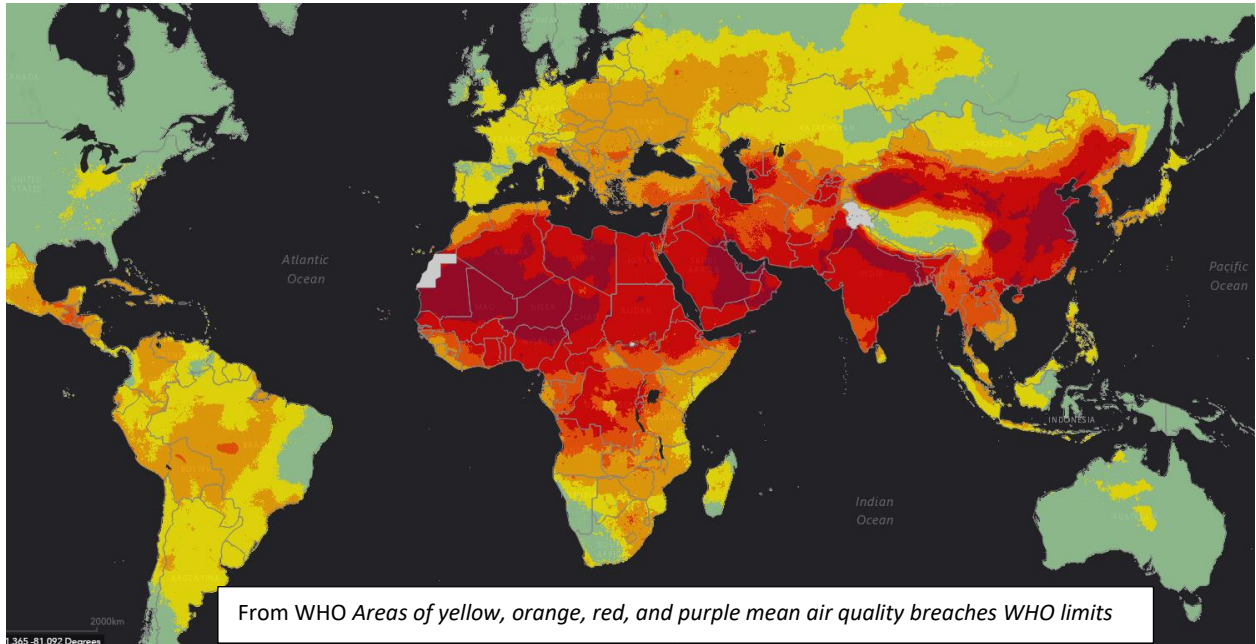


# Monitoring Surface PM<sub>2.5</sub>: An International Constellation Approach to Enhancing the Role of Satellite Observations



**Lead Authors:** Kondragunta, Shobha (NOAA) and Veihelmann, Ben (ESA)

**Contributing Authors:**

Chatfield, Robert (NASA)  
Chin, Mian (NASA)  
Christopher, Sundar (University of Alabama Huntsville)  
Clements, Andrea (EPA)  
Dickerson, Phil (EPA)  
Da Silva, Arlindo (NASA)  
Delgado, Ruben (University of Maryland Baltimore County)  
Diner, David (NASA JPL)  
Fougnie, Bertrand (EUMETSAT)  
Garrigues, Sebastien (ECMWF)  
Giles, David (NASA)  
Gupta, Pawan (NASA/USRA)  
Hashimoto, Makiko (JAXA)  
Henderson, Barron (EPA)  
Holben, Brent (NASA)  
Huff, Amy (IM Systems Group)  
Kahn, Ralph (NASA)  
Kim, Jhoon (Yonsei University)  
Knowland, K. Emma (NASA/Morgan State University)  
Koplitz, Shannon (EPA)  
Laszlo, Istvan (NOAA)  
Lefer, Barry (NASA)  
Levy, Rob (NASA)  
Liu, Hongqing (IM Systems Group)  
Liu, Yang (Emory University)  
Loyola, Diego (DLR)  
Lyapustin, Alexei (NASA)  
Martin, Randall (Washington University)  
Mishra, Manoj (ISRO)  
Muva, Ramana (ISRO)  
Natraj, Vijay (NASA JPL)  
Newchurch, Michael (University of Alabama Huntsville)  
Pierce, Brad (University of Wisconsin – Madison)  
Saide, Pablo (University of California Los Angeles)  
Szykman, James J (EPA)  
Tanaka, Taichu (JMA)  
Torres, Omar (NASA)  
van Donkelaar, Aaron (Dalhousie University)  
Wang, Jun (U of Iowa)  
Welton, Judd (NASA)  
Zhang, Hai (IM Systems Group)

## Executive Summary

Exposure to particulate pollution is a severe burden to public health worldwide. Information on near-surface concentrations of particulate matter (PM) is needed on a global scale: as input to air quality services for citizens, to support policy makers in evaluating the efficacy of pollution abatement measures, and to help environmental agencies verify compliance with standards on pollution levels and related emissions.

Satellite observations do offer valuable information on PM. However, satellite observations alone are not sufficient to provide the needed PM products. A combination of ground-based measurements, satellite observations, and information from atmospheric chemistry and transport models is needed for monitoring and forecasting near-surface PM concentrations. Optimal application of satellite observations for PM estimation has not yet been achieved.

A host of space-borne sensors capture different aspects of PM: imagers observe the horizontal distribution of the vertically integrated burden, multi-angle and polarimetric imagers also allow constraining particle size and type, spectrometers provide some information on the vertical distribution as well as spectral absorption and speciation fractions of absorbers in smoke and dust, lidars capture the vertical distribution of the particle load along narrow tracks. Although some products like aerosol optical depth are mature, many products capturing particle properties remain qualitative. A synergetic exploitation of these capabilities is needed to enhance accuracy of the PM distribution globally.

The present whitepaper takes stock of the current and planned sensors with strong potential for constraining PM, and of schemes used for generating particulate pollution products and services. Specific and actionable recommendations are made to strengthen the role of satellites in constraining PM levels and to help creating satellite-informed particulate pollution products.

## Recommendations

1. Pursue the exploitation of the near-real time (NRT) information on Particulate Matter (PM) from meteorological imagers.
2. Pursue the use of aerosol layer height information from satellites for constraining surface PM. Pursue the development of fast forward operators for assimilating vertical distribution information from spectrometers.
3. Pursue the use of particle property information from multi-angle and multi-angle polarimetric imagers for constraining surface PM.
4. Continue efforts to establish, monitor, and enhance the consistency of AOD and other aerosol products relevant to PM from space-borne sensors. Continue and strengthen related efforts made by the AEROSAT community.
5. Pursue the development of synergetic retrievals in order to combine the best available information on aerosol amount, type (proxy for composition), and vertical distribution from multiple sensors.
6. Continue efforts to establish, monitor, and enhance the radiometric calibration consistency of space-borne multi-spectral imagers. Continue and strengthen related efforts made by the Global Space-based Inter-Calibration System (GSICS).
7. Pursue scientific developments to identify ways to improve the consistency of the representation of aerosol between models and satellite products.
8. Reinforce efforts to improve uncertainty estimates in satellite aerosol products, in order to facilitate their use in data assimilation schemes.
9. Continue and reinforce the efforts made by the AEROCOM community to evaluate and improve the skill of aerosol models and the capability of aerosol assimilation schemes.
10. Pursue the development of schemes for the assimilating Earth radiances measured by space-borne sensors.
11. Create ground-based validation sites with collocated in-situ PM sensors, aerosol remote sensing sensors, measurements of near-surface extinction, and active sensors that characterize the vertical aerosol distribution.
12. Pursue calibration of low-cost PM<sub>2.5</sub> sensors and develop correction methodologies.
13. Develop tools for enhanced data processing including machine learning algorithms.
14. Facilitate coordination of data access for stakeholders.

## Contents

Executive Summary.....	3
Recommendations.....	4
List of Abbreviations and Acronyms .....	10
1. Introduction.....	14
2. Current and Planned Sensors that Provide Aerosol Information.....	17
2.1. Multispectral Satellite Imagers .....	18
2.2. Hyperspectral Imagers (Spectrometers) in LEO and GEO Orbits.....	20
2.3. Multi-Angle Polarimeters in LEO.....	21
2.4. Space-borne Lidar .....	21
2.5. Aerosol Measurements from Ground.....	22
<b>2.5.1. Ground-based in situ PM Sensors</b> .....	22
<b>2.5.2. Ground-based AOD (AERONET)</b> .....	23
<b>2.5.3. Ceilometers and Lidars</b> .....	23
3. Satellite Observations.....	23
3.1. Consistency of Aerosol Optical Depth Products .....	24
3.2. Merged AOD Products .....	25
<b>3.2.1. Merging Multiple LEO Products</b> .....	26
<b>3.2.2. Merging Multiple GEO Products</b> .....	26
<b>3.2.3. Merging GEO-LEO AOD Products</b> .....	27
<b>3.2.4. Merging AOD from Satellites and Simulations</b> .....	29
3.3. Aerosol Vertical Distribution.....	30
3.4. Synergistic Retrievals .....	32
<b>3.4.1. Retrieving a Suite of Aerosol Products from Multi-spectral Imager and Imaging Spectrometer</b> .....	32
<b>3.4.2. Multiple Views by Combining Multiple Sensors</b> .....	32
3.5. The Retrieval Challenge .....	33
3.6. Earth Radiance Data.....	33
4. Estimating Surface PM <sub>2.5</sub> .....	34
4.1. Statistical Methods .....	35
4.2. Geophysical Scaling Methods .....	36

4.3. Geophysical Scaling Method using Multiple Satellite AOD Products .....	37
4.4. Statistical Methods with Dynamic Updating of Regression Parameters .....	40
4.5. Assimilation of Aerosol Products .....	42
<b>5. Validation of Aerosol Products and Model Skill .....</b>	<b>45</b>
References .....	46
Appendix A: Summary of Individual Satellite Sensors that Provide Aerosol Information .....	69
A1. Geostationary Sensors .....	69
<b>A1.1. The INSAT Series .....</b>	<b>69</b>
<b>A1.2. The GOES-R Series .....</b>	<b>69</b>
<b>A1.3. The Himawari Series .....</b>	<b>73</b>
<b>A1.4. The GEOKOMPSAT Series .....</b>	<b>74</b>
<b>A1.5. The MetoSat Series .....</b>	<b>74</b>
<b>A1.6. The FengYun-4 (FY-4) Series .....</b>	<b>74</b>
<b>A1.7. The Geostationary Ocean Color Imager (GOCI) Series.....</b>	<b>75</b>
A2. Geostationary Spectrometers.....	75
<b>A2.1. GEO-KOMPSAT-2B GEMS.....</b>	<b>76</b>
<b>A2.2. Tropospheric Emissions: Measurement of Pollution (TEMPO) .....</b>	<b>76</b>
<b>A2.3. Sentinel-4 UVN .....</b>	<b>76</b>
A3. Polar-Orbiting Imagers.....	77
<b>A3.1. MODIS.....</b>	<b>77</b>
<b>A3.2. MISR.....</b>	<b>79</b>
<b>A3.3. Visible Infrared Imaging Radiometer Suite (VIIRS) .....</b>	<b>80</b>
<b>A3.4. METImage.....</b>	<b>81</b>
<b>A3.5. MAIA.....</b>	<b>81</b>
<b>A3.6. OceanSat.....</b>	<b>83</b>
A4. Polar-Orbiting Spectrometers.....	84
<b>A4.1. Sentinel-5P TROPOMI .....</b>	<b>84</b>
<b>A4.2. Sentinel-5 UVNS .....</b>	<b>84</b>
<b>A4.3. GaoFen-5 EMI.....</b>	<b>85</b>
A5. Polarimeters.....	85
<b>A5.1. GaoFen-5 DPC.....</b>	<b>85</b>
<b>A5.2. Metop-SG 3MI.....</b>	<b>86</b>
<b>A5.3. Copernicus Carbon Dioxide Monitoring (CO2M) .....</b>	<b>86</b>
<b>A5.4. CALIOP .....</b>	<b>86</b>
<b>A5.5. Atmosphere Observing System (AOS).....</b>	<b>87</b>

---

A6. Ground-Based Sensors.....	87
<b>A6.1. Surface PM<sub>2.5</sub></b> .....	87
<b>A6.2. AERONET</b> .....	88
<b>A6.3. Ceilometer and Lidar Networks</b> .....	89
<b>A6.4. Surface Particulate Matter Network (SPARTAN)</b> .....	91

## List of Figures

Figure 1.	Schematic view of a satellite-informed PM monitoring scheme .....	16
Figure 2.	High quality NOAA VIIRS AOD at 550 nm for 3 January 2020. ....	25
Figure 3.	Merged high-quality NOAA GEO/LEO AOD at 550 nm for 17-18 UTC on 1 December 2020.....	28
Figure 4.	Merged NASA GEO/LEO AOD at 550 nm for 15 March 2020. ....	29
Figure 5.	The combined AOD (A), simulated $\eta$ ( $PM_{2.5}/AOD$ ) (B), and combined $PM_{2.5}$ estimates (C) for 1998-2018.. ..	<b>Error! Bookmark not defined.</b>
Figure 6.	Geophysical $PM_{2.5}$ and Annual mean geophysical $PM_{2.5}$ versus coincident annual mean in situ values for 2015. ....	<b>Error! Bookmark not defined.</b>
Figure 7.	Hourly $PM_{2.5}$ estimates: (a) from ABI AOD using GWR algorithm; (b) from ABI AOD using the climatological relations based on Geophysical approach. ....	41
Figure 8.	Comparison between hourly $PM_{2.5}$ observations (x-axis) to model-estimated concentrations (y-axis) for Thailand in 2018, with MERRA-2 reanalysis derived surface $PM_{2.5}$ and a machine learning estimated $PM_{2.5}$ using MERRA-2 AOD, aerosol and meteorology fields as input parameters .....	42
Figure A 1.	Example MAIA step-and-stare sequence, showing the case of 5 discrete view angles....	82
Figure A 2.	Layout of the MAIA satellite instrument.....	83
Figure A 3.	DPC fine mode aerosol optical depth at 865 nm at 3.3 km x 3.3 km resolution for 23-30 November 2018.....	85
Figure A 4.	Global AERONET .....	89
Figure A 5.	Global Atmospheric Watch (GAW) Aerosol Lidar Observation Network (GALION) stations.....	91
Figure A6.	Global Surface Particulate Matter Network.....	91

## List of Tables

Table 1.	Guidelines for ambient air pollution by PM set by the WHO, the EU and the EPA. ....	15
Table 2.	Typical capabilities of the various satellite sensor classes. ....	18
Table 3.	Schematic for developing use cases.....	43
Table A 1.	Characteristics of sensors on current and planned LEO satellites relevant for PM monitoring.....	70
Table A 2.	Characteristics of sensors on current and planned GEO satellites relevant for PM monitoring.....	71

## List of Abbreviations and Acronyms

3MI	Multi-viewing, Multi-channel, Multi-polarization Imager
AAE	aerosol absorption exponent
ABI	Advanced Baseline Imager
AC	atmospheric composition
AC-VC	Atmospheric Composition – Virtual Constellation
ADEOS	Advanced Earth Observing Satellite
ADNET	Asian Dust Lidar Network
AE	Ångström exponent
AEH	aerosol effective height
AERONET	Aerosol Robotic Network
AEROSAT	Aerosol Satellite Network – international organization of aerosol remote-sensing experts
AGRI	Advanced Geosynchronous Radiation Imager
AHI	Advanced Himawari Imager
AI	aerosol index
ALH	aerosol layer height
AMI	Advanced Meteorological Imager
AMOD	Aerosol Mass and Optical Depth
AOCH	aerosol optical centroid height
AOD	aerosol optical depth
API	Application Programming Interface
ASDC	Atmospheric Science Data Center
ATLID	ATmospheric LIDar
AVHRR	Advanced Very High Resolution Radiometer
CALIOP	Cloud Aerosol Lidar with Orthogonal Polarization
CALIPSO	Cloud-Aerosol Lidar and Infrared Pathfinder Satellite Observation
CAMS	Copernicus Atmosphere Monitoring Service
CATS	Cloud and Aerosol Transport System
CCD	charge-coupled device
CCMM	coupled chemistry-meteorology model
CGMS	Coordinated Group of Meteorological Satellites
CMA	Chinese Meteorological Administration
CMAQ	Community Multiscale Air Quality model
COMS	Communication, Oceanographic, and Meteorological Satellite
CONUS	continental United States
CSN	Chemical Speciation Network
CTM	chemical transport model
CV	cross validation
DA	data assimilation
DB	Deep Blue
DFS	Degrees of Freedom of Signal
DIAL	Differential Absorption Lidar

---

DISCOVER-AQ	Deriving Information on Surface conditions from Column and Vertically Resolved Observations Relevant to Air Quality
DNB	Day-Night Band
DPC	Directional Polarimeter Camera
DRAGON	Distributed Regional Aerosol Gridded Observation Networks
DSCOVR	Deep Space Climate Observatory
DT	Dark Target
EARLINET	European Aerosol Research Lidar Network
ECMWF	European Centre for Medium-Range Weather Forecasts
EEA	European Environment Agency
EMI	Environmental Mapping Instrument
EORC	Earth Observing Research Center
EPA	Environmental Protection Agency
EPS	Enterprise Processing System
ESA	European Space Agency
ESR	estimation of surface reflectance
EUMETSAT	European Organisation for the Exploitation of Meteorological Satellites
FCI	Flexible Combined Imager
FEM	Federal Equivalent Method
FMF	fine mode fraction
FRM	Federal Reference Method
FY	FengYun
GALION	Global Atmospheric Watch (GAW) Aerosol Lidar Observation Network
GAM	generalized additive model
GASP	GOES Aerosol and Smoke Product
GAW	Global Atmospheric Watch
GBD	Global Burden of Disease study
GCAS	GEostationary Coastal and Air Pollution Events (GEO-CAPE) Airborne Simulator
GEFS	Global Ensemble Forecast System
GEMS	Geostationary Environment Monitoring Spectrometer
GEO	geostationary orbit
GEO-KOMPSAT	Geostationary Earth Orbit-Korea Multi Purpose SATellite
GEOS-Chem	Goddard Earth Observing System chemistry model
GeoXo	Geostationary Extended Observations
GK	Geostationary Earth Orbit-Korea Multi Purpose SATellite
GLAS	Geoscience Laser Altimeter System
GOCART	Georgia Tech/Goddard Global Ozone Chemistry Aerosol Radiation and Transport model
GOCI	Geostationary Ocean Color Imager
GOES	Geostationary Operational Environmental Satellite
GOME	Global Ozone Monitoring Experiment
GRASP	Generalized Retrieval for Aerosol and Surface Properties
GRM	geostatistical regression model
GSICS	Global Space-based Inter-Calibration System
GWR	geographically weighted regression
HSRL	High Spectral Resolution Lidar
ICARE	Cloud-Aerosol-Water-Radiation Interactions
ICESat	Ice, Cloud, and land Elevation Satellite
IFS	Integrated Forecasting System

---

IMPROVE	Interagency Monitoring of Protected Visual Environments
INSAT	Indian National Satellite
IOT	in orbit test
ISRO	Indian Space Research Organisation
JAXA	Japan Aerospace Exploration Agency
JMA	Japan Meteorological Agency
LALINET	Latin America Lidar Network
LCS	Land Cover Similarity
LEO	low Earth orbit
LME	linear mixed-effects
LUT	look-up table
MAIA	Multi-Angle Imager for Aerosols
MAIAC	Multi Angle Implementation of Atmospheric Correction
MAP	Multi-Angle Polarimeter
MERIS	Medium Resolution Imaging Spectrometer
MERRA	Modern-Era Retrospective Analysis for Research and Application
MetOp-SG	Meteorological Operational Satellite - Second Generation
MISR	Multi-angle Imaging Spectroradiometer
ML	machine learning
MODIS	MODerate resolution Imaging Spectroradiometer
MOSDAC	Meteorological & Oceanographic Satellite Data Archival Centre
MPLNET	Micro-Pulse Lidar Network
MRM	minimum reflectance method
MSG	Meteosat Second Generation
MTG	Meteosat Third Generation
MTG-I	Meteosat Third Generation-Imager
MTG-S	Meteosat Third Generation-Sounder
MWIR	middle wavelength infra-red
NDACC	Network for the Detection of Atmospheric Composition Change
NDVI	Normalized Difference Vegetation Index
NIR	near infra-red
NRMSD	normalized root mean square difference
NWS	National Weather Service
SCIAMACHY	SCanning Imaging Absorption spectroMeter for Atmospheric CartographY
SPARTAN	Surface PARTiculate mAtter Network
OCM	Ocean Colour Monitor
OCO	Orbiting Carbon Observatory
OE	optimal estimation
OMI	Ozone Monitoring Instrument
OMPS	Ozone Mapping and Profiler Suite
OPC	optical particle counter
OSSE	Observing System Simulation Experiment
OTB	Orbital Test Bed
PA	PurpleAir
PACE	Plankton, Aerosols, Clouds, and Ecosystems
PAMS	Photochemical Assessment Monitoring Stations
PARASOL	Polarization & Anisotropy of Reflectances for Atmospheric Sciences coupled with Observations from a Lidar

---

PBL	planetary boundary layer
PM	particulate matter
PMap	Polar Multi-sensor Aerosol properties
POLDER	Polarization and Directionality of the Earth's Reflectance
PTA	Primary Target Area (MAIA)
RF	random forest
RMSE	root mean square error
RSR	relative spectral response
S4	Sentinel-4
S5	Sentinel-5
S5P	Sentinel-5 Precursor
SAA	single scattering albedo
SAGE	Stratospheric Aerosol and Gas Experiment
SeaWiFS	Sea-viewing Wide Field-of-View Sensor
SEVIRI	Spinning Enhanced Visible and Infrared Imager
SNPP	Suomi-National Polar-orbiting Partnership
SNR	signal-to-noise ratio
SRB	solar reflectance bands
SRON	Netherlands Institute for Space Research
STA	Secondary Target Area (MAIA)
SWIR	shortwave infra-red
TEMPO	Tropospheric Emissions: Monitoring of Pollution
TIR	thermal infra-red
TOMS	Total Ozone Mapping Spectrometer
TRACER-AQ	Tracking Aerosol Convection interactions Experiment-Air Quality
TROPOMI	TROPOspheric Monitoring Instrument
UCN	Unified Ceilometer Network
US	United States
UV	ultraviolet
UVN	Ultraviolet-Visible-Near-Infrared instrument
UVNS	Ultraviolet-Visible-Near-Infrared-Shortwave-Infrared instrument
VEDAS	Visualization of Earth observation Data and Archival System
VII	Visible Infrared Imager
VIIRS	Visible Infrared Imaging Radiometer Suite
VIS	visible
VNIR	visible and near infra-red
WHO	World Health Organization
WMO	World Meteorological Organization
WRF-Chem	Weather Research and Forecasting model coupled with Chemistry
XGBoost	extreme gradient boosting
YAER	Yonsei Aerosol Retrieval

## 1. Introduction

Satellite observations are an underutilized resource for constraining global particulate matter (PM) concentrations. Air pollution by PM is recognized to be a major threat to human health. A large part (90%) of the world population lives in places where the air quality guidelines set by the World Health Organization (WHO) are not met; limits set for PM are often exceeded, especially in urban areas in the Eastern Mediterranean region, the African and South-East Asian regions and low-income areas within the Western Pacific region. Air pollution caused 4.2 million premature deaths (~60 per 10<sup>5</sup> inhabitants) worldwide in 2016 (WHO, 2018a; WHO, 2018b). In Europe, in the same reference year, 75 premature deaths per 10<sup>5</sup> inhabitants have been reported to be attributable to PM (European Environment Agency, 2019).

PM refers to solid or liquid phase particles suspended in ambient air. Coarse particles originate mainly from soil (mineral dust) or from sea spray (sea salt). Fine and ultrafine particles are formed primarily by condensation from the gas phase. Many of the precursor gases involved in this secondary particle formation originate from fossil fuel combustion. Fine and ultrafine particles often consist of a mixture of elemental carbon, organic compounds, metals, nitrates, and sulfates. PM is often classified based on the particle size: the labels PM<sub>10</sub>, PM<sub>2.5</sub> and PM<sub>1</sub> refer to particles with a median diameter smaller than 10 µm, 2.5 µm, and 1 µm, respectively. This classification accounts for the fact that smaller particles tend to have more severe adverse health effects than larger ones. Particles larger than 2.5 µm are largely filtered in the lung by the bronchi and bronchioles, whereas smaller particles can pass this barrier, enter the bloodstream, and cause a wide range of health problems including cardiovascular diseases, asthma, allergies, and even gene mutations. The overall toxicity of PM is determined by both the particle size and its chemical composition (e.g. Nel, 2005).

Legal standards regulating near-surface air pollution levels including PM<sub>10</sub> and PM<sub>2.5</sub> have been established e.g. by the WHO (WHO, 2005), the European Union European Commission 2008), and the United States Environmental Protection Agency (US EPA) (US EPA, 2020) (see Table 1). While setting thresholds is necessary for the formulation of targets and for reporting, there seems to be no limit below which health impacts can be excluded (Di et al., 2017a; Di et al., 2017b). National environmental agencies operate networks of ground-based stations where the concentrations of various trace gases and PM are measured in situ, and use the data records from these stations for exposure estimation, verifying compliance with air quality standards and assessing the effectiveness of air pollution abatement measures. For example, the US EPA monitors air quality in the US in line with several legislative mandates such as the Clean Air Act (US EPA, 1990); the European Environmental Agency (EEA) coordinates the air quality reporting based on measurements from national networks in the European countries.

A growing number of information services focus on air quality. Daily analyses and forecasts of the atmospheric composition with regional or even global coverage are obtained using atmospheric models describing weather, transport, and chemistry, such as ECMWF's Integrated Forecasting System (IFS; <https://www.ecmwf.int/en/publications/ifs-documentation>), NOAA's Global Ensemble Forecast System (GEFS; <https://www.noaa.gov/media-release/noaa-upgrades-global-ensemble-forecast-system>), the global forecasting system of the Copernicus Atmosphere Monitoring Service (CAMS; <https://atmosphere.copernicus.eu/cams-upgrades-its-global-forecasting-system-0>), that are run on high-performance supercomputers. Advanced techniques, including data assimilation methods, are employed to ingest information from satellite or in situ observations into the models. Building on analysis and forecast data, numerous downstream services, including smartphone applications, disseminate warnings related to the current local air quality. In such applications, the overall air quality

is often captured by a single air quality index that is computed based on the concentrations of a small set of key pollutants including PM<sub>10</sub> and PM<sub>2.5</sub> (e.g., AirNow, <https://www.airnow.gov>).

**Table 1.** Guidelines for ambient air pollution by PM set by the WHO, the EU and the US EPA.

Pollutant	Averaging period	Organization	Limit [ $\mu\text{g}/\text{m}^3$ ]	Percentile	Maximum number of exceedances
PM <sub>10</sub>	1 day	WHO	45 <sup>(1)</sup>	99 <sup>th</sup>	3
		EU	50	-	35
		EPA	150	-	1 (averaged over 3 years)
	Calendar year	WHO	20 <sup>(1)</sup>	-	-
		EU	40	-	-
PM <sub>2.5</sub>	1 day	WHO	15 <sup>(1)</sup>	99 <sup>th</sup>	3
	1 day	EPA	35	98 <sup>th</sup>	1 (averaged over 3 years)
	Calendar year	WHO	5 <sup>(1)</sup>	-	-
		EU	25	-	-
	3 years	EPA	12 <sup>(2)</sup> , 15 <sup>(3)</sup>	-	-

(1) [https://www.who.int/news-room/fact-sheets/detail/ambient-\(outdoor\)-air-quality-and-health](https://www.who.int/news-room/fact-sheets/detail/ambient-(outdoor)-air-quality-and-health)

(2) Primary Standards protect public health, including the health of sensitive groups

(3) Secondary Standards protect public welfare (visibility, crops, vegetation, and buildings)

For the characterization of PM in a given spatial and temporal domain, many parameters need to be known, including the number density, size distribution, microphysical properties, hygroscopicity, and vertical distribution. Three main information sources are typically used to characterize PM: ground-based instruments, satellite sensors, and atmospheric modeling. In practice, only a few pieces of information are available from each of these information source, which makes the estimation of PM concentrations and the monitoring of near-surface particle pollution a highly under-constrained problem. Therefore, in current estimation and monitoring schemes, data from a combination of the three information sources is exploited. Atmospheric models capture the scientific understanding of the driving processes including sources, transport and sinks of the pollutants. Satellite observations are complementary to ground based data. Both are key ingredients to meaningful and accurate estimates of pollution levels from the local to the global scale. In practice, satellite-informed particulate pollution products and services integrate prior information and information from the various types of observations either by data assimilation or by applying statistical methods, as schematically sketched in Figure 1. At present, there are various approaches to PM estimation that do exploit satellite observations. These approaches vary depending on the specific type of application, ranging from the attribution of mortality rates to real time alerts and warnings. The improvement of existing schemes and the development of new concepts for PM estimation is currently a dynamic area of research. However,

an optimal application of satellite observations for PM estimation has not yet been achieved, and opportunities exist for the greater utilization of satellite data on a global scale.

Space-borne sensors do have a strong potential to constrain particulate pollution: multispectral imagers provide valuable information on the horizontal distribution of the aerosol burden. Their synoptic view is key to evaluating the consistency of ground-based stations and for covering the gaps between stations. Observations from passive satellite sensors are sensitive to the total column aerosol optical depth (AOD; i.e., the vertically integrated extinction coefficient) but are limited in their capability to resolve the vertical profile. Lidars (active sensors) have the unique capability of resolving the vertical distribution of aerosol but are limited in their horizontal sampling. Spectrometric measurements at strong atmospheric gas absorption features also allow constraining the vertical distribution of trace gas precursors of PM. Polarimetric, multispectral, and multidirectional observations bring information on the aerosol amount, size and type. Geostationary sensors capture the diurnal evolution of pollution fields. Satellite sensors can capture emission events such as from wildfires that are not predictable by models.

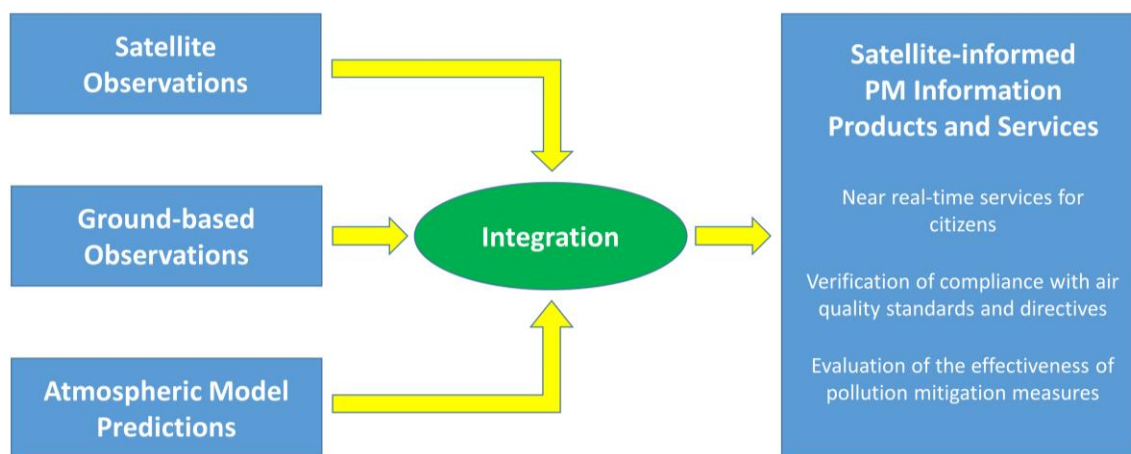


**Figure 1.** Schematic view of a satellite-informed PM monitoring scheme. In this context, satellite observations can be observed radiances converted to reflectances or derived Level 2 products such as aerosol optical depths, aerosol index, layer height etc.

However, the link between the data products from these kinds of sensors and near-surface PM concentrations is complex. Aerosol optical properties that govern the satellite observations depend on the hygroscopic state of the particles and hence on the ambient humidity, whereas PM concentrations refer to particles at controlled relative humidity (typically within 30% to 60%). Parameters such as AOD retrieved from imagers rely on prior assumptions on particle size distribution, vertical distribution, and microphysics. The treatment of surface reflectance and clouds in aerosol retrieval schemes can have a substantial influence on the data products. Error characterization of aerosol products is difficult, especially for products based on discrete aerosol models. The consistent interpretation of PM information from satellites in the context of information from other sources, such as ground based measurements and models, is one of the main challenges that must be addressed in the development of satellite-informed PM monitoring. **The objective of the present whitepaper is to strengthen the role of satellites in constraining particulate pollution levels, specifically near-surface PM<sub>2.5</sub> concentrations.**

**The ambitious long-term goal is to create a satellite-informed PM pollution monitoring system. The present whitepaper is meant to help take a step in that direction.**

To this end, this white paper looks at all necessary elements and the various satellite sensors in a constellation perspective. An inventory is made of the current and planned sensors with relevant capabilities for constraining PM. The state-of-the-art schemes used for generating particulate pollution products and services are discussed. Specific and actionable recommendations are made on the development and enhancement of satellite-informed particulate pollution products. The optimal use of all available information is meant to improve air quality services for citizens and for policy makers. Satellite-informed PM products are meant to offer environmental agencies an additional source of information that complements the data products from in situ networks.

The white paper theme “satellite observations of aerosol for air quality” was picked up by the Atmospheric Composition – Virtual Constellation (AC-VC) community, recognizing that it was not covered by other inter-agency coordinating groups such as the International Aerosol Satellite Network (AEROSAT) or the Coordinated Group of Meteorological Satellites (CGMS). Sessions on this topic were held at the AC-VC meeting first in 2017 and at subsequent meetings in which the new initiative took shape, a new active topical sub-group emerged, and the scope of the present white paper was devised.

The white paper is organized as follows: The current and planned satellite sensors with aerosol observing capabilities are identified and their specific potential for constraining near-surface PM is discussed in Section 2. Typical capabilities and limitations are discussed for sensor classes. Details on specific satellites and instruments in these classes are given in Appendix A. The consistency of current satellite aerosol products, and methods to harmonize products, are discussed in Section 3. The statistical and geophysical approaches currently used to constrain PM using satellite data and potential improvements to current methods are discussed in Section 4. The role that aerosol chemistry and transport models including data assimilation of satellite aerosol observations is presented in Section 5. Finally, the white paper recommends how future satellite sensors that can fill in some identified gaps, discuss development of tools for enhanced data processing including machine learning algorithms, activities needed to establish and monitor the consistency of the PM relevant information in various satellite aerosol products, and coordination of data access for stakeholders.

## **2. Current and Planned Sensors that Provide Aerosol Information**

Today, a variety of space-borne sensors are used for observing atmospheric aerosol. The last two decades have seen a tremendous growth in the use of remotely sensed aerosol products for various applications. Some specific applications include using the near real time aerosol imagery (true color, AOD, false color, etc.) in operational air quality forecasting, using AOD to derive surface  $PM_{2.5}$ , using AOD to improve model first guesses, and using AOD to derive fire emission amounts and properties. The collection of high quality AOD data enabled the scientific community to quickly use it to demonstrate the improvements in air quality during the lockdown measures around the globe (Gkatzelis et al., 2021). The use of satellite AOD to monitor urban/industrial pollution and its trend to understand the efficacy of various environmental regulations is very much an ongoing activity. More recently, blended AOD products from models and observations scaled to surface  $PM_{2.5}$  have been used to document the impact on human health (Castillo et al., 2021)

A comprehensive overview of satellite instruments observing atmospheric aerosols is given by Lee et al. (2009) and by Lenoble et al. (2013) among others. Here, we focus on the sensors with observation capabilities covering the lower troposphere that are relevant for PM monitoring. The satellite sensors can be grouped into a set of classes: multispectral and/or multi-viewing imagers, hyper-

spectral imagers (spectrometers), polarimetric multispectral imagers with multiple viewing directions, and lidars. Ground-based sensors are classified as in situ, passive remote sensing, or active remote sensing. Typical aerosol observation capabilities of these sensor classes are listed in Table 2. Specific strengths and limitations of the observations made by these sensors for PM applications are discussed in the subsequent sections (2.1 to 2.5). In Appendix A, individual sensors on current and planned satellites that fall into these classes are described in more detail and summarized in Tables A1 and A2.

**Table 2.** Typical capabilities of the various satellite sensor classes.

Sensor class		Horizontal coverage and resolution	Revisit time / temporal sampling	Information content
Multispectral imagers	LEO	Global, sub-km resolution	Daily	Amount (AOD), size (Ångström coefficient) over land
	GEO	Full disc, sub-km resolution	~10 minutes	
Multispectral imagers with multiple viewing directions in LEO		Global, ~1 km resolution	Few days	Amount (AOD), size (Ångström coefficient), some info on particle shape and light-absorption
Hyperspectral imagers (spectrometers)	LEO	Global, ~10 km resolution	Daily	Amount (AOD), size (Ångström coefficient), vertical distribution (ALH with ~1 DFS from O <sub>2</sub> signatures), spectral absorption and absorber concentrations
	GEO	Partial disc, ~10 km resolution	Hourly	
Polarimetric multispectral imagers with multiple viewing directions in LEO		Global, ~5 km resolution	Few days	Amount (AOD), size (Ångström coefficient), particle shape and microphysical properties
Lidars in LEO		Narrow track	Can be weeks	Finely resolved vertical profiles, particle shape (non-sphericity from depolarization)
Ground based spectrometers and radiometers		Local	Can be a few minutes	Amount (AOD), size (Ångström coefficient), microphysical properties from inversion of sky radiances
Ground based lidars		Local	Can be a few minutes	Finely resolved vertical profile, particle shape (non-sphericity from depolarization)

### 2.1. Multispectral Satellite Imagers

Multispectral imagers with spectral channels in the visible, near IR, and IR provide valuable information on the horizontal distribution of the aerosol burden. Spatial resolutions on the order of a km enable the detection of small-scale signatures of emission events and allow measuring between

clouds in broken cloud conditions. The synoptic view from space-borne imagers is key for complementing ground-based observations. Satellite observations are instrumental for evaluating the consistency of ground-based stations by capturing the gradients in concentrations in between the monitors. Various data products that can be derived from multispectral imagers are relevant to PM monitoring: AOD is a measure for the total column aerosol burden and equals the vertically integrated extinction. Usually, AOD is reported at one or more reference wavelengths in the mid-visible (e.g. 0.55  $\mu\text{m}$ ). The Ångström exponent (AE) over ocean, derived from the wavelength dependence of AOD, is related to aerosol particle size, particularly for mono-modal aerosol distributions. Although AOD algorithms for individual sensors (e.g., MODIS, VIIRS, MISR) can vary, the fundamental approach involves identifying clear-sky pixels from cloudy and snow/ice covered pixels and separating the radiance contribution from the surface and aerosols using pre-computed look-up-tables (Hsu et al., 2013; Levy et al., 2015; Jackson et al., 2013; Limbacher and Kahn, 2017; Lyapustin et al., 2018). The AODs from a network of ground-based sun photometers (Aerosol Robotic Network, AERONET) have provided ground truth to validate the satellite retrievals (Holben et al., 1998).

Aerosol remote sensing deals with the fact that the number of unknowns is by far larger than the degrees of freedom of the measured signal. Multispectral imager observations in the visible wavelengths are weakly sensitive to the vertical distribution and microphysical parameters (particle shape, real and imaginary parts of the refractive index, hygroscopic and mixing state, size distribution, etc.). The AOD estimates derived from a multispectral imager do depend on the assumptions made on these other unknowns. Aerosol retrieval schemes necessarily rely on prior information about these parameters or other types of regularization. Often a discrete set of aerosol models is used, and the aerosol model selection is sometimes based on the season and geo-location. Aerosol products report the assumed aerosol type and the set of assumptions made in the retrieval. When AOD data are used for PM applications, assumptions on the aerosol physical/optical properties are made to convert modelled aerosol loads to observables such as AOD. Potential inconsistencies in these assumptions and approaches that aim at avoiding such inconsistencies are discussed in Section 5.

One of the challenges of aerosol retrievals from multispectral imagers is the handling of the surface reflectance. Single-view passive observations of this type do not provide information to separate the surface from aerosol signals in the top-of-atmosphere reflectances. Often, aerosol parameters are retrieved relying on prior information on the surface reflectance. Multi-angle passive imagers such as MISR allow separation of surface from atmospheric contributions, making self-consistent surface-aerosol retrievals possible in many situations (e.g., Martonchik et al., 2009). Geostationary sensors view the same target frequently with varying solar illumination, which is exploited in joint surface and aerosol retrieval schemes (Govaerts et al. 2010; Wagner et al., 2010; Dubovik et al., 2014). Such schemes work on multi-angle and multi-spectral data-cubes obtained by temporally aggregating reflectance measurements. Independent information on surface and aerosol is extracted from the data-cubes exploiting also differences in the temporal and spatial correlation lengths between aerosol and surface variabilities. The surface characteristics obtained by such joint retrieval schemes may be more representative of the actual observing conditions than climatological surface reflectance data, and thus enhance the quality of the aerosol products. This concept was exploited by algorithms such as the Multi-angle implementation of Atmospheric Correction (MAIAC) to simultaneously derive surface reflectance and aerosol optical depth (Lyapustin et al., 2011) using Aqua and Terra MODIS observations. The operational version of MODIS MAIAC algorithm uses the slow rate of change of surface properties in time to characterize the surface spectral ratios, and derive AOD and surface reflectance (BRF) and parameters of the BRDF model which support the follow-on aerosol retrievals (Lyapustin et al., 2018). Prior to MAIAC algorithm development, the NOAA GOES Aerosol and Smoke Product (GASP) algorithm retrieved surface reflectance and aerosol optical depth using single channel reflectance (Knapp, 2002). The GASP algorithm was subsequently adapted by Kim et al (2016) for Geostationary Ocean Color

Imager (GOCI) AOD retrievals. Such concepts should be considered when optimizing the exploitation of geostationary meteorological imager observations for aerosol and PM pollution monitoring.

## 2.2. Hyperspectral Imagers (Spectrometers) in LEO and GEO Orbits

Hyperspectral imagers (spectrometers) are built to capture the spectral absorption signatures of atmospheric trace gases. AOD products can be derived from the measurements of spectrometers using the spectral windows without strong gas absorption features. AOD products from multispectral imagers are often preferred since the products typically have significantly higher spatial resolution compared to hyperspectral imagers. Nevertheless, spectrometers yield unique information on aerosol that is relevant to PM. Information on the vertical aerosol distribution can be extracted from the relative depth and spectral shape of strong absorption features of known trace gases, such as the O<sub>2</sub>-O<sub>2</sub> collision complex, and the O<sub>2</sub>-A and -B bands. The use of O<sub>2</sub> absorption measurements to constrain cloud and aerosol profiles was first proposed by Yamamoto and Wark (1961). The physical basis is that O<sub>2</sub> is uniformly distributed in the atmosphere with a known mixing ratio, and its spectrally-dependent absorption cross sections are reasonably well known (Drouin et al., 2017). Since aerosols and clouds scatter light back to space, they leave distinctive signatures in different parts of the observed O<sub>2</sub> spectra that are associated with their column optical depth and vertical structure. Absorptions in strong O<sub>2</sub> lines are saturated; therefore, any radiance measured in these lines originates from scattering in the upper part of the atmosphere. Outside of O<sub>2</sub> lines, or in weak lines, the atmospheric column absorption is small, and light penetrates lower atmospheric layers, allowing for the quantification of aerosols and other clouds near the surface. By studying O<sub>2</sub> and O<sub>2</sub>-O<sub>2</sub> absorption signatures, the vertical distribution of aerosols and clouds can be quantified (Xu et al., 2019, Park et al., 2016). Aerosol layer height (ALH) products approximate the aerosol vertical distribution by one single homogeneous layer with a fixed vertical thickness. ALH estimates thus obtained tend to be accurate for cases with medium to high optical depth. The product helps in characterizing events with pronounced emission plumes but is of limited use for characterizing near-surface particle pollution with low optical thickness.

However, the vertical distribution information from such spectral signatures is not yet exploited in data assimilation schemes. For this purpose, forward operators (radiative transfer simulators) are needed that allow a fast prediction of observable spectral signatures for a given model state. The computational demands of radiative transfer calculations that account for multiple scattering at fine spectral sampling is challenging. Dedicated efforts are needed to develop fast forward operators.

A series of spectrometers (e.g. Total Ozone Mapping Spectrometer, TOMS), originally designed to measure ozone, also capture aerosol related signatures in the UV. The UV aerosol index (UV AI) is derived from the spectral contrast in the UV and is sensitive to elevated absorbing particles. This index is powerful for detecting aerosol even over clouds, for tracking plumes of desert dust, volcanic ash, and smoke, and for qualitative analyses (Herman et al., 1997; de Graaf et al., 2005). UV spectral reflectance measurements are also exploited to retrieve a combination of AOD, absorbing AOD, and single scattering albedo (Torres et al., 2007; Torres et al., 2020). A combination of UV and Visible spectral bands in the Earth Polychromatic Imaging Camera (EPIC) of DSCOVR satellite parked in the first Lagrangian point (L1) allows for simultaneous retrieval of AOD and spectral aerosol absorption represented by an Angstrom-type two-parameter model (Lyapustin et al., 2021). For strong smoke or dust plumes, the general magnitude and “spectral slope” of absorption helps to derive concentrations/mass fractions of the main absorbers, namely of black and brown carbon (BC/BrC) in BB smoke and of hematite/goethite in mineral airborne dust (e.g., Go et al., 2022). The aerosol speciation retrieval relies on prior knowledge of the refractive index of mentioned species and assumed ALH. The algorithm was originally developed by Schuster et al. (2016) in application to AERONET, and was prototyped by the GRASP team for POLDER/PARASOL data record (e.g., Li et al., 2019). These UV

products are relevant for air quality by the virtue of their capability to capture pollution events with pronounced plumes. The product portfolio of spectrometers often comprises aerosol precursors such as NO<sub>2</sub> and SO<sub>2</sub>. Assimilating trace gas fields in atmospheric models helps to constrain particle production.

### 2.3. *Multi-Angle Polarimeters in LEO*

The multi-angle viewing capability of sensors like MISR advanced the aerosol retrieval capability to parameters beyond AOD. The additional polarimetric capabilities of Multi-Angle Polarimeters (MAPs) further enhances satellite aerosol remote sensing. The first spaceborne MAP measurements were made with the Polarization and Directionality of the Earth's Reflectance (POLDER) instrument on the ADEOS satellite launched in 1996. Since then other MAPs have been launched, e.g. a POLDER instrument on PARASOL launched in 2004 and the Directional Polarimeter Camera (DPM) on GaoFen-5 launched in 2018. Future MAPs include HARP2 and SPEXone on Plankton, Aerosols, Clouds, and Ecosystems (PACE) and Multi-viewing, Multi-channel, Multi-polarization Imager (3MI) with expected launch dates in 2024. A review of polarimetric sensors and methodologies is given by Dubovik et al. (2018) and Hasekamp (2010).

Multi-angle polarimeter measurements contain typically twice the number of Degrees of Freedom of Signal (DFS) compared to observations from a single-view radiometer (Dubovik et al., 2019). This allows for the simultaneous retrieval of AOD and several aerosol parameters that are of key importance for air quality applications constraining the particle size distribution and the aerosol type. However, the application of derived products for air quality services has been hampered by the complexity and computational demands of aerosol retrieval algorithms (Kokhanovsky et al., 2015). Complex retrieval schemes are needed to fully exploit the information content of the multi-angle polarimetric measurement data. Joint retrieval schemes for surface and aerosol characteristics are needed to obtain independent information on surface reflectivity and aerosol characteristics. Algorithms such as the Generalized Retrieval for Aerosol and Surface Properties (GRASP) and the Netherlands Institute for Space Research (SRON) algorithm retrieved and validated aerosol properties derived from polarized measurements over ocean (Hasekamp et al., 2011; Dubovik et al., 2011). Some recent studies used polarized measurements to retrieve aerosol properties and fine mode fraction of AOD over land (Fu et al., 2018; Zhang et al., 2021). At present, it is a challenge to offer the processing capability that can keep pace with the output of these instruments in an operational environment.

The validation of retrieved aerosol parameters other than AOD is challenging since accurate and representative reference data are scarce: reference data from ground based in situ measurements may capture many parameters accurately but are only partially representative for air masses observed by satellites. Ground-based sun photometers (AERONET) provide direct observations of AOD; the other aerosol parameters are observed indirectly with substantial uncertainties for AODs below ~0.4 (Remer et al., 2019).

### 2.4. *Space-borne Lidar*

Lidar measurements have the unique capability of finely resolving the vertical aerosol distribution. The first space-borne lidar was the Geoscience Laser Altimeter System (GLAS) on ICESat, launched in 2003. The Cloud Aerosol Lidar with Orthogonal Polarization (CALIOP; Winker et al., 2009, 2010) provides vertical profile data with ~30 m resolution. Return signals in the three channels (532 nm parallel, 532 nm perpendicular, and 1064 nm) of CALIOP are used to derive profiles of attenuated backscatter, perpendicular backscatter, depolarization ratio, and color ratio between 532 nm and 1064 nm. These profiles allow the identification and characterization of aerosol layers in terms of optical depth and aerosol type (Kim et al., 2018). The strong potential of lidar measurements at three

wavelengths for retrieving aerosol microphysical properties has been shown for an airborne High Spectral Resolution Lidar (HSRL; McLean et al., 2021).

For air quality applications, aerosol profiling within the planetary boundary layer (PBL) is necessary. Even with advanced space-borne lidar systems, it is very challenging to resolve aerosol vertical profiles in the PBL because resolving the aerosol profile at sub-kilometer scales requires accurate knowledge of aerosol optical properties and composition and correct characterization of surface reflection. However, knowledge of the boundary layer height, which can be identified in lidar profile data more reliably, is already very useful to constrain the vertical aerosol distribution in models, especially when assimilating AOD retrievals.

The strongest limitation of lidar observations for direct use in air quality applications is their limited spatial coverage. Nevertheless, several indirect benefits of lidars in this context are important. Lidar data are very helpful in evaluating and improving models in their capability of describing aerosol vertical profiles and constraining aerosol type. Lidar data are a unique source of reference data for validating and improving effective ALH retrievals, such as using O<sub>2</sub> A-band absorption measurements from instruments such as the TROPOspheric Monitoring Instrument (TROPOMI) (de Graaf, personal communication; Nanda et al., 2020), the aerosol plume injection height product from MISR, or the smoke plume height product from MODIS MAIAC (Ciren and Kondragunta, 2014; Lyapustin et al., 2020; Nelson et al., 2013). The MISR derived global climatologies of aerosol plume heights and aerosol types have also contributed to the advancement of the knowledge of aerosol source regions such as biomass burning, dust storms, and urban/industrial aerosols (Gonzalez-Alonso et al., 2019; Kahn et al., 2008; Val Martin et al., 2018).

## 2.5. *Aerosol Measurements from Ground*

In this section, the ground-based sensor types are discussed that are most important for validation and improvement of aerosol and PM products derived from satellite observations and from models. This includes in situ PM sensors, sun photometers, lidars, and ceilometers. A detailed description of the individual instruments and networks are provided in Appendix A.6.

### 2.5.1. **Ground-based in situ PM Sensors**

Ground-based in situ PM sensors are the main source of reference data for the validation and improvement of PM data products from any kind of air quality monitoring system. PM products that are generated by exploiting column-integrated aerosol characteristics from satellite observations are very sensitive to the correct treatment of the aerosol vertical distribution. Ground-based in situ PM measurements are vital to verify and improve this critical step in particular, and the overall success of a satellite informed PM estimation scheme in general.

Ground-based sensors measuring near-surface PM concentrations in situ are unique in their capability to characterize local PM pollution levels. Many sensors of this kind provide size information by reporting PM<sub>2.5</sub> and PM<sub>10</sub> concentrations, while some even report PM<sub>1</sub> data. Some in situ systems also provide information on the chemical composition of the particles. Operational networks of such sensors are run by national environmental agencies for monitoring air quality and the compliance with national air quality standards. Measurement data of such networks are a key ingredient to PM pollution information services as discussed in Section 4. Low-cost in situ sensors are publicly available, but not all sensors are well calibrated. The low-cost sensor data in the US are corrected using the algorithms developed by US EPA (Holder et al., 2020) but the data from Asia, Europe, and other parts of the world are less understood and methodologies to quantify their accuracy and any corrections needed must be developed. Networks of such sensors are operated by public and scientific institutes and players in the

private sector.

### **2.5.2. Ground-based AOD (AERONET)**

AERONET, the multi-wavelength ground-based sun photometer network of AOD measurements, started in the early 1990s prior to the launch of Terra as a “truth” dataset for space-borne AOD retrievals (Holben et al., 1998). AERONET grew from a few stations in the early stages to hundreds (600 as of 2018) of stations across the globe, covering a variety of geographical regions from rural to urban areas, including current and emerging mega cities (<https://aeronet.gsfc.nasa.gov/>). AERONET is a federated program wherein instrument scientists agree to calibrate their sun photometers according to guidelines set forth by NASA and to contribute the data freely to users. An AERONET sun photometer tracks the sun and measures direct solar irradiance and directional sky radiance at different wavelengths. The attenuation of solar irradiance is proportional to the aerosol amount present in the atmosphere, derived as AOD. Observations at multiple wavelengths (UV to visible) provide the spectral dependence of AOD, which is a proxy for particle size. The inversion of direct sky radiance measurements provides information on refractive index, volume size distribution, single scattering albedo, and particle phase function. The aerosol optical and physical properties are extremely important because they not only provide regional aerosol climatologies but they also form the basis for categorizing aerosols into different types (e.g., dust highly absorbing, smoke low absorbing) that are used by satellite aerosol retrieval algorithms. The AOD measured by AERONET sun photometers is never used in any retrieval algorithm other than to verify the retrievals. Most satellite AOD retrieval algorithms use the global AERONET sun photometers to demonstrate algorithm performance metrics. Further description of AERONET is provided in Appendix A6.2.

### **2.5.3. Ceilometers and Lidars**

Ceilometers and lidars are ground-based active laser-based instruments that provide unique information on the vertical profile of atmospheric constituents. Both systems rely on the time delay and the amplitude of backscattered return signals. The main products relevant to aerosol are extinction coefficient profiles and boundary layer height. Some advanced lidar products also provide information on the aerosol type.

The distinguishing characteristics of ceilometers that set them apart from lidars are historically: low cost, robust, single near IR wavelength, lower signal to noise (especially for clear air), commercially available. In addition, ceilometers deployed in most operational networks are operated in black box mode, where only limited variables are provided, such as cloud base and PBL height, but the signal profile data are not utilized and/or archived. Ceilometer networks have produced dense coverage spatially, but with a limited data set. Historically lidar characteristics have included: higher costs, less robust, addition of UV and/or visible wavelengths, polarized observations to determine particle shape, higher signal to noise, provide the lidar signals and more retrieved data variables. A description of lidar and ceilometer networks is provided in Appendix A6.3.

Ground-based data sets supporting the scientific studies and developments aiming at PM estimation would strongly benefit from co-located lidar and ceilometer data. Therefore, campaign supersites and long terms measurement sites with in situ PM and ground based aerosol remote sensing sensors should be complemented with ground-based lidar and ceilometers.

## **3. Satellite Observations**

The premise of this white paper is the use of satellite-derived aerosol products in estimating surface PM. While aerosol algorithms are dictated by the science and capabilities of individual sensors and thus products could have diverse performance metrics, users expect certain standard for the quality of data provided. Consistency of satellite observations and derived products is critical. For example, there cannot be an observable whose long-term trend over a region is increasing when one product is used and decreasing when a different product is used. While biases between different sets of products are expected, they should be corrected so the products are harmonized based on the availability of information on uncertainties and on correlated errors and assumptions made.

Many PM estimation schemes focus on the use of satellite AOD products from one or more sensors. Current approaches to establish and maintain data quality and consistency of AOD products are discussed in Sections 3.1 and related recommendations are made. Some PM estimation schemes exploit satellite radiance products instead of AOD. Section 3.2 is dedicated to discussing the consistency of such radiance products.

Specific needs in this regard depend on the type of application. For example, if the AODs from a given sensor are being used for near real-time estimates of PM<sub>2.5</sub> for operational air quality warnings, then it is important to know the pixel-level uncertainties (Sayer et al., 2020). For certain applications that need fine spatial and temporal coverage with minimal gaps, data from multiple satellites and sensors are merged. During the merging process, consideration is given to the quality of individual products but it is not practical to transfer pixel-level uncertainties of each sensor to a merged grid.

### *3.1. Consistency of Aerosol Optical Depth Products*

Given the availability of many different AOD products from many different sensors and algorithms, it is prudent to derive a consistent merged AOD product for certain applications. The need to merge AOD products from different sensors/algorithms arises from the need to optimize information content. For example, AOD products from the VIIRS instruments on the Suomi-National Polar-orbiting Partnership (SNPP) and NOAA-20 satellites are derived using the same algorithm, but the spatial coverage of the AOD products is different due to the 50-minute time offset in the equator crossing time of the satellites. Due to the time difference, cloud cover and sun glint are different for the two satellites. Due to these differences, when the two AOD products are merged, the merged products have more spatial coverage compared to the corresponding products from each individual satellite, as shown in Figure 2.

Merging of AOD products from different sensors is also conducted to study long-term trends in AOD, and gaps in certain satellite products have to be bridged. As the MODIS AOD era draws to an end in 2023 with planned orbit lowering maneuvers of NASA, and as the scientific community transitions to using VIIRS AOD products, the merging of MODIS and VIIRS AOD products, when they are both available, is important to adjust for their biases caused by instrument calibration/algorithm differences. For PM<sub>2.5</sub> applications, temporal and spatial coverage is of utmost importance, as filling in the gaps between ground monitors using satellite AOD is the goal. Given this objective, merging different satellite AOD products to improve spatial and temporal coverage is practical.

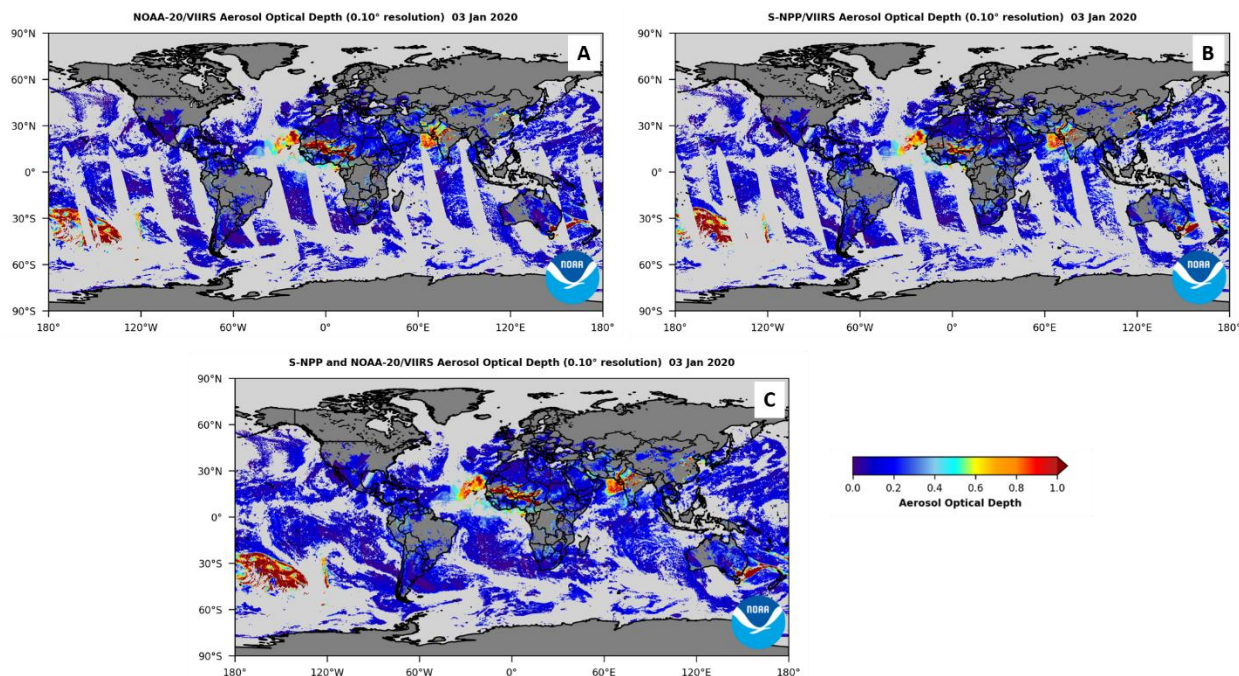


**Figure 2.** High quality NOAA VIIRS AOD at 550 nm for 3 January 2020 from NOAA-20 (A), SNPP (B), and merged NOAA-20 and SNPP (C).

Documenting the diversity in multi-satellite AOD products at both regional and global scales is a key step in this direction. Biases in the observations and departure between observations can significantly affect the data assimilation outputs (Zhang and Reid, 2005), and the spatial and temporal structure of the systematic differences between satellite products needs to be properly understood and quantified in order to account for them in the assimilation process (Dee et al., 2005). Schutgens et al. (2020) reported results of an extensive analysis of 9 different algorithms (14 AOD products) using daily average AOD aggregated to  $1^\circ$  resolution. The study shows difference in regional biases, which tend to cancel out in the merged products (e.g., Sogacheva et al., 2020), different random error associated with quality of cloud screening and measurement noise, including differences from the same algorithm but different sensor (e.g., MODIS on Terra and Aqua platforms). The AeroSat initiative coordinates scientific activities on satellite aerosol products, including intercomparisons of products, and aims to make more consistent definitions, tools, and formats used. Continuing these activities is recommended to monitor the consistency of existing satellite aerosol products and to pursue making them more consistent.

### 3.2. Merged AOD Products

It has been shown that, despite differences in information content, sampling, calibration, cloud masking, and algorithmic assumptions, merged products can be robust and outperform products from individual sensors. Merged products benefit from complementary spatial-temporal sampling of the individual products and allow creating long-term data records covering the lifetimes of multiple sensors. The quality of a merged data product is indicative for the consistency of the ingredients, needed for combined use in a data assimilation scheme. Examples are given for merged products from multiple LEO sensors (3.2.1), multiple GEO sensors (3.2.2), the combination of LEO and GEO sensors (3.2.3), and satellites and simulations (3.2.4).

### 3.2.1. Merging Multiple LEO Products

The AeroSat community, comprising aerosol algorithm developers and product users, decided during their annual meeting in 2019 that it is in the best interests of product users to develop and document best practices for merging various satellite products. The AeroSat community is interested in using satellite data for climate applications and long-term trend analysis in different parts of the world; thus, the procedures developed by this group are primarily Level 3 gridded monthly mean AOD datasets, typically at  $1^\circ \times 1^\circ$  spatial resolution. Merging Level 3 AOD data helps with building AOD datasets that are spatially and temporally consistent.

Though the purpose is different, some of the  $PM_{2.5}$  applications that are of interest to the air quality community are also related to long-term changes in pollution and its impact on human health. Thus, it is important to summarize the methods used to create merged datasets by the AeroSat community. Sagacheva et al. (2020) collected multiple satellite sensors including products from different algorithms for the same sensor from 1995 to 2017.

For the creation of the merged dataset, Sagacheva et al. (2020) took two different approaches. In one approach, they used comparisons of each individual satellite dataset to AERONET AOD data to derive metrics such as correlation coefficient, bias, root mean square error, and percentage of data points within the expected error. Each of the 10 different satellite AOD products were assigned a rank for these categories and an overall weight was defined based on the sum of all individual ranks for each product. The merged AOD was then derived as weighted mean value of all the available datasets. In another approach, each satellite dataset was adjusted for offset with MODIS AOD and the median of all offset-adjusted AOD datasets was selected to generate the merged dataset.

The merged product appears to be overall better than the individual products. Better agreement with reference measurements from AERONET data and a good robustness were reported by Sagacheva et al. (2020). One of the challenges that remains to be tackled is finding a way to report the uncertainty of the parameters in the combined product.

### 3.2.2. Merging Multiple GEO Products

Lim et al. (2021) developed an ensemble retrieval approach using the Yonsei Aerosol Retrieval (YAER) algorithm to derive merged AOD. In this approach, two different algorithms are run on two different satellites to generate four AOD products, and then a weighted merged product is generated. The two instruments are Advanced Himawari Imagery (AHI) and GOCI; AHI is used as a proxy for Advanced Meteorological Imager (AMI) as the AOD product from AMI is not available. The spatial and spectral characteristics of the instruments are different but the data are mapped to a common resolution of  $6 \text{ km} \times 6 \text{ km}$ . The difference between the two algorithms is in the way surface reflectance is derived. One algorithm that uses the minimum reflectance method is based on the algorithm approach, originally developed by NOAA for its legacy GOES AOD product, GASP (Knapp et al., 2007). The other algorithm estimates surface reflectance from pre-determined spectral surface reflectance ratios between SWIR and visible. For GOCI, because of the absence of a  $2.25 \mu\text{m}$  channel, the  $1.6 \mu\text{m}$  channel is used instead. Due to this difference, the GOCI AOD product from the algorithm using estimated surface reflectance from the  $1.6 \mu\text{m}$  channel can have errors associated with snow covered pixels.

Each individual AOD product was compared to AERONET according to certain matchup criteria to derive root mean square errors. The authors found that the retrieval errors have a Gaussian distribution and discarded the outliers using a 2-sigma standard deviation threshold. The Gaussian center difference and root mean square errors for each product were used to derive the bias corrections and weights for the merged AOD product, respectively. Comparisons of the merged AOD product to

AERONET AOD data show that the fused retrievals are more accurate than any given individual AOD product.

### **3.2.3. Merging GEO-LEO AOD Products**

#### **3.2.3.1. NOAA Method**

NOAA currently generates AOD products from a suite of satellite sensors on geostationary and polar-orbiting satellites. These include GOES-16 Advanced Baseline Imager (ABI), GOES-17 ABI, SNPP VIIRS, and NOAA-20 VIIRS. NOAA has developed the Enterprise Processing System (EPS) algorithm that retrieves AOD over both dark vegetated as well as bright surfaces; it is currently run on both VIIRS instruments and soon will be implemented for the ABIs. The outputs of the EPS algorithm include “high”, “medium”, and “low” quality AOD; the “high” and “medium” quality AODs (termed “top 2 qualities”) are recommended for air quality applications. The SNPP VIIRS and NOAA-20 VIIRS equator crossing times are different by ~50 minutes, and they can at times observe the same scene from different viewing geometry. Analysis of several years of AOD data from the two VIIRS sensors showed that they are consistent at a statistically significant level and can therefore be mathematically averaged without any adjustments to individual AODs.

When the ABI AOD data are available at the same time as VIIRS for a given scene, the AOD data must be weighted in the merging process. Weighted averaging with constant coefficients is adopted, namely arithmetic averaging is used among the GEO or LEO products, and the combination adopts the weights of 0.4 and 0.6 for the GEO and LEO AOD, respectively. These constant weight values are derived from the overall statistics of the validation of the GEO/LEO retrievals against the ground AERONET measurements. The GEO/LEO sensors include GOES-16 ABI, GOES-17 ABI, SNPP VIIRS, and NOAA-20 VIIRS. The spatial and temporal resolutions can be specified as inputs to generate the gridded GEO/LEO averaged AOD at 550 nm for the high, medium and low-quality data individually. Figure 3 shows the hourly (17-18 UTC) merged GEO/LEO high-quality AOD on 1 December 2020. A more sophisticated merging scheme, with weights based on surface characteristics and sensor scan angle, is being considered to improve the consistency of the GEO/LEO merged AOD product. The refresh rate and spatial resolution of the merged AOD product vary depending on the US National Weather Service (NWS) requirements. The merged AOD product is currently available on a 1-hour temporal scale for regional model applications and 3-hour temporal scale for global model applications. Spatial resolutions for the global model and regional model are  $0.25^\circ$  and  $0.03^\circ$  respectively. In addition to merged AOD, the output also includes the of number of pixels used for grid averaging, minimum and maximum AOD, and the standard deviation.

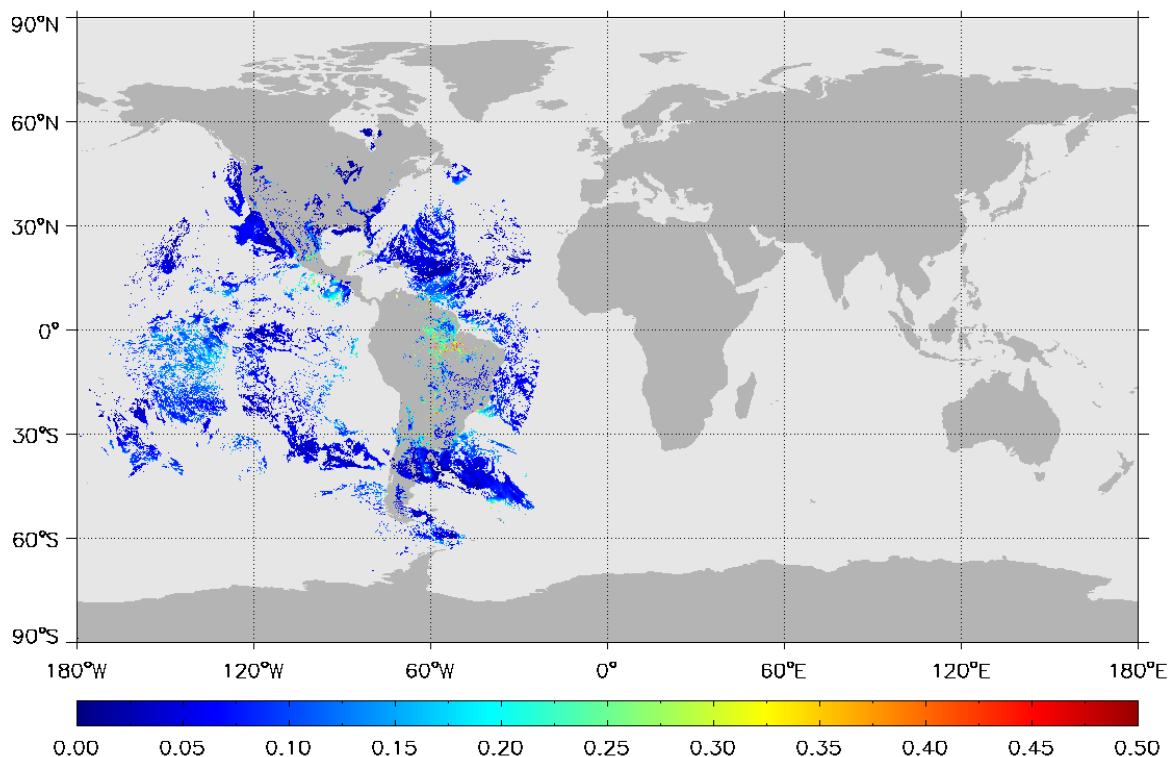


**Figure 3.** Merged high-quality NOAA GEO/LEO AOD at 550 nm for 17-18 UTC on 1 December 2020.

### 3.2.3.2. NASA Method

NASA applied its Dark Target (DT) AOD algorithm (see Section 2.3.1) to multiple geostationary and polar-orbiting satellite sensors globally to retrieve merged AOD that is quality controlled and composited for 30-minute temporal resolution and  $0.25^\circ \times 0.25^\circ$  spatial resolution. The DT algorithm currently runs on six sensors, including GOES-16 and -17 ABI, Himawari-8 AHI, Terra and Aqua MODIS, and SNPP VIIRS. Due to minor differences in available spectral channels and spatiotemporal resolutions, specific adjustments to the DT algorithm are made for each sensor (Levy et al., 2013; Gupta et al., 2018; Sawyer et al., 2020). In the core algorithm, assumptions on aerosols models, surface reflectance, and other decision-making remain unchanged.

The retrieved AODs from each sensor are first aggregated in a 30-minute interval and then averaged over a  $0.25^\circ \times 0.25^\circ$  latitude-longitude grid for the global region. In addition to the simple arithmetic mean, the median, standard deviation, minimum, maximum, and the number of pixels for each grid and time stamps are saved. The Level 2 AOD data are generated at 10 km nadir resolution from the ABIs, MODISs, and AHI, whereas VIIRS data have 6 km resolution. The native pixel size for each individual sensor grows from nadir to edge of the swath as a function of viewing geometry of the sensor. This changing pixel size, specifically at the edge, can create some empty grid cells in cases where pixel size becomes larger than the  $0.25^\circ$  grid size. To avoid empty grids in the merged product, grid filling is applied while considering viewing geometry following the method developed for MODIS sensors (Gupta et al., 2020). The AOD merging is done separately for data corresponding to retrievals with best quality flags and all quality flags.

The output file includes individual sensor AODs as well as merged AOD. In addition to AODs at 550 nm, future work will include AODs at blue and red channels for land and ocean and near-infrared

channel only over the ocean. Also, solar geometry, individual sensor geometry, aerosol-cloud fractions, and a land-ocean flag will be made available in each file. Merged AOD data are produced every 30 minutes for the entire globe. Figure 4 is an example of AOD from the individual sensors and the merged data sets for 15 March 2020. To date, limited variable outputs for one year have been processed, and the merged product has been tested for consistency and cross-validated against ground measurements by AERONET. More research on refining the merging algorithm is underway and providing AERONET AODs for each grid is under consideration.

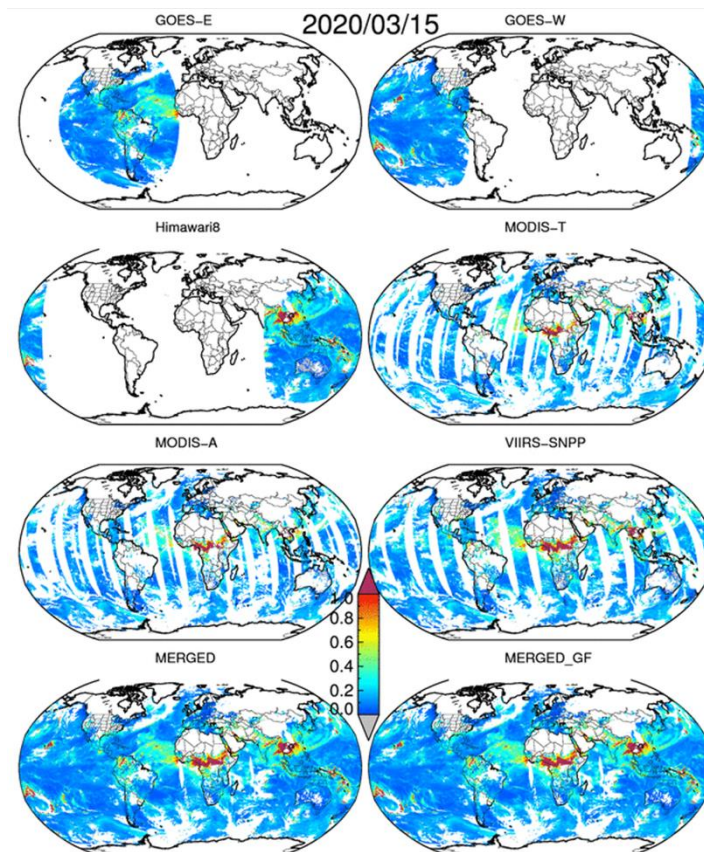


**Figure 4.** Merged NASA GEO/LEO AOD at 550 nm for 15 March 2020.

### 3.2.4. Merging AOD from Satellites and Simulations

The need to merge multiple available AOD products with models to derive  $PM_{2.5}$  was first framed by van Donkelaar et al. (2010) when they attempted to derive surface  $PM_{2.5}$  globally. The algorithm to combine AOD information from satellites and simulations was recently also summarized by Hammer et al. (2020). The first step is the common calibration of the separate AOD sources. Each source is translated onto a common grid. For a consistent definition of uncertainty, each AOD source is compared with AERONET AOD.

Satellite retrieved AOD and simulated AOD have different sources of errors, therefore their uncertainties need to be accounted for differently. For cloud-free and snow-free daytime scenes, one of

the main sources of uncertainty associated with satellite retrieved AOD is the surface treatment used in the retrieval. Therefore, one of the techniques used is to sample the daily satellite AOD retrievals to within  $0.25^\circ$  of each AERONET site and bin according to the Normalized Difference Vegetation Index (NDVI), which represents seasonally based changes in vegetation. Local calibrations are calculated at each AERONET site as the median slope and offset from reduced major axis linear regression of retrieved AOD with the AERONET values. The local calibrations are then expanded globally by calculating each pixel as the weighted average of all AERONET site-specific local calibrations, using inverse squared distance and the inverse of the Land Cover Similarity (LCS) defined by the MODIS land cover product. The LCS allows similar mixtures of land cover to be weighted more strongly.

The residual uncertainty between the calibrated and observed AOD at each AERONET site is then calculated as the normalized root mean square difference (NRMSD). Local NRMSD values are globally extended using inverse squared distance and LCS, following the approach used for the local calibration factors.

For the simulated AOD, to account for errors due to species-specific emissions and assumed aerosol microphysical properties, the relative uncertainty is calculated by applying the simulated fractional aerosol composition to each daily AERONET observation following van Donkelaar et al. (2013). The local calibration factors are calculated as the absolute error of each species at each station as a function of magnitude. The local calibration factors are then extended globally using inverse distance squared and the cross-correlation weighted average of each AERONET site to each global pixel. The residual uncertainty is calculated as the component-specific NRMSD, and is extended globally using the inverse squared distance and cross correlation.

The daily AOD values are used to calculate monthly mean values. Missing AOD and  $PM_{2.5}$  values within areas of more than 50% coverage are approximated using the interpolated ratio with the same data source during other years, or if necessary the interpolated ratio with simulated values during the same period. Monthly AOD values from all sources are combined using a weighted average, weighted by the product of the inverse residual AOD NRMSD, the inverse absolute percent difference between calibrated and uncalibrated AOD and the local data density.

### 3.3. *Aerosol Vertical Distribution*

The vertical distribution of aerosols is key to estimating surface  $PM_{2.5}$  from total-column AOD; it is also important in the retrieval of trace gases such as  $NO_2$  from satellites. If the aerosol profile is well resolved, then the aerosol amount confined to a well-mixed planetary boundary layer ( $AOD_{PBL}$ ) can be used to estimate surface  $PM_{2.5}$ . Although they cannot provide aerosol vertical distribution information with the same level of accuracy as lidar, passive remote sensing techniques can retrieve effective ALH with much more (and often nearly global) spatial coverage and higher temporal resolution. Indeed, as summarized in the literature (Xu et al., 2018), a growing number of techniques have been developed to retrieve ALH from space, including: (a) a limb/occultation method, which is best for characterizing the aerosols in the upper troposphere and stratosphere (such as from OMPS and SAGE), (b) a stereo photogrammetry method based on multi-angle observations (such as from MISR), (c) a UV and deep-blue method that either uses or does not use polarization (such as those applied to OMI and POLDER), (d) an infrared method, which is best for retrieving dust layer height over ocean (and to some degree, smoke layer height near the fire source region, (Lyapustin et al., 2020), and (e) oxygen absorption spectroscopy such as using the  $O_2$  A-band from LEO instruments including POLDER and MERIS (Dubuisson et al., 2009) and TROPOMI (Wu et al., 2008; Nanda et al., 2020), SCIAMACHY (Kokhanovsky and Rozanov 2010; Sanghavi et al., 2012), GOME/GOME-2 (Sanders et al., 2015), OCO-2 (Zeng et al., 2020), OMI (Chimot et al., 2017; Park et al., 2016), and ground-based observations (Zeng et al. 2018), as well using the  $O_2$ -A and -B bands from DSCOVR EPIC (Xu et al., 2017; Xu et al., 2019), and the  $O_2$ - $O_2$  ( $O_4$ )

absorption bands from GEMS (Park et al., 2016). The references here are not meant to be exhaustive; for details please see a review by (Xu et al., 2018).

ALH is a general term used here to describe the aerosol vertical distribution information retrieved from the passive sensing techniques. The meaning of ALH indeed depends on the measurement technique and algorithm used. Since aerosol distribution is sometimes continuous in the vertical dimension, though aerosol transported above the PBL often accumulates in relatively thin (<~1 km) layers of relative stability in the free troposphere (Kahn et al., 2007; Val Martin et al., 2010). As such, defining a layer of aerosol above the PBL can sometimes be subjective. Nevertheless, in the literature, several specific terminologies regarding ALH have been used, including the aerosol optical centroid height (AOCH), the aerosol stereo height, aerosol plume height, and aerosol effective height. AOCH refers to the altitude at which the aerosol extinction profile peaks (Xu et al., 2017). Aerosol stereo height is often referred as the aerosol plume height or the aerosol plume top, although its altitude corresponds to the layer of maximum spatial contrast in multi-angle imagery, and it can indeed be somewhere below the thinnest aerosol at the top of the plume. Retrieval of AOCH however does not have this requirement. The definition of aerosol effective height varies by different algorithm and depends on how the shape of the aerosol vertical profile is defined in the algorithm, but often it is defined as the altitude that provides the best fit to the satellite measurement that contain the aerosol layer height information.

To date, only TROPOMI provides ALH data operationally and globally, and to some degree, the MODIS MAIAC thermal algorithm retrieves smoke layer height at the fire source region; for sensors like MISR, the best-quality aerosol plume heights require running an interactive computer program, but this MISR Interactive eXplorer (MINX) technique has already been applied to tens of thousands of smoke, dust, and volcanic plumes. The recently launched GEMS instrument retrieves ALH using O<sub>2</sub>-O<sub>2</sub> absorption. The first comparison of TROPOMI ALH retrievals with those derived from CALIOP at the global scale reveals that the ALH from TROPOMI has a mean negative bias of 2.4 km over land and negative bias of 1 km over ocean (Nanda et al., 2020), and the bias becomes larger as surface reflectance increases. At the same time, several techniques have demonstrated that using the O<sub>2</sub>-B band or O<sub>4</sub> band to derive ALH over land is helpful to mitigate the negative impact of high surface reflectance often observed in the O<sub>2</sub>-A band over land ALH retrieval (Xu et al., 2017; Xu et al., 2019; Park et al., 2016).

Overall, techniques of passive ALH retrieval from space are at varying levels of maturity and further work is needed to improve the product readiness and accuracy and have enhanced treatment of O<sub>2</sub> absorption spectroscopy, the surface reflectance and aerosol optical properties, and the shape of aerosol profile in the retrieval algorithm. However, with existing production of ALH data from TROPOMI and planned production of ALH from GEMS, an era of routine ALH globally is emerging. Future missions such as 3MI on MetOp-SG, the Sentinel-4 and Sentinel-5 missions, and the MAIA, TEMPO, and PACE, will provide the measurements in the UV and O<sub>2</sub> (A, B, or O<sub>4</sub>, and other) absorption bands, some at multiple angles and/or with polarization. These future missions will enable the development of new ALH retrieval techniques and offer enhancements to existing techniques that can be applied globally and operationally in the near future.

In brief, an era of operational production of ALH data at high spatial resolution (<10 km) globally and high temporal resolution (hourly) over the Northern Hemisphere is emerging in the second decade of 21<sup>st</sup> century. AC-VC will work with the community by facilitating the cross-validation of different aerosol layer height products, the exchange of algorithm developments among different teams and groups, and potential development of new algorithms from multiple GEO sensors and their synergy with LEO sensors.

At high AOD, it might be difficult to obtain an accurate estimate of AOD from remote sensing, but with an adequate radiative transfer code, retrieving particle properties in smoke and volcanic plumes with AOD  $\geq 4$ . The practical upper limit on total-column AOD retrieval is about 7 at a given wavelength, as beyond that, it is no longer possible to see through the column to the surface. However, in these circumstances, it can still be possible to retrieve particle microphysical properties. Most satellite

retrieval algorithms make different assumptions about the surface for land and ocean, and this often leads to significantly different algorithms overall, including the choice of spectral bands, the approach for filtering radiances, cloud screening, etc. This inevitably leads to discontinuities, between land and water. Lower bounds on AOD and particle property retrievals depend in part on surface properties. Generally, dark, uniform surfaces allow for higher-confidence aerosol retrievals. As a practical matter, a lower AOD bound on AOD retrieval is around 0.02 under ideal conditions, and good-quality particle property retrievals, e.g., from MISR, require mid-visible AOD around 0.15 to 0.2. Over urban areas, where the surface tends to be complex and fairly bright, the effective lower bounds on aerosol retrieval are usually higher.

### *3.4. Synergistic Retrievals*

In the past decade, increasing efforts have been made to explore the combination of measurements from multiple sensors in order to obtain aerosol products with a better performance or to retrieve more aerosol parameters as compared to a retrieval using data from a single sensor. To date, most multi-sensor retrieval algorithms are still in the research and development stage, but the results have been promising. For an enhancement of PM estimation, the best available information on aerosol amount, type, and vertical distribution needs to be brought together. More research and development on synergetic satellite products is also needed to make a step in this direction.

#### **3.4.1. Retrieving a Suite of Aerosol Products from Multi-spectral Imager and Imaging Spectrometer**

The high spatial resolution of multi-spectral imagers is a key feature in aerosol observation: one of the most important benefits of a small footprint size is the high yield of observation with little or no contamination by clouds. High spatial resolution is also valuable when observing localized emissions, e.g. from fires or volcanic events. Imaging spectrometer products typically have significantly lower spatial resolution but offer additional and complementary spectral information. While imagers are strong in constraining AOD, many spectrometers additionally capture height information that can be extracted from the UV reflectance or from oxygen absorption signatures (e.g.,  $O_2-O_2$ ,  $O_2-A$ ,  $O_2-B$ ), and allow for distinguishing of mineral dust from other aerosol types using an absorption feature of mineral dust in the UV. High spatial resolution information on clouds and scene heterogeneity is used to enhance the aerosol retrieval from spectrometer data. For example, the synergies between the TEMPO spectrometer and the ABI on GOES-16 and between the GEMS spectrometer and AHI on Himawari-8 are being explored. The spectrometers on the atmospheric Sentinels (Sentinel-4, -5, and -5P/TROPOMI) benefit from using imager data for cloud masking and treatment of scene heterogeneity, but the full exploitation of the synergy is subject to future developments.

Multi-spectral multi-viewing imagers with polarimetric capabilities (such as 3MI) or without (such as MISR) offer valuable information on the aerosol amount and type but little information on the vertical aerosol distribution. This information should be exploited in synergy with the height information that can be extracted from the spectrometer measurements (e.g., UV,  $O_2-O_2$ ,  $O_2-A$ ,  $O_2-B$ ). A dedicated product offering 3MI and Sentinel-5 radiance data on a common spatial grid is being considered by EUMETSAT in order to facilitate the development of retrievals schemes exploiting this synergy.

#### **3.4.2. Multiple Views by Combining Multiple Sensors**

In some satellite constellations, multiple sensors view the same target at the same time from different directions. This is the case for the geostationary imagers of the GOES-R series and the

upcoming TEMPO spectrometer. Similarly, the future Geostationary Extended Observations (GeoXO) system will also comprise imagers and spectrometers that offer such multi-viewing observations. This capability will enable inferring the height of aerosol plumes and clouds based on parallax features, and a better characterization of surface reflectance and aerosol properties (Wang et al., 2014).

### 3.5. *The Retrieval Challenge*

Particulate pollution is governed by many parameters including the near-surface particle number density, the size distribution, and the chemical composition. The information contained in satellite observations is sufficient to retrieve only a subset of these parameters, even for the most powerful sensors or combination of sensors. Aerosol algorithms must deal solve an under-constrained problem. Also, the available aerosol information varies depending on the observation conditions (e.g., sun-satellite geometry, surface reflectance, cloud conditions, aerosol characteristics). Aerosol retrieval remains a challenge and is subject to continuous research and development. PM estimation taking aerosol products from satellites relies on these developments.

### 3.6. *Earth Radiance Data*

Aerosol retrieval algorithms use observed radiance data that are converted to reflectances to derive AOD and other aerosol properties. Space agencies that operate satellite sensors coordinate under Global Space-based Inter-Calibration System (GSICS) to develop procedures for sensor calibration in a consistent manner to achieve consistent accuracies in derived Level 2 products such as AOD. Sources of calibration errors (e.g., diffuser degradation) are identified and corrected using similar techniques so radiance data among different sensors are well calibrated and accurate even if different aerosol algorithms are used by various Level 2 product developers. The current generation of imagers such as MODIS, VIIRS, AHI, ABI, etc., will continue to make measurements for the next several decades. Therefore, assuring consistency in calibration of radiances used to generate multi-instrument and multi-decade aerosol products is important. For typical multispectral imagers/sensors, the key performance parameters that could have direct impact on radiometric calibration and AOD data are: relative spectral response (RSR), signal-to-noise ratio (SNR), nonlinearity, calibration accuracy (absolute and relative), calibration stability (short- and long-term), polarization responsivity, stray light rejection and crosstalk, and response versus scan-angle (for scanning radiometers). Working under the umbrella of the World Meteorological Organization (WMO) supported GSICS, space agencies ensure that calibration parameters are established pre-launch and monitored in orbit regularly to identify any calibration instability. These practices depend on vicarious calibration, onboard calibration, inter-satellite comparisons, and systematic ground-based or sub-orbital coincident measurements to keep track of calibration. When instrument calibration changes occur or artifacts are identified, product developers are expected to reprocess the data to account for those changes and deliver a consistent dataset to the users.

Establishing how calibration errors impact AOD is not straightforward because the algorithms are multi-spectral and there can be competing and compensating errors. Calibration errors can also influence the AOD product through the impact on the upstream cloud mask algorithm. Typically, when calibration changes are identified (usually via comparisons with ground truth, typically AERONET for AOD), the AOD product is regenerated with updated calibration and then the reprocessed AOD data are compared to ground truth again to demonstrate that due to calibration improvements, AOD are meeting the specified requirements in terms of accuracy/bias, precision, and root mean square error.

Users of AOD have been fortunate that there are two MODIS instruments and two VIIRS instruments currently operating. Because the algorithm to derive AOD from MODIS is the same for

Aqua and Terra, time series analysis of the two products on monthly time scales can shed light on calibration differences and drifts. In fact, Terra MODIS suffered an anomaly in 2003, rendering onboard calibration impossible, and the sensor's calibration drifted from that of Aqua MODIS. Sayer et al. (2015) discuss the Terra MODIS calibration adjustments to account for the drift and how reprocessed AOD with new calibration improved the product accuracy and brought the AOD data closer to that from Aqua MODIS. Lyapustin et al. (2014) developed technique to remove residual calibration trends from both Terra and Aqua MODIS and cross-calibrate the older and less stable MODIS Terra to MODIS Aqua making them, effectively, the same sensor. This calibration is applied in MODIS land discipline processing Collection 6 and higher and in MAIAC algorithm. Schutgens et al. (2020) mentions the "remarkable" stability and agreement between MAIAC Terra and Aqua AOD which is partly a consequence of the applied calibration enhancement. A similar analysis has recently been completed at NASA to remove residual trends and cross-calibrate the VIIRS SNPP and N20 to MODIS Aqua, which will allow to create a consistent MODIS-VIIRS AOD record and extend the MODIS long-term record into the future.

In the same way, NOAA currently has two VIIRS instruments in orbit on the SNPP and NOAA-20 satellites. Comparisons of AODs from the two VIIRS instruments for data acquired between 1 November 2018 and 1 February 2019 showed that NOAA-20 VIIRS AOD is biased higher than that of SNPP VIIRS by 0.017 over land and lower by -0.016 over ocean. These differences are attributed to calibration offset at all reflective solar bands (Table 3, Uprety et al., 2020; Cao et al., 2021). When each of its wavelength radiances in the NOAA SNPP VIIRS AOD algorithm was adjusted with offsets to match the NOAA-20 calibration, the differences in retrieved AODs were similar to those observed between SNPP and NOAA-20 VIIRS AODs derived with their respective operational (at launch) calibrations ([https://www.star.nesdis.noaa.gov/jpss/documents/AMM/N20/Aerosol\\_AOD\\_Validated.pdf](https://www.star.nesdis.noaa.gov/jpss/documents/AMM/N20/Aerosol_AOD_Validated.pdf)). This exercise demonstrated that both absolute calibration biases as well as changing calibration over time need to be monitored to ascertain the accuracy of retrieved AOD and its use in deriving surface PM<sub>2.5</sub>.

**Table 3.** VIIRS Reflective Solar Bands and calibration bias between NOAA-20 and SNPP VIIRS.

<b>Band (Wavelength)</b>	<b>Calibration Bias (NOAA-20/SNPP VIIRS)</b>
M1 (412 nm)	-3%
M2 (445 nm)	-1.7%
M3 (488 nm)	-2.6%
M4 (550 nm)	-3.2%
M5 (672 nm)	-5%
M7 (865 nm)	-3.8%
M8 (1240 nm)	-2.7%
M9 (1378 nm)	-1.2%
M10 (1610 nm)	-1.9%
M11 (2250 nm)	-2.2%

#### 4. Estimating Surface PM<sub>2.5</sub>

Given the large public health burden due to PM<sub>2.5</sub> exposure worldwide (Cohen et al., 2017), there is a pressing need for a surface PM<sub>2.5</sub> product at high spatial and temporal resolution to assess various adverse health outcomes linked to PM<sub>2.5</sub> pollution (Pope and Dockery, 2006). Maps of near-

surface PM concentrations with contiguous spatial coverage are needed for estimating exposure and for epidemiological studies. It has been reported that with the current limited number of PM measurement stations, it is not possible to infer reliable estimates for locations without monitoring by using simple spatial interpolation (Miller et al., 2007; Zeger et al., 2000). With global coverage, satellite remote sensing has been used to estimate surface  $PM_{2.5}$  to complement ground monitoring networks both spatially and temporally (Hoff and Christopher, 2009).

Most passive satellite sensors that provide an aerosol product report AOD as a measure for the total column aerosol amount. Deriving near-surface PM concentrations from AOD values is difficult. Challenges are related to uncertainties in the microphysical properties of the particles, their size distribution and vertical distribution, hygroscopic state, etc. Currently, there is a variety of approaches to constrain near-surface PM using satellite AOD data and a variety of auxiliary information, outlined in Sections 4.1 to 4.4. A review of strategies for using satellite-based products in modeling  $PM_{2.5}$  is provided by Sorek-Hamer et al. (2020). The present white paper aims at formulating a set of best practices for constraining near-surface PM using a combination of satellite aerosol observations, ground-based observations, and the information from atmospheric chemistry and transport models.

It is worth emphasizing that  $PM_{2.5}$  is not measured at 0% relative humidity (RH), but rather is operationally defined by the conditions of the instrument of laboratory used for the measurement. In the United States the RH is often defined as within 30%-40% following US EPA protocols, but some networks (e.g., Interagency Monitoring of Protected Visual Environment, IMPROVE) employ different protocols. European  $PM_{2.5}$  measurements are often at 45%-55% RH. Relationships derived between AOD and  $PM_{2.5}$  need to account for geographic variation in the definition of  $PM_{2.5}$  across networks and jurisdictions.

#### 4.1. Statistical Methods

The simplest form of using AOD to predict  $PM_{2.5}$  is to correlate them in a linear regression model with  $PM_{2.5}$  surface concentrations as the dependent variable and collocated satellite AOD in space and time as the independent variable (Christopher and Gupta, 2020; Wang and Christopher, 2003). After model fitting, a  $PM_{2.5}$  value can be predicted by a given AOD using this relationship. This relationship then can be used to estimate the spatiotemporal patterns of  $PM_{2.5}$  in grid cells with satellite AOD coverage where ground monitors of  $PM_{2.5}$  are not available. The validity of such simplistic relationships is limited, as they do not even capture basic features such as vertical distribution or hygroscopicity.

Therefore, multiple regression techniques have been developed, which include meteorological variables such as relative humidity, temperature, PBL height, wind speed, and wind direction, to predict  $PM_{2.5}$  (Gupta and Christopher, 2009; Liu et al., 2005). These meteorological variables are usually obtained from a numerical model that contains all the meteorological and other relevant parameters. While it is tempting to use any and all information to see if it improves the correlation coefficient, it is important to ensure that this is based on the physics of the problem and only include parameters that are most important for estimating  $PM_{2.5}$ . For example, columnar humidity is an important factor because of particle hygroscopic growth. Wind speed is important because the speed of the air mass over the  $PM_{2.5}$  location governs how the spatiotemporal collocations must be matched. Regardless, results indicate that the improvement in predictability of  $PM_{2.5}$  from AOD is region specific because meteorology, aerosol sources, and the ability of satellite sensors to provide accurate AOD retrievals for the region are specific to different regions (Chu et al, 2016).

The relationship between satellite AOD and surface  $PM_{2.5}$  concentration has strong spatiotemporal heterogeneities. Early studies often assumed linear and static linkages between  $PM_{2.5}$  and AOD as well as other ancillary variables, resulting in relatively low and sometimes unstable prediction accuracy. When estimated  $PM_{2.5}$  values are compared to observed  $PM_{2.5}$  values that were

not used in the training, the linear correlation coefficient ( $R^2$ ) is often lower than 0.6. Various more sophisticated and flexible statistical modeling techniques have been reported in the literature since then to account for the spatiotemporal variability of the  $PM_{2.5}$ -AOD relationship, including the generalized additive model (GAM) (Liu et al., 2009), geographically weighted regression model (GWR) (Bai et al., 2016; Hu et al., 2013; Ma et al., 2014; Song et al., 2014), linear mixed-effects model (LME) (Chudnovsky et al., 2012; Lee et al., 2011; Zheng et al., 2016), hierarchical models (Hu et al., 2014; Kloog et al., 2014; Liu et al., 2009), Bayesian down-scalers (Chang et al., 2013; Geng et al., 2018; Wang et al., 2018), and data fusion models that combine satellite retrievals and chemical transport model simulation results (Friberg et al., 2018). These efforts have greatly improved the prediction skill at regional to global scales with the cross validation (CV)  $R^2$  generally increased to 0.6-0.8. In recent years, machine learning algorithms, such as random forest (RF) (Hu et al., 2017; Mhawish et al., 2020; Vu et al., 2019; Wei et al., 2020), extreme gradient boosting (XGBoost) (Reid et al., 2015; Xiao et al., 2018; Just et al., 2020), and neural network (Park et al., 2020), ensemble-based machine learning (Di et al., 2019; Yazdi et al., 2020) among others have also been applied to  $PM_{2.5}$  prediction. Compared to advanced statistical models, machine learning algorithms have better ability to address the complex non-linear relationships between  $PM_{2.5}$  and AOD, and thus often have greater model accuracy (CV  $R^2$  is generally higher than 0.8).

The successful application of statistical models requires a sufficient training dataset generated from collocated satellite AOD and ground-based  $PM_{2.5}$  measurements in a study region (Liu, 2013). In many parts of the globe, either the ground observations are not available or the satellite AOD retrievals are not available due to persistent cloud cover, bright surfaces, etc. The lack of a sufficient training dataset in these locations restricts the use of statistical models for estimating surface  $PM_{2.5}$  from AOD

Advanced geostatistical regression models (GRMs) are emerging in which a set of aerosol products are used to “calibrate” the regression coefficients. For example, a GRM is foreseen to transform the aerosol properties retrieved from MAIA radiance and polarization imagery to  $PM$  concentrations from surface  $PM$  monitors. Sources of training data include  $PM_{2.5}$  and  $PM_{10}$  networks operated by environmental agencies in the MAIA target areas, the Chemical Speciation Network (CSN) and IMPROVE network (Solomon et al., 2014), the Surface PARTiculate mAtter Network (SPARTAN) (Snider et al., 2015), additional SPARTAN stations and a set of second generation Aerosol Mass and Optical Depth (AMODv2) speciated  $PM$  samplers (an upgrade of the instrument described in Wendt et al., 2019), and several aethalometers.

Aerosol predictors in the MAIA GRMs are not limited to AOD. Using AERONET inversion products, Sorek-Hamer et al. (2019) found that other optical components contribute to distinguishing between nitrate, elemental carbon, and dust. Supplementary geospatial data including population and roadway densities and meteorological information such as PBL height and wind speed from the Weather Research and Forecasting model coupled with Chemistry (WRF-Chem) will be used as ancillary predictors. A Bayesian framework with prescribed probabilistic distributions of the model coefficients will be used to integrate this information. Speciated  $PM$  maps would be generated at 1-km spatial resolution. To fill in spatial gaps (e.g., due to clouds) and to generate  $PM$  products on days when a particular target area is not observed by the satellite, a separate set of GRMs will use the surface  $PM$  monitors to correct biases in  $PM$  estimated by WRF-Chem. At locations with both satellite-based and WRF-Chem-based  $PM$  estimates, the results will be merged using an ensemble averaging approach (Murray et al., 2019). MAIA data processing and product archival and distribution will take place at the NASA Atmospheric Science Data Center (ASDC).

#### 4.2. Geophysical Scaling Methods

In the absence of routine ground-based PM<sub>2.5</sub> monitoring networks, the scaling method may be applied, as it does not require ground measurements for model development. The scaling method uses a chemical transport model (CTM) to simulate the association between AOD and PM<sub>2.5</sub>, and then calculates satellite-derived PM<sub>2.5</sub> using Equation 1:

$$\text{Satellite-derived PM}_{2.5} = \eta \times \text{Satellite AOD} \quad (1)$$

where  $\eta$  as introduced by van Donkelaar et al. (2010) is the ratio of the simulated PM<sub>2.5</sub> to simulated AOD (Liu et al, 2004).

The scaling method can provide PM<sub>2.5</sub> concentration estimates over regions with sparse or no routine air quality monitoring. However, without the calibration of ground measurements, the scaling model tends to have higher prediction errors in estimated PM<sub>2.5</sub> than that derived from statistical models.

Liu et al. (2004) applied Equation 2 to MISR data over the contiguous US, making joint use of the Goddard Earth Observing System chemistry (GEOS-Chem) and Georgia Tech/Goddard Global Ozone Chemistry Aerosol Radiation and Transport (GOCART) models. This method was extended by van Donkelaar et al. (2006, 2010) to use a combination of MISR and MODIS data, and has been further studied and refined in later publications to generate global maps of near-surface PM<sub>2.5</sub> concentrations and track multi-year trends (Boys et al., 2014; van Donkelaar et al., 2016a; van Donkelaar et al., 2021). Data from the Sea-viewing Wide Field-of-View Sensor (SeaWiFS) (Sayer et al., 2012) was later incorporated to provide a longer time series.

These satellite-based maps of PM<sub>2.5</sub> have been used in the Global Burden of Disease (GBD) and many other health studies. Dey et al. (2012) applied the CTM-based AOD-to-PM<sub>2.5</sub> scaling approach to a decade of MISR data to study PM<sub>2.5</sub> over the Indian subcontinent, and applied linear scaling to correct for a systematic underestimation of PM concentration relative to surface samplers. Philip et al. (2014) extended the scaling approach in conjunction with MODIS and MISR data to estimate the concentrations of chemical constituents of PM<sub>2.5</sub> (including sulfate, nitrate, ammonium, organic matter, black carbon, and dust) using PM<sub>2.5</sub> component concentrations from GEOS-Chem to generate species-specific values of  $\eta$ . Comparisons with surface measurements over North America showed high correlation coefficients and slopes near unity for sulfate, nitrate, and ammonium, and weaker yet positive correlations for the other constituents.

Numerical model simulations still have challenges in properly characterizing aerosol spatial, temporal, and vertical distributions, thereby leading to uncertainties in the estimation of  $\eta$ . Studies have shown that large uncertainties in estimated PM<sub>2.5</sub> can result from uncertainties in the modeled AOD-PM<sub>2.5</sub> relationship (Jin et al., 2019). Recognizing these issues of lower accuracy, more recently, statistical methods have been applied to calibrate the predictions from the geophysical scaling approach (van Donkelaar et al., 2016; Hammer et al., 2020; van Donkelaar et al., 2021) where the residuals of the scaling method derived PM<sub>2.5</sub> were applied to the GWR model to improve the estimates of PM<sub>2.5</sub>.

#### 4.3. Geophysical Scaling Method using Multiple Satellite AOD Products

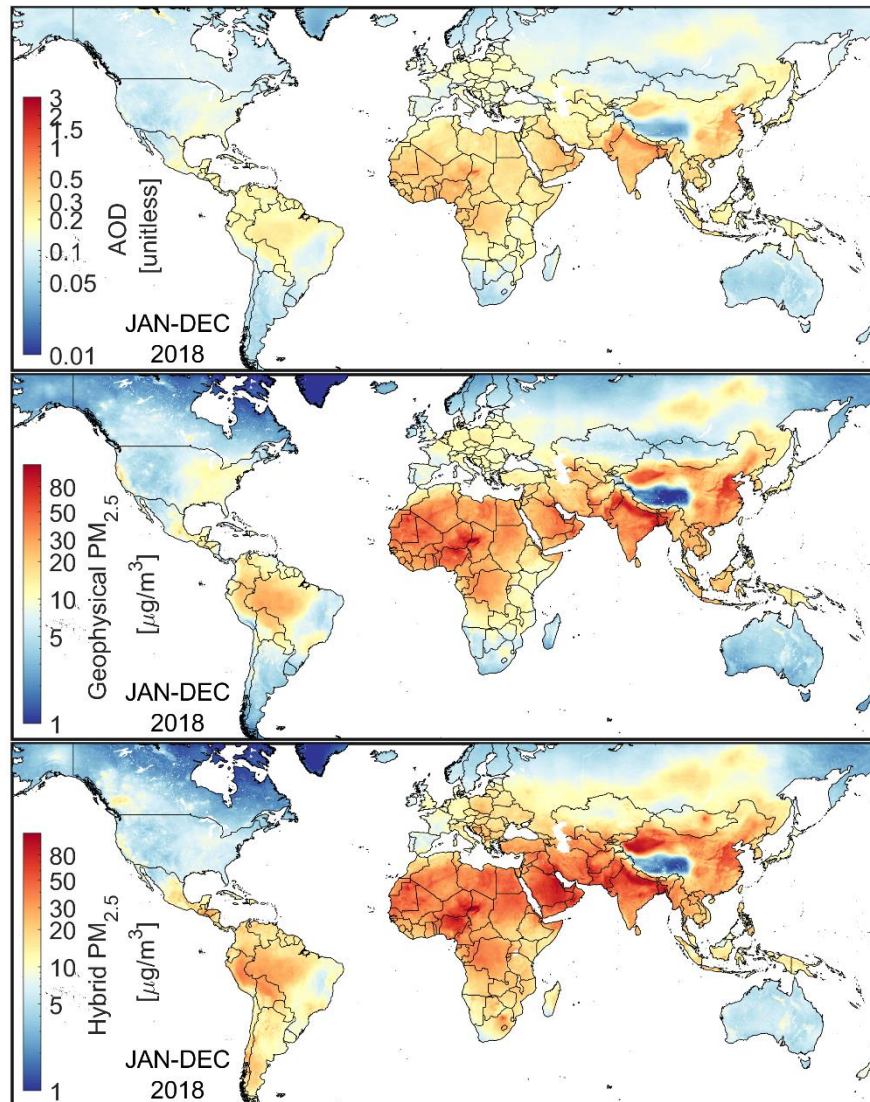
A large community relies upon annual estimates of PM<sub>2.5</sub> derived from a geophysical scaling framework. This approach, as recently described by van Donkelaar et al. (2021) begins with AOD from multiple datasets. As described in section 3.2, these AOD datasets are combined to a monthly mean on a 0.01° grid using consistent uncertainty definitions determined using AERONET-based comparisons. Satellite retrievals comprise most (>90%) of the population-weighted AOD due to their accuracy in regions with significant population density, while simulated AOD provides larger contributions in locations where seasonal snow-cover and cloud-cover inhibit satellite retrievals. Spatial information

from the 1 km MAIAC AOD retrieval is incorporated for the finest scale features at 0.01°, whereas several satellite sources are incorporated to represent AOD features at 0.1°.

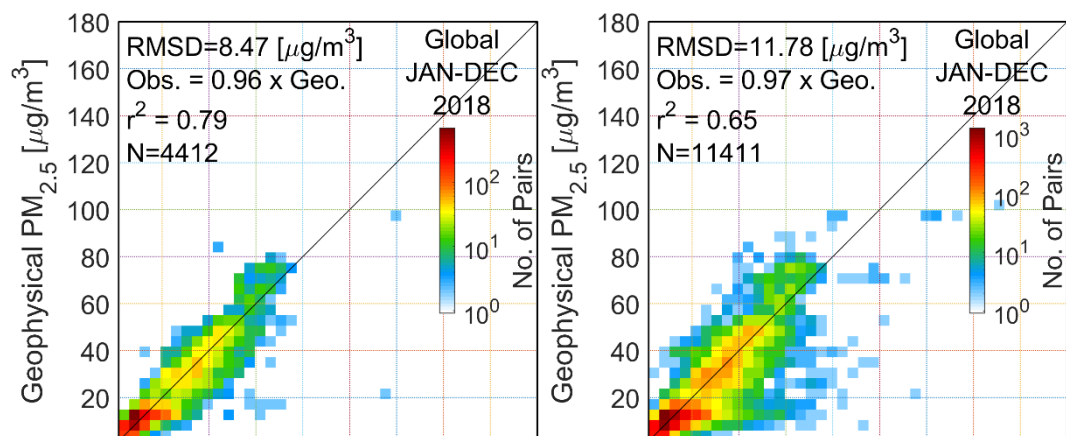
Geophysical surface PM<sub>2.5</sub> concentrations obtained from the combined AOD by applying the simulated PM<sub>2.5</sub> to AOD ratio ( $\eta$ ). This ratio implicitly and dynamically accounts for the effects of changing meteorology and composition via the chemical transport model simulation that is used for its calculation. Similarly, the impact of sampling frequency and overpass time can be accounted for within the definition of  $\eta$ .

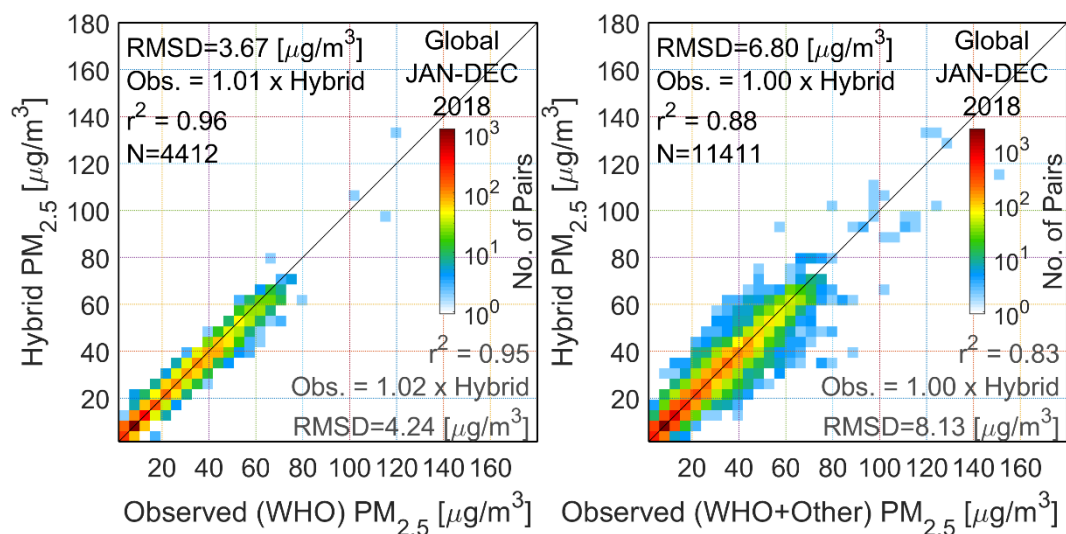
This geophysical framework is often augmented by statistical fusion with ground-based monitors to produce a hybrid PM<sub>2.5</sub> estimate. Geographically Weighted Regression (GWR; van Donkelaar et al. 2016; Hammer et al. 2020; van Donkelaar et al. 2021) and Bayesian Hierarchical Modeling (Shaddick et al. 2018) have both been used to predict and account for residual biases in the geophysical PM<sub>2.5</sub> estimates. The predictor variables used to produce these hybrid values are associated with uncertainties in the simulated relation of PM<sub>2.5</sub> to AOD, such as simulated aerosol types, sub-grid topographical variation and urban surfaces.

Figure 5 shows the combined AOD, geophysical PM<sub>2.5</sub>, and hybrid PM<sub>2.5</sub> estimates for 2018 from van Donkelaar et al. (2021). Elevated PM<sub>2.5</sub> concentrations are apparent over East Asia and South Asia reflecting a wide variety of sources as extensively discussed in the literature. Enhancements over North Africa and the Middle-East are driven by regional mineral dust sources. Lower concentrations over North America and western Europe reflect regional emission controls. Evaluation of these geophysical estimates versus ground-based measurements, shown in Figure 6, yields significant agreement with  $R^2=0.79$  and a slope of 0.96 versus the widely used annual mean PM<sub>2.5</sub> concentrations compiled by the World Health Organization. This agreement offers promise for satellite-derived PM<sub>2.5</sub> in regions with low monitor density, as the geophysical estimates are independent of ground monitor data. The statistically fused (hybrid) GWR estimates for 2018 further enhance this agreement, with 10-fold out-of-sample cross validated agreement of  $R^2=0.95$  and slope of 1.01. This high level of agreement demonstrates the added value in incorporating ground-based observations into the geophysical estimates. Expansion of the ground-based PM<sub>2.5</sub> dataset by including data from the literature and from unvalidated networks such as OpenAQ reinforces the greater uncertainty that exists in poorly monitored regions and the need for additional ground-based monitoring.



**Figure 5.** Annual mean combined AOD, geophysical and hybrid PM<sub>2.5</sub> for 2018 from van Donkelaar et al. (2021).





**Figure 6:** Comparison of geophysical and hybrid  $PM_{2.5}$  with ground-based observations in the World Health Organization (WHO) database, and additionally other available ground-based sites. Grey text for the hybrid plots corresponds to cross-validated comparisons.

#### 4.4. Statistical Methods with Dynamic Updating of Regression Parameters

Statistical methods can be significantly enhanced by updating the parameters of the regression model dynamically in a daily or hourly manner using surface  $PM_{2.5}$  measurements and satellite AOD. Approaches to derive surface  $PM_{2.5}$  can be different based on the application, and therefore the uncertainties of the derived  $PM_{2.5}$  may also be drastically different. The question is about the tolerance and the requirement of the specific application. While benchmarks can be laid out for the level of certainty with which surface  $PM_{2.5}$  should be derived, they cannot be the same for human health/mortality estimates done on annual mean basis compared to hourly and daily estimates of surface  $PM_{2.5}$  for issuing pollution alerts and warning. These disparities also bring forth the differences in concentration ranges and the algorithm approach to estimate surface  $PM_{2.5}$  with same level of certainty across all concentration ranges. In near real-time, during a pollution event related to dense smog in China, a dust storm in Africa, or smoke from forest fires, hourly  $PM_{2.5}$  concentrations can reach up to  $1000 \mu\text{g}/\text{m}^3$  whereas when annual means are computed, the concentrations are a hundred times smaller. Given the large dynamic range of concentrations, care must be taken in placing demands on an algorithm or method that scales AOD to surface  $PM_{2.5}$  and expected uncertainty. NOAA has been deriving surface  $PM_{2.5}$  from satellite AOD (MODIS) over the continental United States (CONUS) using a climatological  $PM_{2.5}$ -AOD regression relation based on the geophysical scaling approach. However, because the  $PM_{2.5}$ -AOD relationship can change over time, this method can have large errors when the relationship deviates from the climatological scaling factors.

NOAA, NASA, and US EPA have partnered to develop a near real-time surface  $PM_{2.5}$  product using NOAA's Advanced Baseline Imager (ABI) AOD product for dissemination to users via US EPA's AirNow website (<https://www.airnow.gov/>). This effort is based on converting ABI AODs to surface  $PM_{2.5}$  using a GWR algorithm (Zhang and Kondragunta, 2021). However, the parameters of the regression model are derived dynamically in a daily or hourly manner using surface  $PM_{2.5}$  measurements from regulatory monitors and AOD from ABI on the GOES-16 or GOES-17 satellite instead of the climatological  $PM_{2.5}$ -AOD relationship. On these shorter timescales, the algorithm performs much better than using simple climatological relationships derived using scaling methods. The estimated daily  $PM_{2.5}$  from VIIRS AOD has a cross validation CV  $R^2$  of 0.59 with surface measured  $PM_{2.5}$ , bias of

0.09  $\mu\text{g}/\text{m}^3$  and root mean square error (RMSE) of 5.66  $\mu\text{g}/\text{m}^3$ . The estimated hourly  $\text{PM}_{2.5}$  from ABI AOD has a CV  $R^2$  of 0.44, bias of 0.04  $\mu\text{g}/\text{m}^3$ , and RMSE of 4.53  $\mu\text{g}/\text{m}^3$  (Figure 7). The algorithm will run in near real-time at NOAA to provide  $\text{PM}_{2.5}$  estimates over the CONUS to the air quality community. It is anticipated that the data will be available within two hours of data capture.

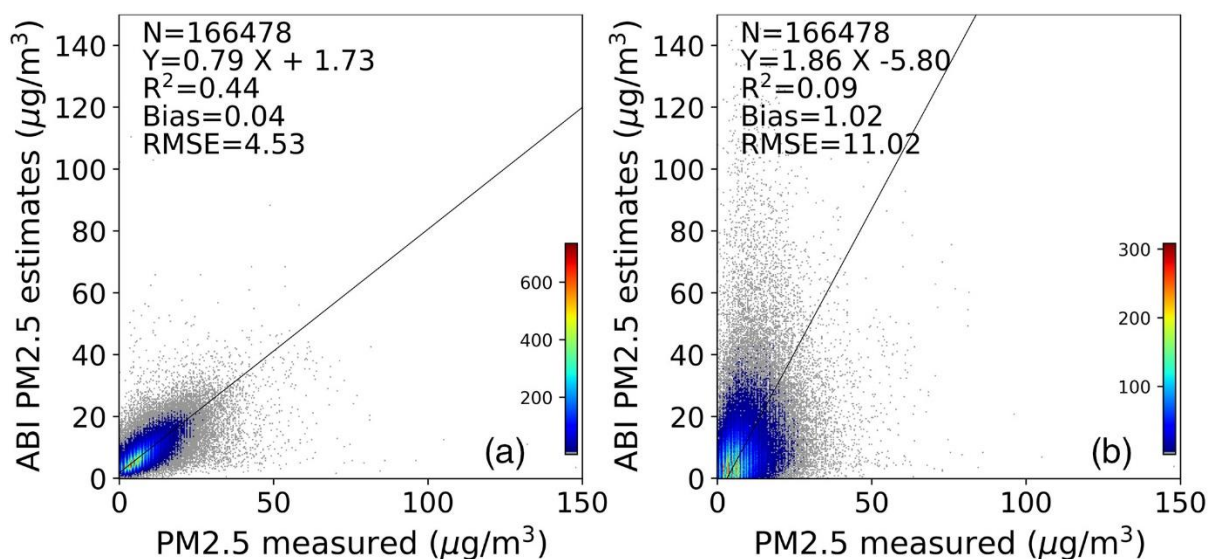


**Figure 7.** Hourly  $\text{PM}_{2.5}$  estimates: (a) from ABI AOD using GWR algorithm; (b) from ABI AOD using the climatological relations based on Geophysical approach. ABI, Advanced Baseline Imager; AOD, aerosol optical depth; GWR, geographically weighted regression. From Zhang and Kondragunta (2021).

With sufficient training data, machine learning (ML) techniques – such as those mentioned in Section 4.1 – can be used to improve upon the simulated AOD- $\text{PM}_{2.5}$  relationships used to estimate  $\text{PM}_{2.5}$  at higher temporal frequency than the annual mean (e.g., Carmona et al., 2020; Gupta et al., 2021). Using NASA’s Modern-Era Retrospective Analysis for Research and Application, version 2 (MERRA-2; Gelaro et al., 2017) combined meteorology and aerosol reanalysis product, in combination with surface measurements of  $\text{PM}_{2.5}$ , Carmona et al. (2020) and Gupta et al. (2021) developed ML models to estimate  $\text{PM}_{2.5}$  in regions of the world which can have relatively high  $\text{PM}_{2.5}$  concentrations (an urban area in Northeastern Mexico and Thailand, respectively). MERRA-2 is a coupled chemistry-meteorology model (CCMM) with both meteorology and aerosol data assimilation and outputs a global gridded product available at a horizontal resolution of  $0.5^\circ \times 0.625^\circ$ . As shown in Figure 8 (Gupta et al. 2021), MERRA-2 has the aerosol components to calculate  $\text{PM}_{2.5}$  but is expected to have representative errors when comparing the grid-box average to point source measurements (Figure 8, left). The ML techniques can overcome these errors, drastically improving the predictive capability when using simulated aerosol output (Figure 8, right), and can be used not only in retrospective studies but also for bias correcting  $\text{PM}_{2.5}$  forecasts.

These ML and statistical techniques can improve regional estimates of PM and add value to existing global datasets, especially where global models face obvious challenges.

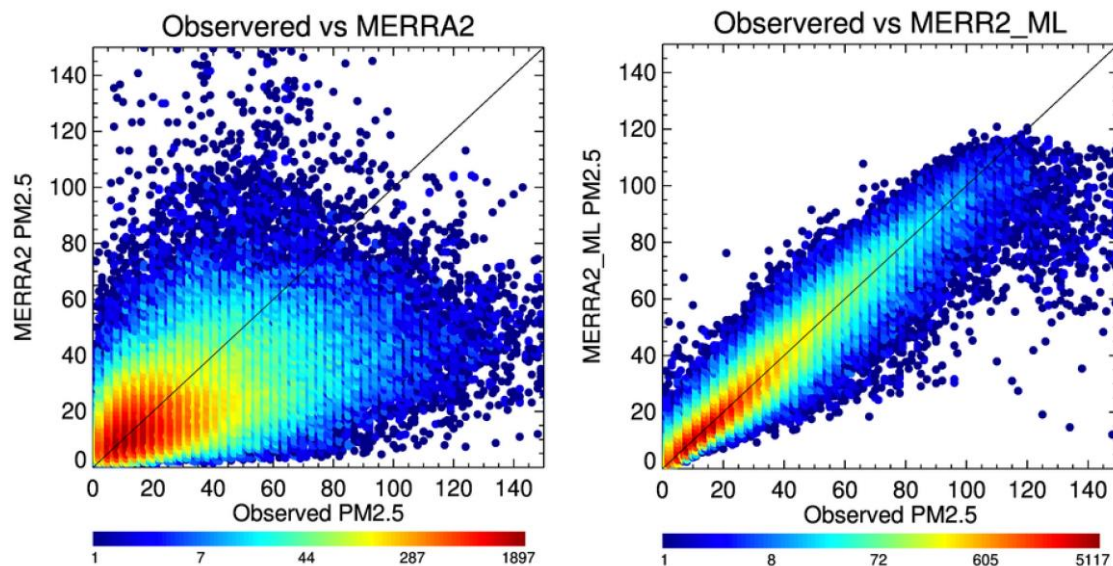


**Figure 8.** Comparison between hourly  $PM_{2.5}$  observations (x-axis) to model-estimated concentrations (y-axis) for Thailand in 2018, with MERRA-2 reanalysis derived surface  $PM_{2.5}$  (left) and a machine learning estimated  $PM_{2.5}$  using MERRA-2 AOD, aerosol and meteorology fields as input parameters (right). From Gupta et al. (2021).

#### 4.5. Assimilation of Aerosol Products

Atmospheric composition (AC) models describe sources and sinks of atmospheric components, related chemical processes and transport. AC models with a focus on aerosol capture primary sources, secondary particle formation, hygroscopic growth and many other driving processes. Data Assimilation (DA) can be used to combine heterogeneous sets of satellite and ground-based aerosol observations with model information in an optimal way. DA systems are used to initialize forecast simulations of  $PM_{2.5}$  with various lead times and to generate reanalyses which can provide consistent long time series of climate data record. Such methods benefit from 1) a more realistic representation of key physical and chemical processes influencing  $PM_{2.5}$ , which ensures better consistency between  $PM_{2.5}$  estimate and the other atmospheric parameters, and 2) the potential of Earth observations to reduce the uncertainties in the initial conditions used to forecast aerosols. Though costly to implement and sometimes having spatial resolutions that are coarser than observations, DA systems account for all sources of uncertainties (e.g. emissions) and can provide a more comprehensive error budget for  $PM_{2.5}$  compared to empirical methods.

There are multiple operational systems that incorporate aerosol data assimilation. The Copernicus Atmospheric Monitoring Service (CAMS) relies on the ECMWF/IFS (ECMWF Integrated Forecast System) model and assimilates MODIS and Polar Multi-sensor Aerosol properties (PMAp) AOD to provide the best initial conditions for global forecast of aerosol mixing ratios and PM variables (Morcrette et al., 2009; Remy et al., 2019). While the NASA and Naval Research Lab aerosol forecast systems utilize AOD assimilation for their global aerosol forecast systems (Randles et al., 2017; Zhang et al., 2014), the NOAA National Weather Service (NWS) currently relies on the Community Multiscale Air Quality (CMAQ) model without data assimilation to inform their hourly  $PM_{2.5}$  forecasts for the US; AOD assimilation to improve CMAQ predictions is under testing at NOAA (Tang et al., 2017; Kumar et al., 2019).

Aerosol DA systems can be evaluated in multiple ways, which include checking that the uncertainties in the analyzed fields are lower than those of the model background (Saide et al., 2013), comparison against independent satellite or ground-based observations of the assimilated variable or a different variable such as aerosol absorption or PM (Buchard et al., 2017; Saide et al., 2020) and looking at variables resulting from processes involving interactions with aerosols such as downward solar radiation, cloud properties or meteorological surface parameters (Saide et al., 2015; Randles et al., 2017).

The source of uncertainties in DA systems concern both the AC model and the satellite retrievals. Uncertainties in aerosol models include uncertainties in the forcing data sets, particularly the large range of anthropogenic, biogenic, and biomass burning emission sources, uncertainties in the aerosol optical properties and their spatiotemporal variability, inaccuracies in the representation of the complex emission (e.g., at times satellite observations are not timely, especially smoke from fires which cannot be currently measured at night), deposition and aging processes which are strongly coupled with meteorology and chemistry (Ryder et al., 2019), the characterization of the variability of secondary organic aerosol optical properties (Tsigaridis et al., 2014), the representation of dust absorbing properties (Balkanski et al., 2021), inaccuracies in the observation operator used in the DA system (Liu et al., 2011, Tang et al., 2017, Cheng et al., 2019), discrepancies between satellite retrieval and its model equivalent due to use of distinct/limited aerosol models, and radiative transfer model assumptions. In addition, the impact of DA can diminish after 1-2 days. This is in part due to replacement of air masses but also because of emissions biases, such as persistence of fires releasing emissions at the same rate in the forecast period that dominate over the forecasting window (Ye et al., 2021). Satellite retrieval uncertainties include cloud contamination, radiometric calibration issues, the instrument information content (which varies with geometry configuration and is not always sufficient to properly separate the aerosol and the surface reflectance signal), the simplified assumptions used in the forward radiative transfer model, the representation of the surface anisotropy particularly over bright surfaces, and the low number of aerosol models which may fail to properly represent the diversity of aerosol physicochemical properties at global scale (Garrigues et al., 2022). A critical challenge in predicting  $PM_{2.5}$  from an aerosol model and DA is related to the speciation of aerosols and a lack of vertical profile information from the imagers. Total AOD does not provide constraints on the model aerosol species. The application of the increments is generally weighted by a priori ratios between species mixing ratio provided by the background error covariance matrix.

The role of DA in enhancing  $PM_{2.5}$  prediction is envisioned to grow as advancements in satellite sensors and products occur. Specifically, an ability to separate AOD into fine mode and coarse mode, information on absorbing AOD, spectral AOD, Angstrom Exponent (AE) over land and ocean, Single Scattering Albedo (SSA), thermal infrared observations for dust, aerosol vertical distribution from lidar backscatter measurements should help to distinguish between aerosol species and to estimate their optical properties more accurately. At the outset, some of this information from satellites may be qualitative but opportunities exist to exploit the data and iterate between product development/enhancement and usage in the models. Additionally, assimilating clear-sky satellite radiance measurements is emerging as an alternative approach to assimilating aerosol products from satellites. Schemes that assimilate infrared radiance data have been applied successfully in operational weather forecast services. Following this strategy also in the visible was until recently impossible because of the heavy computational burden of radiative transfer computation including multiple scattering. The evolution of computing power has opened this path to be explored.

Assimilating clear-sky satellite radiance could facilitate the synergetic use of observations from distinct satellites and should ensure better consistency with the modelled aerosol optical properties which is a great source of uncertainty in AOD retrievals (Benedetti et al., 2018). It should also improve the use of multi-satellite observations over non-optimal surfaces such as cloudy regions, bright land

surfaces, and glint regions over the ocean. However, further development efforts are needed to design appropriate observation operators in the UV-VIS spectral domain and pre-processing steps such as data quality check and cloud screening.

Failure of aerosol DA systems to achieve consistency between AOD and surface  $PM_{2.5}$  performance can be due to many reasons, including misrepresentation of vertical distribution of aerosols, meteorological variables important for the AOD computation (e.g., relative humidity), speciation of aerosols, and optical properties calculations. Due to the large list of factors potentially explaining inconsistencies, field campaigns, in conjunction with long-term ground-based measurements can be very useful to understand the issues as they provide a large array of observations to disentangle the different factors, with some of these observations not being available from standard observational sites. An example study is reported in Saide et al. (2020), where aircraft observations were used to show that issues in optical properties computations were mostly responsible for worsening performance in  $PM_{2.5}$  predictions during a Chinese haze event when assimilating AOD and provided ways to address them.

The quality of aerosol information obtained by data assimilation suffers from inconsistencies in the representation of aerosols and assumptions made in satellite retrievals and in the atmospheric model system. Inconsistencies in aerosol parameters tend to be hard to avoid, since aerosol retrieval schemes typically employ a discrete set of aerosol classes while atmospheric models work in a continuous parameter space. ALH products from satellites provide an effective scattering height that is not uniquely linked to the vertical profiles of particle number densities and other particle properties. The cloud state in the model can deviate from the true cloud state that influences the satellite observation. Resulting misinterpretations are hard to eliminate by cloud masking, also since the distinction between aerosol and clouds is to some degree arbitrary. Research and development are needed to identify way to mitigate these inconsistencies.

The use of satellite products in DA depends critically on the completeness and quality of the product uncertainty. Observational error (diagnostic and prognostic) information should be standardized between various satellite products and their use in DA system; observation errors should be prognostic and derived from proper optimal interpolation approaches (Sayer et al., 2020). Information on correlation errors between products along with spatial and temporal correlations are frequently missing. The ongoing work within the AEROSAT/AEROCOM community can be leveraged. Investments need to be made to observe on the ground aerosol optical properties spatially and temporally with good geographic coverage to represent diverse aerosol sources. Without correlative ground observations, validation of aerosol properties other than AOD and their assimilation into models will become challenging. Many satellite products that capture aerosol parameters fall short on providing such estimates. Formal uncertainty estimation is difficult for algorithms in which discrete aerosol models or even different retrieval strategies are used and selected depending on scene parameters. The uncertainty of prior information used may not be available. The reporting of the a posteriori uncertainty including co-variances is usually missing, especially for parameters with very different character (e.g. amount, layer altitude, and particle size).

Enhanced ground-based independent observation are needed to evaluate model forecasts. The validation of satellite AOD is extensive because a network of ground observations via AERONET exists. As additional aerosol parameters (e.g., ALH) are considered in DA, reference networks of lidars and ceilometers need to be exploited. Measurements should be used for closure studies which evaluate uncertainties in each of these components of the aerosol DA system. Ideally, this would include sustained, comprehensive measurements of surface  $PM_{2.5}$ , aerosol speciation, aerosol size distributions along with profiles of aerosol extinction, backscatter, and mixed layer heights (e.g., ceilometers, MPLNet, HSRL). These measurements should be collocated ground based remote sensing of aerosol optical properties from both visible (AERONET) and UV (Pandora) instruments so that multi-spectral

aerosol retrievals can be validated. The EPA Photochemical Assessment Monitoring Stations (PAMS) Enhanced Monitoring Plans ([https://www.epa.gov/sites/production/files/2019-11/documents/pams\\_monitoring\\_network\\_and\\_emp\\_plan\\_guidance.pdf](https://www.epa.gov/sites/production/files/2019-11/documents/pams_monitoring_network_and_emp_plan_guidance.pdf)) and NCore Multipollutant Monitoring Network (<https://www3.epa.gov/ttnamti1/ncore.html>) could provide many of these capabilities for long-term validation of satellite aerosol retrievals and assessment of the fidelity of assimilated PM<sub>2.5</sub> analyses. These long-term measurements would allow robust statistical comparisons between surface PM<sub>2.5</sub> and satellite AOD retrievals to quantify the uncertainty of the satellite based PM<sub>2.5</sub> estimates. These long-term ground-based measurements should be complemented with airborne profiling of aerosol speciation, size distributions, and extinction for rigorous testing of the assumptions that go into the aerosol retrievals as well as the fidelity of the forecast models used in the aerosol assimilation system.

## 5. Validation of Aerosol Products and Model Skill

The link between satellite remote sensing data with local near-surface PM is the central problem discussed in this white paper. Related scientific studies and development efforts would benefit from co-located measurements made with ground-based aerosol remote sensing and in situ PM sensors. Ideally, such measurements would be combined with additional active instruments to help constrain the scenario including, in particular, the aerosol vertical distribution but also many other scene characteristics. This type of comprehensive set of instrumentation is likely possible only at a few supersites during a limited campaign period. The combination of fully automated and low-cost sensors might be possible for many stations for an extended period of time.

The next phase for the CEOS community is develop use cases to demonstrate how estimated PM<sub>2.5</sub> information is aiding various decision support systems such as the provision of air quality alerts, diagnosing impact of smoke on human health, air quality monitoring in areas with sparse ground monitoring, designing new regulations, changes to prescribed burning to limit pollution in downwind regions, etc. These use cases will provide insights into the application capabilities and limitations for specific decision support systems and capacity building.

## References

- Adams, K., D.S. Greenbaum, R. Shaikh, A.M. van Erp, and A.G. Russell (2015), Particulate matter components, sources, and health: Systematic approaches to testing effects. *J. Air Waste Manag. Assoc.* 65, 544-558.
- Anderson, T. L., Masonis, S. J., Covert, D. S., Ahlquist, N. C., Howell, S. G., Clarke, A. D., and McNaughton, C. S. (2003), Variability of aerosol optical properties derived from in situ aircraft measurements during ACE-Asia, *J. Geophys. Res.*, 108, 8647, doi:10.1029/2002JD003247, D23.
- Bai, Y., L. Wu, K. Qin, Y. Zhang, Y. Shen, and Y. Zhou (2016), A Geographically and Temporally Weighted Regression Model for Ground-Level PM<sub>2.5</sub> Estimation from Satellite-Derived 500 m Resolution AOD, *Remote Sensing*, 8(3), 262.
- Barkjohn, K.K., Gantt, B., Clements, A.L. (2021), Development and application of a United States-wide correction for PM<sub>2.5</sub> data collected with the PurpleAir sensor, *Atmos. Meas. Tech.*, 14, 4617–4637, <https://doi.org/10.5194/amt-14-4617-2021>.
- Barreto, Á., et al., (2016), The new sun-sky-lunar Cimel CE318-T multiband photometer – a comprehensive performance evaluation, *Atmos. Meas. Tech.*, 9, 631-654.
- Bell, M.L., F. Dominici, K. Ebisu, S.L. Zeger, and J.M. Samet (2007), Spatial and temporal variation in PM<sub>2.5</sub> chemical composition in the United States for health effects studies. *Environ. Health Perspect.* 115, 989–995.
- Benedetti, A., Reid, J. S., Knippertz, P., Marsham, J. H., Di Giuseppe, F., Rémy, S., Basart, S., Boucher, O., Brooks, I. M., Menut, L., Mona, L., Laj, P., Pappalardo, G., Wiedensohler, A., Baklanov, A., Brooks, M., Colarco, P. R., Cuevas, E., da Silva, A., Escribano, J., Flemming, J., Huneeus, N., Jorba, O., Kazadzis, S., Kinne, S., Popp, T., Quinn, P. K., Sekiyama, T. T., Tanaka, T., and Terradellas, E. (2018), Status and future of numerical atmospheric aerosol prediction with a focus on data requirements, *Atmos. Chem. Phys.*, 18, 10615–10643, <https://doi.org/10.5194/acp-18-10615-2018>.
- Bernard, E.; Moulin, C.; Ramon, D.; Jolivet, D.; Riedi, J.; Nicolas, J.-M. (2011), Description and validation of an AOT product over land at the 0.6  $\mu$ m channel of the SEVIRI sensor onboard MSG. *Atmos. Meas. Tech.*, 4, 2543–2565.
- Bessho, K., Date, M. Hayashi, A. Ikeda, T. Imai, H. Inoue, Y. Kumagai, T. Miyakawa, H. Murata, T. Ohno, A. Okuyama, R. Oyama, Y. Sasaki, Y. Shimazu, K. Shimoji, Y. Sumida, M. Suzuki, H. Taniguchi, H. Tsuchiyama, D. Uesawa, H. Yokota, and R. Yoshida, (2016), An introduction to Himawari-8/9 – Japan’s new-generation geostationary meteorological satellites, *J. Meteor. Soc. Japan*, 94, 151–183, DOI:10.2151/jmsj.2016-009.
- Buchard, V., Randles, C. A., da Silva, A. M., Darmenov, A., Colarco, P. R., Govindaraju, R., Ferrare, R., Hair, J., Beyersdorf, A. J., Ziemba, L. D., and Yu, H. (2017), The MERRA-2 Aerosol Reanalysis, 1980 Onward. Part II: Evaluation and Case Studies, *Journal of Climate*, 30, 6851-6872, 10.1175/jcli-d-16-0613.1.

Cao, C., B. Zhang, X. Shao, W. Wang, S. Uprety, T. Choi, S. Blonski, Y. Gu, Y. Bai, L. Lin and S. Kalluri (2021). "Mission-Long Recalibrated Science Quality Suomi NPP VIIRS Radiometric Dataset Using Advanced Algorithms for Time Series Studies." *Remote Sensing* 13(6): 1075., doi:10.3390/rs13061075

Castillo, M. D., Kinney, P. L., Southerland, V., Arno, C. A., Crawford, K., van Donkelaar, A., et al. (2021). Estimating intra-urban inequities in PM<sub>2.5</sub>-attributable health impacts: A case study for Washington, DC. *GeoHealth*, 5, e2021GH000431. <https://doi.org/10.1029/2021GH000431>  
Chang, H. H., X. Hu, and Y. Liu (2013), Calibrating MODIS aerosol optical depth for predicting daily PM<sub>2.5</sub> concentrations via statistical downscaling, *J Expos Sci Environ Epidemiol*, 24(4), 398-404, doi:10.1038/jes.2013.90.

Chauhan, P., N. Sanwlani and R.R. Navalgund (2009), Aerosol optical depth variability in the north-eastern Arabian Sea during winter monsoon: a study using in-situ and satellite measurements. *Indian J. Mar. Sci.*, 38(4), 390-396, 2009.

Cheng, X., Liu, Y., Xu, X., You, W., Zang, Z., Gao, L., Chen, Y., Su, D., and Yan, P. (2019), Lidar data assimilation method based on CRTM and WRF-Chem models and its application in PM<sub>2.5</sub> forecasts in Beijing, *Science of The Total Environment*, 682, 541-552, <https://doi.org/10.1016/j.scitotenv.2019.05.186>.

Chimot, J., Veefkind, J. P., Vlemmix, T., de Haan, J. F., Amiridis, V., Proestakis, E., Marinou, E., and Levelt, P. F. (2017), An exploratory study on the aerosol height retrieval from OMI measurements of the 477 nm O<sub>2</sub> – O<sub>2</sub> spectral band using a neural network approach, *Atmos. Meas. Tech.*, 10, 783–809, <https://doi.org/10.5194/amt-10-783-2017>.

Choi, M., Kim, J., Lee, J., Kim, M., Je Park, Y., Jeong, U., Kim, W., Holben, B., Eck, T. F., Lim, J. H., and Song, C. K. (2016), GOCI Yonsei Aerosol Retrieval (YAER) algorithm and validation during DRAGON-NE Asia 2012 campaign, *Atmos. Meas. Tech.*, 9, 1377-1398, doi:10.5194/amt-9-1377-2016.

Choi, M.J., Jhoon Kim, Jaehwa Lee, Mijin Kim, Young-Je Park, Brent Holben, Thomas F. Eck, Zhengqiang Li, Chul H. Song (2018), GOCI Yonsei aerosol retrieval version 2 aerosol products: improved algorithm description and error analysis with uncertainty estimation from 5-year validation over East Asia, *Atmospheric Measurement Technique*, 11, 385-408 doi:10.5194/amt-11-385-2018.

Choi, M., H. Lim, J. Kim, S. Lee, T. F. Eck, B. N. Holben, M. J. Garay, E. J. Hyer, P. E. Saide, and H. Liu (2019), Validation, comparison, and integration of GOCI, AHI, MODIS, MISR, and VIIRS aerosol optical depth over East Asia during the 2016 KORUS-AQ campaign, *Atmos. Meas. Tech.*, 12, 1–23, doi:10.5194/amt-12-1-2019.

Christopher, S., and P. Gupta (2020), Global Distribution of Column Satellite Aerosol Optical Depth to Surface PM<sub>2.5</sub> Relationships, *Remote Sensing*, 12(12), 1985.

Chu, Y., Liu, Y., Li, X., Liu, Z., Lu, H., Lu, Y., Mao, Z., Chen, X., Li, N., Ren, M., Liu, F., Tian, L., Zhu, Z., Xiang, H. (2016), A review on predicting ground PM<sub>2.5</sub> concentration using satellite aerosol optical depth. *Atmosphere (Basel)*. 7, 129. <https://doi.org/10.3390/atmos7100129>.

Chudnovsky, A. A., H. J. Lee, A. Kostinski, T. Kotlov, and P. Koutrakis (2012), Prediction of daily fine particulate matter concentrations using aerosol optical depth retrievals from the Geostationary

Operational Environmental Satellite (GOES), *J. Air Waste Manage. Assoc.*, 62(9), doi:10.1080/10962247.2012.695321.

Ciren P, Kondragunta S. (2014), Dust aerosol index (DAI) algorithm for MODIS. *J Geophys Res Atmos.*;119 doi: 10.1002/2013JD020855.

Cohen, A. J., et al. (2017), Estimates and 25-year trends of the global burden of disease attributable to ambient air pollution: an analysis of data from the Global Burden of Diseases Study 2015, *The Lancet*, 389(10082), 1907-1918, doi:10.1016/S0140-6736(17)30505-6.

Das, I., M. Mohan and K. Krishnamoorthy (2002), Detection of marine aerosols with IRS P4-Ocean Colour Monitor. *Proc. Indian Acad. Sci. (Earth Planet. Sci.)*, 111, 425-435.

Das, I., and M. Mohan (2003), Detection of marine aerosols using ocean colour sensors. *Mausam*, 54, 327-334.

Descheemaeker, M., Plu, M., Marécal, V., Claeys, M., Olivier, F., Aoun, Y., Blanc, P., Wald, L., Guth, J., Sič, B., Vidot, J., Piacentini, A., and Josse, B. (2019), Monitoring aerosols over Europe: an assessment of the potential benefit of assimilating the VIS04 measurements from the future MTG/FCI geostationary imager, *Atmos. Meas. Tech.*, 12, 1251–1275, <https://doi.org/10.5194/amt-12-1251-2019>, 2019.

de Graaf, M., Stammes, P., Torres, O., and Koelemeijer, R. B. A. (2005), Absorbing Aerosol Index: Sensitivity analysis, application to GOME and comparison with TOMS, *J. Geophys. Res.*, 110, D01201, doi:10.1029/2004JD005178.

de Souza, P., R.A. Kahn, J.A. Limbacher, E.A. Marais, F. Duarte, and C. Ratti, (2020), Combining low-cost, surface-based aerosol monitors with size-resolved satellite data for air quality applications. *Atm. Meas. Tech.* 13, 5319–5334, doi:10.5194/amt-13-5319-2020.

Dey, S. and R. P. Singh (2002), Retrieval of aerosol parameters using IRS P4 OCM data over the Arabian Sea and the Bay of Bengal. *Current Science*, 83, 1235-1240.

Di, Q., H. Amini, L. Shi, I. Kloog, R. Silvern, J. Kelly, M.B. Sabath, C. Choirat, P. Koutrakis, A. Lyapustin, Y. Wang, L.J. Mickley, J. Schwartz, An ensemble-based model of PM<sub>2.5</sub> concentration across the contiguous United States with high spatiotemporal resolution, *Environ. Int.*, 130, 2019, 104909, <https://doi.org/10.1016/j.envint.2019.104909>.

Diner, D.J., J.C. Beckert, T.H. Reilly, C.J. Bruegge, J.E. Conel, R.A. Kahn, J.V. Martonchik, T.P. Ackerman, R. Davies, S.A.W. Gerstl, H.R. Gordon, J-P. Muller, R. Myneni, R.J. Sellers, B. Pinty, and M.M. Verstraete, (1998), Multiangle Imaging SpectroRadiometer (MISR) description and experiment overview, *IEEE Trans. Geosci. Remt. Sensing* 36, 1072-1087; doi: 10.1109/36.700992.

Diner, D.J., A. Davis, B. Hancock, G. Gutt, R.A. Chipman, and B. Cairns (2007). Dual photoelastic modulator-based polarimetric imaging concept for aerosol remote sensing. *Appl. Opt.* 46, 8428-8445.

Diner, D.J., A. Davis, B. Hancock, S. Geier, B. Rheingans, V. Jovanovic, M. Bull, D.M. Rider, R.A. Chipman, A.-B. Mahler, and S.C. McClain (2010). First results from a dual photoelastic-modulator-based polarimetric camera. *Appl. Opt.* 49, 2929-2946.

Diner D.J., S.W. Boland, M. Brauer, C. Bruegge, K.A. Burke, R. Chipman, L. Di Girolamo, M.J. Garay, S. Hasheminassab, E. Hyer, M. Jerrett, V. Jovanovic, O.V. Kalashnikova, Y. Liu, A.I. Lyapustin, R. V. Martin, A. Nastan, B.D. Ostro, B. Ritz, J. Schwartz, J. Wang, and F. Xu (2018), Advances in multiangle satellite remote sensing of speciated airborne particulate matter and association with adverse health effects: from MISR to MAIA. *J. Appl. Remote Sens.* 12, 042603.

Drouin, B. J., D. C. Benner, L. R. Brown, M. J. Cich, T. J. Crawford, V. M. Devi, et al. (2017), Multispectrum analysis of the oxygen A-band, *J. Quant. Spect. Radiat. Transfer*, 186, 118–138, doi:10.1016/j.jqsrt.2016.03.037.

Dubovik, O., Herman, M., Holdak, A., Lapyonok, T., Tanré, D., Deuzé, J. L., et al. (2011), Statistically optimized inversion algorithm for enhanced retrieval of aerosol properties from spectral multi-angle polarimetric satellite observations. *Atmos. Meas. Tech.* 4, 975–1018. doi: 10.5194/amt-4-975-2011.

Dubovik, O., T. Lapyonok, P. Litvinov, M. Herman, D. Fuertes, F. Ducos, A. Lopatin, A. Chaikovsky, B. Torres, Y. Derimian, X. Huang, M. Aspetsberger, and C. Federspiel (2014), *GRASP: a versatile algorithm for characterizing the atmosphere*, SPIE: Newsroom, Published Online: September 19, 2014. doi:10.1117/2.1201408.005558.

Dubovik, O., et al. (2019), Polarimetric remote sensing of atmospheric aerosols: Instruments, methodologies, results, and perspectives, *Journal of Quantitative Spectroscopy and Radiative Transfer*, 224, 474-511, <https://doi.org/10.1016/j.jqsrt.2018.11.024>.

Dubovik, O. and M. D. King (2000), A flexible inversion algorithm for retrieval of aerosol optical properties from Sun and sky radiance measurements," *J. Geophys. Res.*, 105, 20 673-20 696.

Dubovik, O., A. Smirnov, B. N. Holben, M. D. King, Y.J. Kaufman, T. F. Eck, and I. Slutsker (2000), Accuracy assessments of aerosol optical properties retrieved from AERONET sun and sky-radiance measurements, *J. Geophys. Res.*, 105, 9791-9806.

Dubovik, O., B.N.Holben, T.F.Eck, A.Smirnov, Y.J.Kaufman, M.D.King, D.Tanre, and I.Slutsker (2002), Variability of absorption and optical properties of key aerosol types observed in worldwide locations, *J.Atm.Sci.*, 59, 590-608.

Dubovik, O., A. Sinyuk, T. Lapyonok, B. N. Holben, M. Mishchenko, P. Yang, T. F. Eck, H. Volten, O. Munoz, B. Veihelmann, W. J. van der Zande, J-F Leon, M. Sorokin, and I. Slutsker (2006), Application of spheroid models to account for aerosol particle nonsphericity in remote sensing of desert dust. *J. Geophys. Res.*, 111, doi:10.1029/2005JD006619.

Dubovik, O., et al. (2019), Polarimetric remote sensing of atmospheric aerosols: Instruments, methodologies, results, and perspectives, *Journal of Quantitative Spectroscopy and Radiative Transfer*, 224, 474-511, <https://doi.org/10.1016/j.jqsrt.2018.11.024>.

Dubovik, O., Fuertes, D., Litvinov, P., et al. (2021), A comprehensive Description of Multi-Term LSM for Applying Multiple a Priori Constraints in Problems of Atmospheric Remote Sensing: GRASP Algorithm, Concept, and Applications. *Front. Remote Sens.* 2: 706851, 2021. Doi:10.3389/frsen.2021.706851

Dubuisson, P., R. Frouin, D. Dessailly, L. Duforêt, J.-F. Léon, K. Voss, et al. (2009), Estimating the altitude of aerosol plumes over the ocean from reflectance ratio measurements in the O<sub>2</sub> A-band, *Remote Sens. Environ.*, 113, 1899–1911, doi:10.1016/j.rse.2009.04.018.

Eck, T.F., B.N.Holben, J.S.Reid, O.Dubovik, A.Smirnov, N.T.O'Neill, I.Slutsker, and S.Kinne (1999), Wavelength dependence of the optical depth of biomass burning, urban and desert dust aerosols, *J. Geophys. Res.*, 104, 31 333-31 350.

European Environment Agency (EEA) (2019), Air quality in Europe — 2019 report.

European Commission (EC) (2008), European Air Quality Directive, 2008/50/EC, Brussels.

European Space Agency (ESA) (2017), ESA Special Publication SP-1334 2nd. ed.: Sentinel-4: ESA's Geostationary Atmospheric Mission for Copernicus Operational Services, <https://esamultimedia.esa.int/multimedia/publications/SP-1334/SP-1334.pdf>  
[https://www.esa.int/Applications/Observing\\_the\\_Earth/Copernicus/Sentinel-4\\_and\\_-5](https://www.esa.int/Applications/Observing_the_Earth/Copernicus/Sentinel-4_and_-5)

Feenstra, B., V. Papapostolou, S. Hasheminassab, H.Zhang, B.Der Boghossian, D. Cocker, A.Polidori (2019), Performance evaluation of twelve low-cost PM<sub>2.5</sub> sensors at an ambient air monitoring site, *Atmospheric Environment*, 216, 116946, <https://doi.org/10.1016/j.atmosenv.2019.116946>.

Franklin, M., K. Chau, O.V. Kalashnikova, M.J. Garay, T. Enebish, and M. Sorek-Hamer (2018), Using Multi-Angle Imaging SpectroRadiometer Aerosol Mixture Properties for Air Quality Assessment in Mongolia. *Remote Sens.* 10, 1317; doi:10.3390/rs10081317.

Friberg, M.D., R.A. Kahn, J.A. Limbacher, K.W. Apple, and J.A. Mulholland (2018), Constraining chemical transport PM<sub>2.5</sub> modeling using surface station measurements and satellite retrievals: Application over the San Joaquin valley. *Atmosph. Chem. Phys.* 18, 12891–12913, doi: 10.5194/acp-18-12891-2018.

Fu, G., and Hasekamp, O. (2018), Retrieval of aerosol microphysical and optical properties over land using a multimode approach. *Atmos. Meas. Tech.* 11, 6627–6650. doi: 10.5194/amt-11-6627-2018.

Garrigues, S., Remy, S., Chimot, J., Ades, M., Flemming, J., Kipling, Z., Inness, A., et al Monitoring multiple satellite Aerosol Optical Depth (AOD) products within the Copernicus Atmospheric Monitoring Service (CAMS) data assimilation system. Submitted to ACP, February 2022

Geng, G., N. L. Murray, D. Tong, J. S. Fu, X. Hu, P. Lee, X. Meng, H. H. Chang, and Y. Liu (2018), Satellite-Based Daily PM<sub>2.5</sub> Estimates During Fire Seasons in Colorado, *Journal of Geophysical Research: Atmospheres*, 123(15), 8159-8171, doi:10.1029/2018JD028573.

Giles, D. M., Sinyuk, A., Sorokin, M. G., Schafer, J. S., Smirnov, A., Slutsker, I., Eck, T. F., Holben, B. N., Lewis, J. R., Campbell, J. R., Welton, E. J., Korkin, S. V., and Lyapustin, A. I. (2019), Advancements in the Aerosol Robotic Network (AERONET) Version 3 database – automated near-real-time quality control algorithm with improved cloud screening for Sun photometer aerosol optical depth (AOD) measurements, *Atmos. Meas. Tech.*, 12, 169-209, <https://doi.org/10.5194/amt-12-169-2019>.

Gkatzelis, G.I., J.B. Gilman, S.S. Brown, H. Eskes, A.R. Gomes, A.C. Lange, B.C. McDonald, J. Peischl, A. Petzold, C. Thompson, A. Kiendler-Scharr (2021). The Global Impacts of COVID-19 Lockdowns on Urban Air Pollution: A Review. *Elementa: Science of Anthropocene*. 9 (1): 00176.

doi: <https://doi.org/10.1525/elementa.2021.00176>

Go, S., J. Kim, J. Mok, H. Irie, J. Yoon, O. Torres, N. A. Krotkov, G. Labow, M. Kim, J.-H. Koo, M. Choi, H. Lim (2020), Ground-based retrievals of aerosol column absorption in the UV spectral region and their implications for GEMS measurements, *Remote Sensing of Environ.*, 245, 111759, doi:10.1016/j.rse.2020.111759.

Go, S., Lyapustin, A., Schuster, G. L., Choi, M., Ginoux, P., Chin, M., Kalashnikova, O., Dubovik, O., Kim, J., da Silva, A., Holben, B., and Reid, J. S.: Inferring iron-oxide species content in atmospheric mineral dust from DSCOVR EPIC observations, *Atmos. Chem. Phys.*, 22, 1395–1423, <https://doi.org/10.5194/acp-22-1395-2022>, 2022.

Gonzalez-Alonso, L., Martin, M.V. and Kahn, R.A. (2019), Biomass-burning smoke heights over the Amazon observed from space, *Atmospheric Chemistry and Physics*, 19 (3), 1685-1702. ISSN 1680-7316.

Goto, D., M.i Kikuchi, K. Suzuki, M. Hayasaki, M. Yoshida, T. M. Nagao, M. Choi, J. Kim, N. Sugimoto, A. Shimizu, E. Oikawa, T. Nakajima (2019), Aerosol model evaluation using two geostationary satellites over East Asia in May 2016, *Atmospheric Research*, 217 93–113, doi: 10.1016/j.atmosres.2018.10.016

Govaerts, Y. M., S. Wagner, A. Lattanzio, and P. Watts (2010), Joint retrieval of surface reflectance and aerosol optical depth from MSG/SEVIRI observations with an optimal estimation approach: 1. Theory, *J. Geophys. Res.*, 115, D02203, doi:10.1029/2009JD011779.

Gupta, P., and S. A. Christopher (2009), Particulate matter air quality assessment using integrated surface, satellite, and meteorological products: Multiple regression approach, *J. Geophys. Res.-Atmos.*, 114, doi:D1420510.1029/2008jd011496.

Gupta, P., Remer, L. A., Levy, R. C., and Mattoo, S. (2018a), Validation of MODIS 3 km land aerosol optical depth from NASA's EOS Terra and Aqua missions, *Atmos. Meas. Tech.*, 11, 3145–3159, <https://doi.org/10.5194/amt-11-3145-2018>.

Gupta, P., Doraiswamy, P., Levy, R., Pikelnaya, O., Maibach, J., Feenstra, B., et al. (2018b), Impact of California fires on local and regional air quality: The role of a low-cost sensor network and satellite observations, *GeoHealth*, 2, 172– 181. <https://doi.org/10.1029/2018GH000136>

Gupta, P.; Remer, L.A.; Patadia, F.; Levy, R.C.; Christopher, S.A. (2020), High-Resolution Gridded Level 3 Aerosol Optical Depth Data from MODIS. *Remote Sens.*, 12, 2847. <https://doi.org/10.3390/rs12172847>.

Hammer, M. S., et al. (2020), Global Estimates and Long-Term Trends of Fine Particulate Matter Concentrations (1998-2018), *Environ. Sci. Technol.*, doi:10.1021/acs.est.0c01764.

Hasekamp, O. P. (2010), Capability of multi-viewing-angle photo-polarimetric measurements for the simultaneous retrieval of aerosol and cloud properties, *Atmos. Meas. Tech.*, 3, 839–851, <https://doi.org/10.5194/amt-3-839-2010>.

Hasekamp, O. P., Litvinov, P., and Butz, A. (2011). Aerosol properties over the ocean from PARASOL multiangle photopolarimetric measurements. *J. Geophys. Res.* 116:D14204. doi: 10.1029/2010JD015469.

Herman, J. R., Bhartia, P. K., Torres, O., Hsu, C., Seftor, C., and Celarier, E. (1997), Global distribution of UV-absorbing aerosols from Nimbus 7/TOMS data, *J. Geophys. Res.*, 102( D14), 16911– 16922, doi:10.1029/96JD03680.

Holben, B. N., T. F. Eck, I. Slutsker, D. Tanre, J. P. Buis, and A. Setzer (1998), AERONET—A federated instrument network and data archive for aerosol characterization, *Remote Sens. Environ.*, 66, 1–16, doi:10.1016/S0034-4257(98)00031-5.

Holben, B. N., T. F. Eck, I. Slutsker, A. Smirnov, A Sinyuk, J. Schafer, D. Giles, O. Dubovik (2006), Aeronet's Version 2.0 quality assurance criteria, Proc. SPIE 6408, Remote Sensing of the Atmosphere and Clouds, 64080Q, doi:10.1117/12.706524

Holben, B. N., Kim, J., Sano, I., Mukai, S., Eck, T. F., Giles, D. M., Schafer, J. S., Sinyuk, A., Slutsker, I., Smirnov, A., Sorokin, M., Anderson, B. E., Che, H., Choi, M., Crawford, J. H., Ferrare, R. A., Garay, M. J., Jeong, U., Kim, M., Kim, W., Knox, N., Li, Z., Lim, H. S., Liu, Y., Maring, H., Nakata, M., Pickering, K. E., Piketh, S., Redemann, J., Reid, J. S., Salinas, S., Seo, S., Tan, F., Tripathi, S. N., Toon, O. B., and Xiao, Q. (2018), An overview of mesoscale aerosol processes, comparisons, and validation studies from DRAGON networks, *Atmos. Chem. Phys.*, 18, 655-671, <https://doi.org/10.5194/acp-18-655-2018>.

Hoff, R. H. and S. A. Christopher (2009) Remote Sensing of Particulate Pollution from Space: Have We Reached the Promised Land?, *Journal of the Air & Waste Management Association*, 59:6, 645-675, DOI: [10.3155/1047-3289.59.6.645](https://doi.org/10.3155/1047-3289.59.6.645)

Holder, A. L., A. K. Mebust, L. A. Maghran, M. R. McGown, K. E. Stewart, D. M. Vallano, R. A. Elleman, K. R. Baker, (2020), Field Evaluation of Low-Cost Particulate Matter Sensors for Measuring Wildfire Smoke. *Sensors*, 20, 4796; doi:10.3390/s20174796.

Hsu, N.C., M.-J. Jeong, C. Bettenhausen, A.M. Sayer, R. Hansell, C.S. Seftor, J. Huang and S.-C. Tsay (2013), Enhanced Deep Blue aerosol retrieval algorithm: The second generation. *Journal of Geophysical Research: Atmospheres*, 118, 9296-9315.

Hu, X., L. Waller, M. Al-Hamdan, W. Crosson, M. Estes Jr, S. M. Estes, D. A. Quattrochi, J. A. Sarnat, and Y. Liu (2013), Estimating ground-level PM<sub>2.5</sub> concentrations in the southeastern U.S. using geographically weighted regression, *Environmental Research*, 121, 1-10, doi:<http://dx.doi.org/10.1016/j.envres.2012.11.003>.

Hu, X., et al. (2014), Estimating ground-level PM<sub>2.5</sub> concentrations in the Southeastern United States using MAIAC AOD retrievals and a two-stage model, *Remote Sens. Environ.*, 140(0), 220-232, doi:<http://dx.doi.org/10.1016/j.rse.2013.08.032>.

Hu, X., J. Belle, X. Meng, A. Wildani, L. A. Waller, M. J. Strickland, and Y. Liu (2017), Estimating PM<sub>2.5</sub> Concentrations in the Conterminous United States Using the Random Forest Approach, *Environ. Sci. Technol.*, 51(12), 6936-6944, doi:10.1021/acs.est.7b01210.

Huang, J., Kondragunta, S., Laszlo, I., Liu, H., Remer, L. A., Zhang, H., Superczynski, S., Ciren, P., Holben, B. N., and Petrenko, M. (2016), Validation and expected error estimation of Suomi-NPP VIIRS aerosol

optical thickness and Ångström exponent with AERONET, *J. Geophys. Res. Atmos.*, 121, 7139–7160, doi:10.1002/2016JD024834.

Ingmann, P., Veihelmann, B., Langen, J., Lamarre, D., Stark, H., and Bazalgette Courrèges-Lacoste, G. (2012), Requirements for the GMES Atmosphere Service and ESA's, implementation concept: Sentinels-4/5 and -5p. *Remote Sensing of Environment*, 120: 58–69. doi:10.1016/j.rse.2012.01.023.

Jackson, J. M., H. Liu, I. Laszlo, S. Kondragunta, L. A. Remer, J. Huang, and H.-C. Huang (2013), Suomi-NPP VIIRS aerosol algorithms and data products, *J. Geophys. Res. Atmos.*, 118, 12,673–12,689, doi:10.1002/2013JD020449.

Jeon, W., Y. Choi, P. Percell, A. Hossein Souri, C.-K. Song, S.-T. Kim, and J. Kim (2016), Computationally efficient air quality forecasting tool: implementation of STOPS v1.5 model into CMAQ v5.0.2 for a prediction of Asian dust, *Geosci. Model Dev.*, 9, 3671–3684, 2016, doi:10.5194/gmd-9-3671-2016.

Jethva, H., Torres, O., and Ahn, C. (2018), A 12-year long global record of optical depth of absorbing aerosols above the clouds derived from the OMI/OMACA algorithm, *Atmos. Meas. Tech.*, 11, 5837–5864, <https://doi.org/10.5194/amt-11-5837-2018>.

Jin, Xiaomeng & Fiore, Arlene & Curci, Gabriele & Lyapustin, Alexei & Civerolo, Kevin & Ku, Michael & Donkelaar, Aaron & Martin, Randall. (2019). Assessing uncertainties of a geophysical approach to estimate surface fine particulate matter distributions from satellite-observed aerosol optical depth. *Atmospheric Chemistry and Physics*. 19. 295–313. 10.5194/acp-19-295-2019.

Judd, L. M., Sullivan, J. T., Lefer, B., Haynes, J., Jensen, M. P., Nadkarni, R. (2021), TRACER-AQ Science Plan – An Interagency Cooperative Air Quality Field Study in the Houston, TX Metropolitan Region, [https://www-air.larc.nasa.gov/missions/tracer-aq/docs/TRACERAQ\\_SciencePlan\\_v1.pdf](https://www-air.larc.nasa.gov/missions/tracer-aq/docs/TRACERAQ_SciencePlan_v1.pdf)

Jung, J., A. H. Souri, D. C. Wong, S. Lee, W. Jeon, J. Kim, Y. Choi (2019), The Impact of the Direct Effect of Aerosols on Meteorology and Air Quality Using Aerosol Optical Depth Assimilation During the KORUS-AQ Campaign, *Journal of Geophysical Research: Atmospheres*, 124, 8303–8319, doi:10.1029/2019JD030641.

Just, A.C., K.B. Arfer, J. Rush, M. Dorman, A. Shtein, A. **Lyapustin**, I. Kloog: Advancing methodologies for applying machine learning and evaluating spatiotemporal models of fine particulate matter (PM<sub>2.5</sub>) using satellite data over large regions, *Atmospheric Environment*, 239, 2020, 117649, <https://doi.org/10.1016/j.atmosenv.2020.117649>.

Kahn, R. A., Li, W.-H., Moroney, C., Diner, D. J., Martonchik, J. V., and Fishbein, E. (2007), Aerosol source plume physical characteristics from space-based multiangle imaging, *J. Geophys. Res.*, 112, D11205, doi:10.1029/2006JD007647.

Kahn, R. A., Chen, Y., Nelson, D. L., Leung, F.-Y., Li, Q., Diner, D. J., and Logan, J. A. (2008), Wildfire smoke injection heights: Two perspectives from space, *Geophys. Res. Lett.*, 35, L04809, doi:[10.1029/2007GL032165](https://doi.org/10.1029/2007GL032165).

Kahn, R.A., and B. J. Gaitley (2015), An analysis of global aerosol type as retrieved by MISR. *J. Geophys. Res. Atmos.* 120, 4248-4281, doi:10.1002/2015JD023322.

Kikuchi, M., H. Murakami, K. Suzuki, T. M. Nagao, and A. Higurashi (2018), Improved hourly estimates of aerosol optical thickness using spatiotemporal variability derived from Himawari-8 geostationary satellite, *IEEE Trans. Geosci. Remote Sens.*, 56(6), 3442-3455, doi:10.1109/TGRS.2018.2800060.

Kim, M., Kim, J., Jeong, U., Kim, W., Hong, H., Holben, B., Eck, T. F., Lim, J. H., Song, C. K., Lee, S., and Chung, C.-Y. (2016), Aerosol optical properties derived from the DRAGON-NE Asia campaign, and implications for a single-channel algorithm to retrieve aerosol optical depth in spring from Meteorological Imager (MI) on-board the Communication, Ocean, and Meteorological Satellite (COMS), *Atmos. Chem. Phys.*, 16, 1789–1808, <https://doi.org/10.5194/acp-16-1789-2016>.

Kim, Man-Hae , Ali H. Omar, Jason L. Tackett, Mark A. Vaughan, David M. Winker, Charles R. Trepte, Yongxiang Hu, Zhaoyan Liu, Lamont R. Poole, Michael C. Pitts, Jayanta Kar, and Brian E. Magill (2018), The CALIPSO version 4 automated aerosol classification and lidar ratio selection algorithm, *Atmos. Meas. Tech.*, 11, 6107–6135.

Kim, J., Ukkyo J., M.-H. Ahn, J. H. Kim, R. J. Park, H. Lee, C. H. Song, Y.-S. Choi, K.-H. Lee, J.-M. Yoo, M.-J. Jeong, S. K. Park, K.-M. Lee, C.-K. Song, S.-W. Kim, Y.-J. Kim, S.-W. Kim, M. Kim, S. Go, X. Liu, K. Chance, C. C. Miller, J. Al-Saadi, B. Veihelmann, P. K. Bhartia, O. Torres, G. G. Abad, D. P. Haffner, D. H. Ko, S. H. Lee, J.-H. Woo, H. Chong, S. S. Park, D. Nicks, W. J. Choi, K.-J. Moon, A. Cho, J. Yoon, S.-k. Kim, H. Hong, K. Lee, H. Lee, S. Lee, M. Choi, P. Veefkind, P. Levelt, D. P. Edwards, M. Kang, M. Eo, J. Bak, K. Baek, H.-A. Kwon, J. Yang, J. Park, K. M. Han, B.-R. Kim, H.-W. Shin, H. Choi, E. Lee, J. Chong, Y. Cha, J.-H. Koo, H. Irie, S. Hayashida, Y. Kasai, Y. Kanaya, C. L., J. Lin, J. H. Crawford, G. R. Carmichael, M. J. Newchurch, B. L. Lefer, J. R. Herman, R. J. Swap, A. K H Lau, T. P. Kurosu, G. Jaross, B. Ahlers, M. Dobber, T. McElroy, Y. Choi (2020), New Era of Air Quality Monitoring from Space: Geostationary Environment Monitoring Spectrometer (GEMS), *BAMS*, 101, 1, doi:10.1175/BAMS-D-18-0013.1.

Kinne, Stefan, Michael Schulz, and Philip Stier (2020), An AeroCom–AeroSat study: intercomparison of satellite AOD datasets for aerosol model evaluation, *Atmos. Chem. Phys.*, 20, 12431–12457, <https://doi.org/10.5194/acp-20-12431-2020>.

Kloog, I., A. A. Chudnovsky, A. C. Just, F. Nordio, P. Koutrakis, B. A. Coull, A. Lyapustin, Y. Wang, and J. Schwartz (2014), A new hybrid spatio-temporal model for estimating daily multi-year PM<sub>2.5</sub> concentrations across northeastern USA using high resolution aerosol optical depth data, *Atmospheric Environment*, 95(0), 581-590, doi:http://dx.doi.org/10.1016/j.atmosenv.2014.07.014.

Knapp, K. R., T. H. Vonder Haar, and Y. J. Kaufman (2002), Aerosol optical depth retrieval from GOES-8: Uncertainty study and retrieval validation over South America, *J. Geophys. Res.*, 107(D7), 4055, doi:10.1029/2001JD000505.

Knapp, K. R., Frouin, R., Kondragunta, S., and Prados, A. (2007), Toward aerosol optical depth retrievals over land from GOES visible radiances: determining surface reflectance, *International Journal of Remote Sensing*, 26, 4097-4116, 2007.

- Koelemeijer, R. B. A., C. D. Homan, and J. Matthijsen (2006), Comparison of spatial and temporal variations of aerosol optical thickness and particulate matter over Europe, *Atmos. Environ.*, 40(27), 5304-5315.
- Koffi, B., M. Schulz, F.-M. Breon, J. Griesfeller, D. Winker, Y. Balkanski, et al. (2012), Application of the CALIOP layer product to evaluate the vertical distribution of aerosols estimated by global models: AeroCom phase I results, *J. Geophys. Res.*, 117, doi:10.1029/2011JD016858.
- Koffi, B., et al. (2016), Evaluation of the aerosol vertical distribution in global aerosol models through comparison against CALIOP measurements: AeroCom phase II results, *J. Geophys. Res. Atmos.*, 121, 7254– 7283, doi:10.1002/2015JD024639.
- Kokhanovsky, Alexander A. and Vladimir V. Rozanov (2010), The determination of dust cloud altitudes from a satellite using hyperspectral measurements in the gaseous absorption band, *International Journal of Remote Sensing*, 31:10, 2729-2744, DOI: 10.1080/01431160903085644.
- Kokhanovsky, A. A., Davis, A. B., Cairns, B., Dubovik, O., Hasekamp, O., Sano, I., et al. (2015), Space-based remote sensing of atmospheric aerosols: the multi-angle spectro-polarimetric frontier. *Earth Sci. Rev.* 145, 85–116. doi: 10.1016/j.earscirev.2015.01.012.
- Kondragunta, S., I. Laszlo, H. Zhang, P. Ciren, A. Huff (2020), Air Quality Applications of ABI Aerosol Products from the GOES-R Series. In *The GOES-R Series: A New Generation of Geostationary Environmental Satellites*, Goodman, S.J., Schmit, T.J., Daniels, J., Redmon, R.J. Eds.; Elsevier, Chapter 17.
- Kumar, R., Delle Monache, L., Bresch, J., Saide, P. E., Tang, Y., Liu, Z., da Silva, A. M., Alessandrini, S., Pfister, G., Edwards, D., Lee, P., and Djalalova, I. (2019), Toward Improving Short-Term Predictions of Fine Particulate Matter Over the United States Via Assimilation of Satellite Aerosol Optical Depth Retrievals, *Journal of Geophysical Research: Atmospheres*, 124, 2753-2773.
- Laszlo, I.; Ciren, P.; Liu, H.; Kondragunta, S.; Tarpley, J.D.; Goldberg, M.D. (2008), Remote sensing of aerosol and radiation from geostationary satellites. *Adv. Space Res.*, 41, 1882–1893.
- Laszlo I. and H. Liu (2016), EPS Aerosol Optical Depth algorithm theoretical basis document, v3.0.1.
- Lee, K.H., Z. Li, J.K. Young, A. Kokhanovsky, Y.J. Kim et al. (eds.), (2009), *Atmospheric and Biological Environmental Monitoring*, 13, DOI 10.1007/978-1-4020-9674-7 2, Springer Science+Business Media B.V.
- Lee, J., J. Kim, C. H. Song, J.-H. Ryu, Y.-H. Ahn, and C.K. Song (2010), Algorithm for Retrieval of Aerosol Optical Properties over the Ocean from the Geostationary Ocean Color Imager, *Remote Sensing of Environment*, 114, 1077-1088, doi: 10.1016/j.rse.2009.12.021.
- Lee, H. J., Y. Liu, B. A. Coull, J. Schwartz, and P. Koutrakis (2011), A novel calibration approach of MODIS AOD data to predict PM<sub>2.5</sub> concentrations, *Atmos. Chem. Phys.*, 11(15), 7991-8002, doi:10.5194/acp-11-7991-2011.
- Lee, S., Choi, M., Kim, J., Kim, M., and Lim, H. (2017), Retrieval of Aerosol Optical Depth with High Spatial Resolution using GOCI Data, *Korean Journal of Remote Sensing*, 33(6\_1), 961–970. <https://doi.org/10.7780/KJRS.2017.33.6.1.5>.

- Lee, S., J. Kim, M. Choi, J. Hong, H. Lim, T. F Eck, B. N Holben, J.-Y. Ahn, J. Kim, J.-H. Koo (2019), Analysis of long-range transboundary transport (LRTT) effect on Korean aerosol pollution during the KORUS-AQ campaign, *Atmos. Environment*, 204, 53-67, doi:10.1016/j.atmosenv.2019.02.020.
- Lee, K., Yu, J., Lee, S., Park, M., Hong, H., Park, S. Y., Choi, M., Kim, J., Kim, Y., Woo, J.-H., Kim, S.-W., and Song, C. H. (2020), Development of Korean Air Quality Prediction System version 1 (KAQPS v1): an operational air quality prediction system with focuses on practical issues, *Geosci. Model Dev.*, doi:10.5194/gmd-13-1055-2020.
- Lennartson, E., J. Wang, L. C. Garcia, C. Ge, G. Carmichael, M. Gao, J. Kim, S. Janz (2018), Diurnal variation of aerosol optical depth and PM<sub>2.5</sub> in South Korea: A synthesis from AERONET, Satellite (GOCI), KORUS AQ Observation, and WRF-CHEM model, *Atmos. Chem. Phys.*, 18, 15125–15144, doi: 10.5194/acp-18-15125-2018.
- Lenoble, J., L. Remer and D. Tanre (Eds) (2013), *Aerosol Remote Sensing*, ISBN 978-3-642-17724-8 ISBN 978-3-642-17725-5 (eBook) DOI 10.1007/978-3-642-17725-5 Springer Heidelberg New York Dordrecht London.
- Levy, R.C., L. A. Remer, S. Mattoo, E.F. Vermote and Y.J. Kaufman (2007), Second-generation operational algorithm: Retrieval of aerosol properties over land from inversion of Moderate Resolution Imaging Spectroradiometer spectral radiance. *Journal of Geophysical Research-Atmospheres*, 112, D13211.
- Levy, R. C., Mattoo, S., Munchak, L. A., Remer, L. A., Sayer, A. M., Patadia, F., and Hsu, N. C. (2013), The Collection 6 MODIS aerosol products over land and ocean, *Atmos. Meas. Tech.*, 6, 2989–3034, <https://doi.org/10.5194/amt-6-2989-2013>.
- Levy, R., Hsu, C., et al. (2015), MODIS Atmosphere L2 Aerosol Product, *NASA MODIS Adaptive Processing System*, Goddard Space Flight Center, USA, doi:10.5067/MODIS/MOD04\_L2.006.
- Li, J. (2020), Pollution Trends in China from 2000 to 2017: A Multi-Sensor View from Space. *Remote Sens.* 12, 208; doi:10.3390/rs12020208.
- Li, X., J. Ling, and H. Kan (2019), Air pollution: a global problem needs local fixes. *Nature* 270, 437-439.
- Li, Z. et al. (2016), Simple transfer calibration method for a Cimel Sun-Moon photometer: calculating lunar calibration coefficients from Sun calibration constants. *Appl.Opt.* 55, 7624-7630.
- Li, L., Dubovik, O., Derimian, Y., Schuster, G. L., Lapyonok, T., Litvinov, P., Ducos, F., Fuertes, D., Chen, C., Li, Z., Lopatin, A., Torres, B., and Che, H.: Retrieval of aerosol components directly from satellite and ground-based measurements, *Atmos. Chem. Phys.*, 19, 13409–13443, <https://doi.org/10.5194/acp-19-13409-2019>, 2019.
- Lim, H., Choi, M., Kim, J., Kasai, Y., and Chan, P. (2018), AHI/Himawari-8 Yonsei Aerosol Retrieval (YAER): Algorithm, Validation and Merged Products, *Remote Sens.*, 10, 699-724, <https://doi.org/10.3390/rs10050699>.

- Lim, H., Go, S., Kim, J., Choi, M., Lee, S., Song, C.-K., and Kasai, Y. (2021), Integration of GOCI and AHI Yonsei Aerosol Optical Depth Products During the 2016 KORUS-AQ and 2018 EMERGE Campaigns, *Atmos. Meas. Tech.*, 14, 4575-4592, <https://doi.org/10.5194/amt-14-4575-2021>.
- Lima, C.B., S. S. Prijith, M.V.R. Seshasai, P. V. N. Rao, K. Niranjana, and M. V. Ramana (2019), Retrieval and validation of cloud top temperature from the geostationary satellite INSAT-3D. *Remote Sens.*, 11 (23), 2811.
- Limbacher, J.A., and R.A. Kahn (2014), MISR Research-Aerosol-Algorithm: Refinements for Dark Water Retrievals. *Atm. Meas. Tech.* 7, 1-19, doi:10.5194/amt-7-1-2014.
- Limbacher, J. A. and Kahn, R. A. (2017), Updated MISR dark water research aerosol retrieval algorithm – Part 1: Coupled 1.1 km ocean surface chlorophyll-A retrievals with empirical calibration corrections, *Atmos. Meas. Tech.*, 10, 1539–1555, <https://doi.org/10.5194/amt-10-1539-2017>.
- Liu, Y., Park, R. J., Jacob, D. J., Li, Q., Kilaru, V., and Sarnat, J. A. (2004), Mapping annual mean ground-level PM<sub>2.5</sub> concentrations using Multiangle Imaging Spectroradiometer aerosol optical thickness over the contiguous United States, *J. Geophys. Res.*, 109, D22206, doi:10.1029/2004JD005025.
- Liu, Y., J. A. Sarnat, A. Kilaru, D. J. Jacob, and P. Koutrakis (2005), Estimating ground-level PM<sub>2.5</sub> in the eastern United States using satellite remote sensing, *Environ. Sci. Technol.*, 39(9), 3269-3278.
- Liu, Y., P. Koutrakis, and R.A. Kahn (2007), Estimating PM<sub>2.5</sub> component concentrations and size distributions using satellite-retrieved fractional aerosol optical depth: Part 1 - Development of Methods, *J. Air & Waste Management Assoc.* 57, 1351-1359, doi: 10.3155/1047-3289.57.11.1351.
- Liu, Y., C. J. Paciorek, and P. Koutrakis (2009), Estimating Regional Spatial and Temporal Variability of PM<sub>2.5</sub> Concentrations Using Satellite Data, Meteorology, and Land Use Information, *Environ. Health Perspect.*, 117(6), 886-892, doi:10.1289/ehp.0800123.
- Liu, Z., Liu, Q., Lin, H. C., Schwartz, C. S., Lee, Y. H., and Wang, T. (2011), Three-dimensional variational assimilation of MODIS aerosol optical depth: Implementation and application to a dust storm over East Asia, *Journal of Geophysical Research*, 116, D23206.
- Liu, Y. (2013), New Directions: Satellite driven PM<sub>2.5</sub> exposure models to support targeted particle pollution health effects research, *Atmospheric Environment*, 68, 52-53, doi:10.1016/j.atmosenv.2012.11.043.
- Liu, Y., and D. J. Diner (2017), Multi-Angle Imager for Aerosols: A satellite investigation to benefit public health, *Public Health Rep.*, 132, 14–17, doi:10.1177/0033354916679983.
- Lyapustin, A. I., Y. Wang, I. Laszlo, R. Kahn, S. Korkin, L. Remer, R. Levy, and J. S. Reid, 2011. "Multiangle implementation of atmospheric correction (MAIAC): 2. Aerosol algorithm." *J. Geophys. Res.*, 116 (D3): D03211 [10.1029/2010JD014986]

Lyapustin, A. I., Y. Wang, X. Xiong, G. Meister, S. Platnick, R. Levy, B. Franz, S. Korkin, T. Hilker, J. Tucker, F. Hall, P. Sellers, A. Wu, A. Angal, 2014. "Scientific impact of MODIS C5 calibration degradation and C6+ improvements." *Atmos. Meas. Tech.*, 7: 4353-4365 [10.5194/amt-7-4353-2014]

Lyapustin, A., Wang, Y., Korkin, S., and Huang, D. (2018), MODIS Collection 6 MAIAC algorithm, *Atmos. Meas. Tech.*, 11, 5741–5765, <https://doi.org/10.5194/amt-11-5741-2018>.

Lyapustin, A., Y. Wang, S. Korkin, R. Kahn and D. Winker (2020), MAIAC Thermal Technique for Smoke Injection Height From MODIS, *IEEE Geoscience and Remote Sensing Letters*, 17(5), 730-734, doi: 10.1109/LGRS.2019.2936332.

Lyapustin, A., Go, S., Korkin, S., Wang, Y., Torres, O., Jethva, H. and Marshak, A.: Retrievals of Aerosol Optical Depth and Spectral Absorption from DSCOVER EPIC. *Front. Remote Sens.* 2:645794, doi: 10.3389/frsen.2021.645794, 2021.

Ma, Z., X. Hu, L. Huang, J. Bi, and Y. Liu (2014), Estimating Ground-Level PM<sub>2.5</sub> in China Using Satellite Remote Sensing, *Environ. Sci. Technol.*, 48(13), 7436-7444, doi:10.1021/es5009399.

Martínez. M.A., J. Ruiz, E. Cuevas (2009), Use of SEVIRI images and derived products in a WMO sand and dust storm warning system, *IOP Conf. Ser.: Earth Environ. Sci.*, 7, 012004, doi:10.1088/1755-1307/7/1/012004.

Martonchik, J.V., R.A. Kahn, and D.J. Diner, 2009. Retrieval of Aerosol Properties over Land Using MISR Observations. In: Kokhanovsky, A.A. and G. de Leeuw, ed., *Satellite Aerosol Remote Sensing Over Land*. Springer, Berlin, pp.267-293. ISBN 978-3-540-69396-3.

McLean, W. G. K., Fu, G., Burton, S. P., and Hasekamp, O. P. (2021), Retrieval of aerosol microphysical properties from atmospheric lidar sounding: an investigation using synthetic measurements and data from the ACEPOL campaign, *Atmos. Meas. Tech.*, 14, 4755–4771, <https://doi.org/10.5194/amt-14-4755-2021>, 2021.

Mhawish, A., T. Banerjee, M. Sorek-Hamer, M. Bilal, A. I. Lyapustin, R. Chatfield, and D. M. Broday (2020), Estimation of High-Resolution PM<sub>2.5</sub> over the Indo-Gangetic Plain by Fusion of Satellite Data, Meteorology, and Land Use Variables, *Environ Sci Technol*, 54(13), 7891-7900, doi:10.1021/acs.est.0c01769.

Miller, K. A., D. S. Siscovick, L. Sheppard, K. Shepherd, J. H. Sullivan, G. L. Anderson, and J. D. Kaufman (2007), Long-term exposure to air pollution and incidence of cardiovascular events in women, *N. Engl. J. Med.*, 356(5), 447-458.

Miller, S. D., Lindsey, D. T., Seaman, C. J., and Solbrig, J. E. (2020), GeoColor: A Blending Technique for Satellite Imagery, *Journal of Atmospheric and Oceanic Technology*, 37(3), 429-448, <https://doi.org/10.1175/JTECH-D-19-0134.1>.

Mishra, M. K., A. Misra, P. Gupta, Raj Kumar (2021), Indian Space Research Organization, Novel technique for aerosol retrieval over land using partially sensitive spectral channels, India Patent Application No. 202141046670, filed October 13, 2021.

Mishra, M.K., Rastogi, G., and Chauhan, P. (2014), Operational Retrieval of aerosol optical depth over Indian subcontinent and Indian Ocean using INSAT-3D/Imager product validation. ISPRS - International Archives of the Photogrammetry, Remote Sensing and Spatial Information Sciences, 277-282.

Mishra, M. K. (2018), Retrieval of aerosol optical depth from INSAT-3D imager over Asian landmass and adjoining ocean: Retrieval uncertainty and validation. *Journal of Geophysical Research: Atmospheres*, 123, 5484–5508, <https://doi.org/10.1029/2017JD028116>.

Morcrette, J.-J., Boucher, O., Jones, L., Salmond, D., Bechtold, P., Beljaars, A., Benedetti, A., Bonet, A., Kaiser, J., Razinger, M., Schulz, M., Serrar, S., Simmons, A. J., Sofiev, M., Suttie, M., Tompkins, A. M., and Untch, A. (2009) Aerosol analysis and forecast in the European Centre for medium-range weather forecasts integrated forecast system: Forward modeling, *J. Geophys. Res.-Atmos.*, 114, D06206, <https://doi.org/10.1029/2008JD011235>.

Murray, N., H. Holmes, Y. Liu, and H. Chang (2019), A Bayesian ensemble approach to combine PM<sub>2.5</sub> estimates from statistical models using satellite imagery and numerical model simulation. *Environ. Res.* 178, 10860. Nanda, S., de Graaf, M., Veeffkind, J. P., Sneep, M., ter Linden, M., Sun, J., and Levelt, P. F. (2020), A first comparison of TROPOMI aerosol layer height (ALH) to CALIOP data, *Atmos. Meas. Tech.*, 13, 3043–3059, <https://doi.org/10.5194/amt-13-3043-2020>.

National Research Council (2004). *Research Priorities for Airborne Particulate Matter: IV. Continuing Research Progress*. Washington, DC: The National Academies Press. <https://doi.org/10.17226/10957>.

Nel, A. (2005), Air Pollution–Related Illness: Effects of Particles, *Science*, 308(5723), 804-806.

Nelson, D.L.; Garay, M.J.; Kahn, R.A.; Dunst, B.A. (2013), Stereoscopic Height and Wind Retrievals for Aerosol Plumes with the MISR Interactive eXplorer (MINX). *Remote Sens*, 5, 4593-4628. <https://doi.org/10.3390/rs5094593>.

Pang, J., Liu, Z., Wang, X., Bresch, J., Ban, J., Chen, D., Kim, J. (2018), Assimilating AOD retrievals from GOCI and VIIRS to forecast surface PM<sub>2.5</sub> episodes over Eastern China, *Atmospheric Environment*, 179, 288-304, doi: 10.1016/j.atmosenv.2018.02.011.

Park, M. E., Song, C. H., Park, R. S., Lee, J., Kim, J., Lee, S., Woo, J.-H., Carmichael, G. R., Eck, T. F., Holben, B. N., Lee, S.-S., Song, C. K., and Hong, Y. D. (2014), New approach to monitor transboundary particulate pollution over Northeast Asia, *Atmos. Chem. Phys.*, 14, 659–674, <https://doi.org/10.5194/acp-14-659-2014>.

Park, S. S., Kim, J., Lee, H., Torres, O., Lee, K.-M., and Lee, S. D. (2016), Utilization of O4 slant column density to derive aerosol layer height from a space-borne UV–visible hyperspectral sensor: sensitivity and case study, *Atmos. Chem. Phys.*, 16, 1987–2006, <https://doi.org/10.5194/acp-16-1987-2016>.

Park, S., Shin, M., Im, J., Song, C.-K., Choi, M., Kim, J., Lee, S., Park, R., Kim, J., Lee, D.-W., and Kim, S.-K. (2019), Estimation of ground-level particulate matter concentrations through the synergistic use of satellite observations and process-based models over South Korea, *Atmos. Chem. Phys.*, 19, 1097–1113, <https://doi.org/10.5194/acp-19-1097-2019>.

- Park, S. J. Lee, J. Im, C.-K. Song, M. Choi, J. Kim, S. Lee, R. Park, S.-M. Kim, J. Yoon, D.-W. Lee, L. J. Quackenbush (2020a), Estimation of spatially continuous daytime particulate matter concentrations under all sky conditions through the synergistic use of satellite-based AOD and numerical models, *Science of the Total Environment*, 713, 136516, doi:10.1016/j.scitotenv.2020.136516.
- Park, Y., B. Kwon, J. Heo, X. Hu, Y. Liu, and T. Moon (2020b), Estimating PM<sub>2.5</sub> concentration of the conterminous United States via interpretable convolutional neural networks, *Environmental Pollution*, 256, 113395, doi:https://doi.org/10.1016/j.envpol.2019.113395.
- Patadia, F., R. A. Kahn, J. A. Limbacher, S. P. Burton, R. A. Ferrare, C.A. Hostetler, and J. W. Hair (2013), Aerosol Airmass Type Mapping Over the Urban Mexico City Region From Space-based Multi-angle Imaging. *Atm. Chem. Phys.* 13, 9525–9541, doi:10.5194/acp-13-9525-2013.
- Pope, C.A. III, and D.W. Dockery. (2006), Health effects of fine particulate air pollution: lines that connect. *J. Air Waste Manag. Assoc.* 56, 709-742.
- Popp, C.; Hauser, A.; Foppa, N.; Wunderle, S. (2007), Remote sensing of aerosol optical depth over central Europe from MSG-SEVIRI data and accuracy assessment with ground-based AERONET measurements. *J. Geophys. Res. Space Phys.*, 112.
- Prados, A. I., S. Kondragunta, P. Ciren, and K. R. Knapp (2007), GOES Aerosol/Smoke Product (GASP) over North America: Comparisons to AERONET and MODIS observations, *J. Geophys. Res.*, 112, D15201, doi:10.1029/2006JD007968.
- Randles, C. A., da Silva, A. M., Buchard, V., Colarco, P. R., Darmenov, A., Govindaraju, R., Smirnov, A., Holben, B., Ferrare, R., Hair, J., Shinozuka, Y., and Flynn, C. J. (2017), The MERRA-2 Aerosol Reanalysis, 1980 Onward. Part I: System Description and Data Assimilation Evaluation, *Journal of Climate*, 30, 6823-6850.
- Reid, C. E., M. Jerrett, M. L. Petersen, G. G. Pfister, P. E. Morefield, I. B. Tager, S. M. Raffuse, and J. R. Balmes (2015), Spatiotemporal Prediction of Fine Particulate Matter During the 2008 Northern California Wildfires Using Machine Learning, *Environ. Sci. Technol.*, 49(6), 3887-3896, doi:10.1021/es505846r.
- Rémy, S., Kipling, Z., Flemming, J., Boucher, O., Nabat, P., Michou, M., Bozzo, A., Ades, M., Huijnen, V., Benedetti, A., Engelen, R., Peuch, V.-H., and Morcrette, J.-J. (2019), Description and evaluation of the tropospheric aerosol scheme in the European Centre for Medium-Range Weather Forecasts (ECMWF) Integrated Forecasting System (IFS-AER, cycle 45R1), *Geosci. Model Dev.*, 12, 4627–4659, https://doi.org/10.5194/gmd-12-4627-2019.
- Saide, P. E., Carmichael, G. R., Liu, Z., Schwartz, C. S., Lin, H. C., da Silva, A. M., and Hyer, E. (2013), Aerosol optical depth assimilation for a size-resolved sectional model: impacts of observationally constrained, multi-wavelength and fine mode retrievals on regional scale forecasts, *Atmos. Chem. Phys. Discuss.*, 13, 12213-12261, 10.5194/acpd-13-12213-2013.
- Saide, P. E., J. Kim, C. H. Song, M. Choi, Y. Cheng, G. R. Carmichael (2014), Assimilation of next generation geostationary aerosol optical depth retrievals to improve air quality simulations, *Geophys. Res. Lett.*, 41, 24, 9188-9196, doi:10.1002/2014GL062089.

Saide, P. E., Spak, S. N., Pierce, R. B., Otkin, J. A., Schaack, T. K., Heidinger, A. K., da Silva, A. M., Kacenelenbogen, M., Redemann, J., and Carmichael, G. R. (2015), Central American biomass burning smoke can increase tornado severity in the U.S, *Geophysical research letters*, 2014GL062826, 10.1002/2014gl062826.

Saide, P. E., Gao, M., Lu, Z., Goldberg, D., Streets, D. G., Woo, J.-H., Beyersdorf, A., Corr, C. A., Thornhill, K. L., Anderson, B., Hair, J. W., Nehrir, A. R., Diskin, G. S., Jimenez, J. L., Nault, B. A., Campuzano-Jost, P., Dibb, J., Heim, E., Lamb, K. D., Schwarz, J. P., Perring, A. E., Kim, J., Choi, M., Holben, B., Pfister, G., Hodzic, A., Carmichael, G. R., Emmons, L., and Crawford, J. H. (2020), Understanding and improving model representation of aerosol optical properties for a Chinese haze event measured during KORUS-AQ, *Atmos. Chem. Phys.*, 20, 6455-6478, <https://doi.org/10.5194/acp-20-6455-2020>.

Sanders, A. F. J., J. F. de Haan, M. Sneep, A. Apituley, P. Stammes, M. O. Vieitez, et al. (2015), Evaluation of the operational aerosol layer height retrieval algorithm for Sentinel-5 Precursor: Application to O<sub>2</sub> A band observations from GOME-2A, *Atmos. Meas. Tech.*, 8, 4947–4977, doi:10.5194/amt-8-4947-2015.

Sanghavi, S., J. V. Martonchik, J. Landgraf, and U. Platt (2012), Retrieval of the optical depth and vertical distribution of particulate scatterers in the atmosphere using O<sub>2</sub> A- and B- band SCIAMACHY observations over Kanpur: A case study, *Atmos. Meas. Tech.*, 5, 1099–1119, doi:10.5194/amt-5-1099-2012.

Sawyer, V.; Levy, R.C.; Mattoo, S.; Cureton, G.; Shi, Y.; Remer, L.A. (2020), Continuing the MODIS Dark Target Aerosol Time Series with VIIRS, *Remote Sens.*, 12, 308. <https://doi.org/10.3390/rs12020308>.

Sayer, A. M., N. C. Hsu, C. Bettenhausen, M.-J. Jeong, and G. Meister (2015), Effect of MODIS Terra radiometric calibration improvements on Collection 6 Deep Blue aerosol products: Validation and Terra/Aqua consistency, *J. Geophys. Res. Atmos.*, 120, 12,157–12,174, doi:10.1002/2015JD023878.

Sayer, A. M., Govaerts, Y., Kolmonen, P., Lipponen, A., Luffarelli, M., Mielonen, T., Patadia, F., Popp, T., Povey, A. C., Stebel, K., and Witek, M. L. (2020), A review and framework for the evaluation of pixel-level uncertainty estimates in satellite aerosol remote sensing, *Atmos. Meas. Tech.*, 13, 373–404, <https://doi.org/10.5194/amt-13-373-2020>.

Schafer, J. S., et al. (2014), Intercomparison of aerosol single-scattering albedo derived from AERONET surface radiometers and LARGE in situ aircraft profiles during the 2011 DRAGON-MD and DISCOVER-AQ experiments, *J. Geophys. Res. Atmos.*, 119, doi:10.1002/2013JD021166.

Schafer, J. S., Eck, T. F., Holben, B. N., Thornhill, K. L., Ziemba, L. D., Sawamura, P., Moore, R. H., Slutsker, I., Anderson, B. E., Sinyuk, A., Giles, D. M., Smirnov, A., Beyersdorf, A. J., and Winstead, E. L. (2019), Intercomparison of aerosol volume size distributions derived from AERONET ground-based remote sensing and LARGE in situ aircraft profiles during the 2011–2014 DRAGON and DISCOVER-AQ experiments, *Atmos. Meas. Tech.*, 12, 5289–5301, <https://doi.org/10.5194/amt-12-5289-2019>, 2019.

Schmit, T. J., P. Griffith, M. M. Gunshor, J. M. Daniels, S. J. Goodman, W. J. Lebar (2017), A Closer Look at the ABI on the GOES-R Series. *Bull. Amer. Meteor. Soc.*, 98(4), 681-698.

Schuster, G. L., Dubovik, O., and Arola, A.: Remote sensing of soot carbon – Part 1: Distinguishing different absorbing aerosol species, *Atmos. Chem. Phys.*, 16, 1565–1585, <https://doi.org/10.5194/acp-16-1565-2016>, 2016.

Schutgens, N., A.M. Sayer, A. Heckel, C. Hsu, H. Jethva, G. de Leeuw, P.J.T. Leonard, R.C. Levy, A. Lipponen, A. Lyapustin, P. North, T. Popp, C. Poulson, V. Sawyer, L. Sogacheva, G. Thomas, O. Torres, Y. Wang, S. Kinne, M. Schulz, and P. Stier, An AeroCom/AeroSat study: Intercomparison of Satellite AOD Datasets for Aerosol Model Evaluation, *Atmos. Chem. Phys.*, 20, 12431–12457, <https://doi.org/10.5194/acp-20-12431-2020>.

Shaddick, G., Thomas, M.L., Green, A., Brauer, M., van Donkelaar, A., Burnett, R., Chang, H.H., Cohen, A., Dingenen, R.V., Dora, C., Gumy, S., Liu, Y., Martin, R., Waller, L.A., West, J., Zidek, J.V. and Prüss-Ustün, A. (2018), Data integration model for air quality: a hierarchical approach to the global estimation of exposures to ambient air pollution. *J. R. Stat. Soc. C*, 67: 231-253. <https://doi.org/10.1111/rssc.12227>.

She, Qiannan, Myungje Choi, Jessica H. Belle, Qingyang Xiao, Jianzhao Bi, Keyong Huang, Xia Meng, Guannan Geng, Jhoon Kim, Kebin He, Min Liu, Yang Liu (2020), Satellite-based estimation of hourly PM<sub>2.5</sub> levels during heavy winter pollution episodes in the Yangtze River Delta, China, *Chemosphere* 239 (2020) 124678, doi:10.1016/j.chemosphere.2019.124678.

Sinyuk, A., Holben, B. N., Eck, T. F., Giles, D. M., Slutsker, I., Korokin, S., Schafer, J. S., Smirnov, A., Sorokin, M., and Lyapustin, A. (2020), The AERONET Version 3 aerosol retrieval algorithm, associated uncertainties and comparisons to Version 2, *Atmos. Meas. Tech.*, 13, 3375–3411, <https://doi.org/10.5194/amt-13-3375-2020>, 2020.

Smirnov A., B.N.Holben, T.F.Eck, O.Dubovik, and I.Slutsker (2000), Cloud screening and quality control algorithms for the AERONET database, *Rem.Sens.Env.*, 73, 337-349.

Snider, G., and 34 coauthors (2015), SPARTAN: a global network to evaluate and enhance satellite-based estimates of ground-level particulate matter for global health applications. *Atmos. Meas. Tech.* 8, 505-521.

Sogacheva, L., Popp, T., Sayer, A. M., Dubovik, O., Garay, M. J., Heckel, A., Hsu, N. C., Jethva, H., Kahn, R. A., Kolmonen, P., Kosmale, M., de Leeuw, G., Levy, R. C., Litvinov, P., Lyapustin, A., North, P., Torres, O., and Arola, A. (2020), Merging regional and global aerosol optical depth records from major available satellite products, *Atmos. Chem. Phys.*, 20, 2031–2056, <https://doi.org/10.5194/acp-20-2031-2020>.

Solomon, P.A., D. Crumpler, J.B. Flanagan, R.K.M. Jayanty, E.E. Rickman, and C.E. McDade (2014), U.S. National PM<sub>2.5</sub> Chemical Speciation Monitoring Networks—CSN and IMPROVE: Description of networks. *J. Air Waste Manag. Assoc.* 64, 1410-1438.

Song, W., H. Jia, J. Huang, and Y. Zhang (2014), A satellite-based geographically weighted regression model for regional PM<sub>2.5</sub> estimation over the Pearl River Delta region in China, *Remote Sens. Environ.*, 154(0), 1-7, doi:<http://dx.doi.org/10.1016/j.rse.2014.08.008>.

Sorek-Hamer, M., M. Franklin, O.V. Kalashnikova, M.J. Garay, K. Chau, and D.J. Diner (2019), Characterizing speciated particulate matter over the California Central Valley with AERONET and MISR aerosol products. American Geophysical Union, Fall Meeting 2019, abstract #A13A-06.

Sorek-Hamer, M., R. Chatfield, Y. Liu (2020), Review: Strategies for using satellite-based products in modeling PM<sub>2.5</sub> and short-term pollution episodes. *Environment International*, Volume 144, November 2020, 106057, doi.org/10.1016/j.envint.2020.106057

Tan, Yunhui, Enguang Li, Zhaoyang Zhang, Xingwen Lin, Yonggang Chi, Lei Zhou, Chaofan Wu, Quan Wang (2019), Validation of POLDER-3/GRASP aerosol products using AERONET measurements over China, *Atmospheric Environment*, 215, 116893, <https://doi.org/10.1016/j.atmosenv.2019.116893>.

Tan, Yunhui, Enguang Li, Zhaoyang Zhang, Xingwen Lin, Yonggang Chi, Lei Zhou, Chaofan Wu, Quan Wang (2019), Validation of POLDER-3/GRASP aerosol products using AERONET measurements over China, *Atmospheric Environment*, 215, 116893, <https://doi.org/10.1016/j.atmosenv.2019.116893>.

Tang, Y., Pagowski, M., Chai, T., Pan, L., Lee, P., Baker, B., Kumar, R., Delle Monache, L., Tong, D., and Kim, H. C. (2017), A case study of aerosol data assimilation with the Community Multi-scale Air Quality Model over the contiguous United States using 3D-Var and optimal interpolation methods, *Geosci. Model Dev.*, 10, 4743-4758, 10.5194/gmd-10-4743-2017.

Tang, Die Dongren Liu, Yulei Tang, Barnabas C. Seyler, Xunfei Deng, Yu Zhan (2019), Comparison of GOCI and Himawari-8 aerosol optical depth for deriving full-coverage hourly PM<sub>2.5</sub> across the Yangtze River Delta, *Atmospheric Environment*, 217, 116973, doi:10.1016/j.atmosenv.2019.116973.

Torres, O., Decae, R., Veefkind, P., & de Leeuw, G. (2002), OMI aerosol retrieval algorithm. OMI algorithm theoretical basis document: Clouds, aerosols, and surface UV irradiance, 3(2).

Torres, O., A. Tanskanen, B. Veihelman, C. Ahn, R. Braak, P. K. Bhartia, P. Veefkind, and P. Levelt (2007), Aerosols and Surface UV Products from OMI Observations: An Overview, *J. Geophys. Res.*, 112, D24S47, doi:10.1029/2007JD008809.

Torres, O., H. Jethva, and P.K. Bhartia (2012), Retrieval of Aerosol Optical Depth above Clouds from OMI Observations: Sensitivity Analysis and Case Studies, *Journal. Atm. Sci.*, 69, 1037-1053, doi:10.1175/JAS-D-11-0130.1.

Torres, O., Ahn, C., and Chen, Z. (2013), Improvements to the OMI near UV aerosol algorithm using A-train CALIOP and AIRS observations, *Atmos. Meas. Tech.*, 6, 3257-3270, doi:10.5194/amt-6-3258-2013.

Torres, O., Bhartia, P. K., Jethva, H., and Ahn, C. (2018), Impact of the ozone monitoring instrument row anomaly on the long-term record of aerosol products, *Atmos. Meas. Tech.*, 11, 2701-2715, <https://doi.org/10.5194/amt-11-2701-2018>.

Torres, O., Jethva, H., Ahn, C., Jaross, G., and Loyola, D. G. (2020), TROPOMI Aerosol Products: Evaluation and Observations of Synoptic Scale Carbonaceous Aerosol Plumes during 2018–2020, *Atmos. Meas. Tech. Discuss.*, <https://doi.org/10.5194/amt-2020-124>, in review.

Uprety, S., C. Cao, and X. Shao, 2020, Radiometric consistency between GOES-16 ABI and VIIRS on Suomi NPP and NOAA-20, *J. Appl. Remote Sens.* 14(3), 032407 (2020), doi: 10.1117/1.JRS.14.032407  
US Environmental Protection Agency (EPA) (1990), The Clean Air Act, United States Code as Title 42, Chapter 85, <https://www.epa.gov/clean-air-act-overview/clean-air-act-text>

US Environmental Protection Agency (EPA) (2013), National Ambient Air Quality Standards for Particulate Matter; Final Rule. *Federal Register* 78, No. 10, January 15, 2013/Rules and Regulations.

US Environmental Protection Agency (EPA) (2019), Integrated Science Assessment (ISA) for Particulate Matter (Final Report). U.S. EPA, Washington, DC, EPA/600/R-19/188.

US Environmental Protection Agency (EPA) (2020), National Ambient Air Quality Standards (NAAQS) for PM, <https://www.epa.gov/pm-pollution/national-ambient-air-quality-standards-naaqs-pm>

Val Martin, M., J.A. Logan, R.A. Kahn, F-Y. Leung, D. Nelson, and D. Diner, 2010. Smoke injection heights from fires in North America: analysis of 5 years of satellite observations. *Atm. Chem. Phys.* 10, 1491-1510, doi: 10.5194/ACP-10-1491-2010.

Val Martin, M. R.A. Kahn, and M. Tosca, 2018. A Global Climatology of Wildfire Smoke Injection Height Derived from Space-based Multi-angle Imaging. *Remote Sensing*; 10, 1609, doi:10.3390/rs10101609.

van Donkelaar, A., R.V. Martin, M. Brauer, R.A. Kahn, R. Levy, C. Verduzco, and P. Villeneuve (2010), Global estimates of average ground-level fine particulate matter concentrations from satellite-based aerosol optical depth. *Environ. Health Perspect.* 118, 847-855, doi: 10.1289/EHP.0901623.

van Donkelaar, A., Martin, R. V., Spurr, R. J. D., Drury, E., Remer, L. A., Levy, R. C., and Wang, J. (2013), Optimal estimation for global ground-level fine particulate matter concentrations, *J. Geophys. Res. Atmos.*, 118, 5621– 5636, doi:10.1002/jgrd.50479.

van Donkelaar, A., R. V. Martin, M. Brauer, N. C. Hsu, R. A. Kahn, R. C. Levy, A. Lyapustin, A. M. Sayer, and D. M. Winker (2016), Global Estimates of Fine Particulate Matter using a Combined Geophysical-Statistical Method with Information from Satellites, Models, and Monitors, *Environ. Sci. Technol.*, 50(7), 3762-3772, doi:10.1021/acs.est.5b05833.

van Donkelaar, A., M. S. Hammer, L. Bindle, M. Brauer, J. R. Brook, M. J. Garay, N. C. Hsu, O. V. Kalashnikova, R. A. Kahn, C. Lee, R. C. Levy, A. Lyapustin, A. M. Sayer, and R. V. Martin (2021), Monthly global estimates of fine particulate matter and their uncertainty, *Environmental Science & Technology*, 55 (22), 15287-15300, DOI: 10.1021/acs.est.1c05309.

Vu, B. N., O. Sanchez, J. Bi, Q. Xiao, N. N. Hansel, W. Checkley, G. F. Gonzales, K. Steenland, and Y. Liu (2019), Developing an Advanced PM<sub>2.5</sub> Exposure Model in Lima, Peru, *Remote Sens (Basel)*, 11(6), doi:10.3390/rs11060641.

Wagner, S. C., Y. M. Govaerts, and A. Lattanzio (2010), Joint retrieval of surface reflectance and aerosol optical depth from MSG/SEVIRI observations with an optimal estimation approach: 2. Implementation and evaluation, *J. Geophys. Res.*, 115, D02204, doi:10.1029/2009JD011780.

Wang, J., and S. A. Christopher (2003), Intercomparison between satellite-derived aerosol optical thickness and PM<sub>2.5</sub> mass: Implications for air quality studies, *Geophys. Res. Lett.*, 30(21), doi:10.1029/2003GL018174.

Wang, J., X. Xu, S. Ding, J. Zeng, R. Spurr, X. Liu, et al. (2014), A numerical testbed for remote sensing of aerosols, and its demonstration for evaluating retrieval synergy from a geostationary satellite

constellation of GEO-CAPE and GOES-R, *J. Quant. Spectrosc. Radiat. Transfer*, 146, 510–528, doi:10.1016/j.jqsrt.2014.03.020.

Wang, Y., X. Hu, H. H. Chang, L. A. Waller, J. H. Belle, and Y. Liu (2018), A Bayesian Downscaler Model to Estimate Daily PM<sub>2.5</sub> Levels in the Conterminous US, *International Journal of Environmental Research and Public Health*, 15(9), 1999.

Wendt, E.A., C.W. Quinn, D.D. Miller-Lionberg, J. Tryner, C. L'Orange, B. Ford, A.P. Yalin, J.R. Pierce, S. Jathar, and J. Volckens (2019), A low-cost monitor for simultaneous measurement of fine particulate matter and aerosol optical depth – Part 1: Specifications and testing. *Atmos. Meas. Tech.* 12, 5431–5441.

Wei, J., Li, Z., Cribb, M., Huang, W., Xue, W., Sun, L., Guo, J., Peng, Y., Li, J., **Lyapustin**, A., Liu, L., Wu, H., and Song, Y.: Improved 1 km resolution PM<sub>2.5</sub> estimates across China using enhanced space–time extremely randomized trees, *Atmos. Chem. Phys.*, 20, 3273–3289, <https://doi.org/10.5194/acp-20-3273-2020>, 2020.

Winker, D. M., M. A. Vaughan, A. Omar, Y. Hu, K. A. Powell, Z. Liu, et al. (2009), Overview of the CALIPSO mission and CALIOP data processing algorithms, *J. Atmos. Ocean. Tech.*, 26, 2310–2323, doi:10.1175/2009JTECHA1281.1.

Winker, D. M., J. Pelon, J. A. Coakley Jr., S. A. Ackerman, R. J. Charlson, P. R. Colarco, et al. (2010), The CALIPSO mission: A global 3D view of aerosols and clouds, *Bull. Am. Meteorol. Soc.*, 91, 1211–1230, doi:10.1175/2010BAMS3009.1.

World Health Organization (WHO) (2005), WHO Air quality guidelines – global update 2005, <https://www.who.int/airpollution/publications/aqg2005/en/>

World Health Organization (WHO) (2007), Health relevance of particulate matter from various sources. Report on a WHO workshop Bonn, Germany 26-27 March 2007.

World Health Organization (WHO) (2018a), WHO report “Exposure to ambient air pollution from particulate matter for 2016”, Version 2 April 2018, [https://www.who.int/airpollution/data/AAP\\_exposure\\_Apr2018\\_final.pdf?ua=1](https://www.who.int/airpollution/data/AAP_exposure_Apr2018_final.pdf?ua=1)

World Health Organization (WHO) (2018b), Ambient air quality and health, WHO, available at: [http://www.who.int/en/news-room/fact-sheets/detail/ambient-\(outdoor\)-air-quality-and-health](http://www.who.int/en/news-room/fact-sheets/detail/ambient-(outdoor)-air-quality-and-health) (last access: 5 January 2020)

Wu, L., O. Hasekamp, H. Hu, J. Landgraf, A. Butz, J. aan de Brugh, et al. (2018), Carbon dioxide retrieval from OCO-2 satellite observations using the RemoTeC algorithm and validation with TCCON measurements, *Atmos. Meas. Tech.*, 11, 3111–3130, doi:10.5194/amt-11-3111-2018.

Xiao, Q., Zhang, H., Choi, M., Li, S., Kondragunta, S., Kim, J., Holben, B., Levy, R. C., and Liu, Y. (2016), Evaluation of VIIRS, GOCI, and MODIS Collection 6 AOD retrievals against ground sunphotometer observations over East Asia, *Atmos. Chem. Phys.*, 16, 1255–1269, doi:10.5194/acp-16-1255-2016.

Xiao, Q., H. H. Chang, G. Geng, and Y. Liu (2018), An Ensemble Machine-Learning Model To Predict Historical PM<sub>2.5</sub> Concentrations in China from Satellite Data, *Environ Sci Technol*, 52(22), 13260-13269, doi:10.1021/acs.est.8b02917.

Xie, Yisong, et al. (2019), Retrieval of fine-mode aerosol optical depth based on remote sensing measurements of directional polarimetric camera onboard GF-5 satellite, *Aerospace Shanghai*, 36(S2), 219-226.

Xu, J., Martin, R. V., van Donkelaar, A., Kim, J., Choi, M., Zhang, Q., Geng, G., Liu, Y., Ma, Z., Huang, L., Wang, Y., Chen, H., Che, H., Lin, P., and Lin, N. (2015), Estimating ground-level PM<sub>2.5</sub> in eastern China using aerosol optical depth determined from the GOCI satellite instrument, *Atm. Chem and Phys.*, 15, 13133-13144, doi:10.5194/acp-15-13133-2015.

Xu, F., G. van Harten, D. J. Diner, O.V. Kalashnikova, F.C. Seidel, C.J. Bruegge, and O. Dubovik (2017a), Coupled retrieval of aerosol properties and land surface reflection using the Airborne Multiangle SpectroPolarimetric Imager. *J. Geophys. Res. Atmos.* 122, 7004-7026.

Xu, X., J. Wang, Y. Wang, J. Zeng, O. Torres, Y. Yang, et al. (2017b), Passive remote sensing of altitude and optical depth of dust plumes using the oxygen A and B bands: First results from EPIC/DSCOVR at Lagrange-1 point, *Geophys. Res. Lett.*, 44, 7544–7554, doi:10.1002/2017GL073939.

Xu, X., Wang, J., Wang, Y., and Kokhanovsky, A. (2018), Chapter 1 – Passive Remote Sensing of Aerosol Height, in: *Remote Sensing of Aerosols, Clouds, and Precipitation*, Elsevier, Cambridge, MA, 1–22.

Xu, X., Wang, J., Wang, Y., Zeng, J., Torres, O., Reid, J. S., Miller, S. D., Martins, J. V., and Remer, L. A. (2019), Detecting layer height of smoke aerosols over vegetated land and water surfaces via oxygen absorption bands: hourly results from EPIC/DSCOVR in deep space, *Atmos. Meas. Tech.*, 12, 3269–3288, <https://doi.org/10.5194/amt-12-3269-2019>.

Yamamoto, G., and D. Q. Wark (1961), Discussion of the letter by R.A. Hanel, “Determination of cloud altitude from a satellite”, *J. Geophys. Res.*, 66, 3596, doi:10.1029/JZ066i010p03596.

Yang, J., Z. Q. Zhang, C. Y. Wei, F. Lu, and Q. Guo (2017), Introducing the new generation of Chinese geostationary weather satellites, FengYun-4. *Bull. Amer. Meteor. Soc.*, 98, 1637–1658, <https://doi.org/10.1175/BAMS-D-16-0065.1>.

Yazdi, D., M.; Kuang, Z.; Dimakopoulou, K.; Barratt, B.; Suel, E.; Amini, H.; Lyapustin, A.; Katsouyanni, K.; Schwartz, J. Predicting Fine Particulate Matter (PM<sub>2.5</sub>) in the Greater London Area: An Ensemble Approach using Machine Learning Methods. *Remote Sens.* 2020, 12, 914, <https://doi.org/10.3390/rs12060914>.

Yoshida, M., M. Kikuchi, T.M. Nagao, H. Murakami, T. Nomaki, A. Higurashi (2018), Common Retrieval of Aerosol Properties for Imaging Satellite Sensors, *J. Meteor. Soc. Japan*, 96B, 193-209, DOI:10.2151/jmsj.2018-039.

Zawadzka, O.; Markowicz, K. (2014), Retrieval of Aerosol Optical Depth from Optimal Interpolation Approach Applied to SEVIRI Data. *Remote Sens.*, 6, 7182–7211.

- Zawadzka-Manko, O.; Stachlewska, I.S.; Markowicz, K.M. (2020), Near-Real-Time Application of SEVIRI Aerosol Optical Depth Algorithm, *Remote Sens.*, 12, 1481, <https://doi.org/10.3390/rs12091481>.
- Zeger, S. L., D. Thomas, F. Dominici, J. M. Samet, J. Schwartz, D. Dockery, and A. Cohen (2000), Exposure measurement error in time-series studies of air pollution: concepts and consequences, *Environ. Health Perspect.*, 108(5), 419-426.
- Zeng, Z. C., V. Natraj, F. Xu, T. J. Pongetti, R.-L. Shia, E. A. Kort, et al. (2018), Constraining aerosol vertical profile in the boundary layer using hyperspectral measurements of oxygen absorption, *Geophys. Res. Lett.*, 45, 10772–10780, doi:10.1029/2018GL079286.
- Zeng, Z.-C., S. Chen, V. Natraj, T. Le, F. Xu, A. Merrelli, et al. (2020), Constraining coastal aerosol vertical distribution using OCO-2 O<sub>2</sub> A-band measurements, *Remote Sens. Environ.*, 236, 111494, doi:10.1016/j.rse.2019.111494.
- Zhang, H., and S. Kondragunta (2021), Daily and hourly surface PM<sub>2.5</sub> estimation from satellite AOD, *Earth Space Sci.*, 8, e2020EA001599, <https://doi.org/10.1029/2020EA001599>.
- Zhang, H., Kondragunta, S., Laszlo, I., Liu, H., Remer, L. A., Huang, J., Superczynski, S., and Ciren, P. (2016), An enhanced VIIRS aerosol optical thickness (AOT) retrieval algorithm over land using a global surface reflectance ratio database, *J. Geophys. Res. Atmos.*, 121, 10,717– 10,738, doi:10.1002/2016JD024859.
- Zhang, Hai, Pubu Ciren, Shobha Kondragunta, Istvan Laszlo, (2018), Evaluation of VIIRS dust detection algorithms over land, *J. Appl. Rem. Sens.*, 12(4), 042609, <https://doi.org/10.1117/1.JRS.12.042609>.
- Zhang, Peng; Zhu, Lin; Tang, Shihao; Gao, Ling; Chen, Lin; Zheng, Wei; Han, Xiuzhen; Chen, Jie; Shao, Jiali (2019), General Comparison of FY-4A/AGRI With Other GEO/LEO Instruments and Its Potential and Challenges in Non-meteorological Applications, *Front. Earth Sci.*, 11 January 2019, <https://doi.org/10.3389/feart.2018.00224>.
- Zhang, H., Kondragunta, S., Laszlo, I., and Zhou, M. (2020), Improving GOES Advanced Baseline Imager (ABI) aerosol optical depth (AOD) retrievals using an empirical bias correction algorithm, *Atmos. Meas. Tech.*, 13, 5955–5975, <https://doi.org/10.5194/amt-13-5955-2020>.
- Zhang, Y., Li, Z., Liu, Z., Wang, Y., Qie, L., Xie, Y., Hou, W., and Leng, L. (2021), Retrieval of aerosol fine-mode fraction over China from satellite multiangle polarized observations: validation and comparison, *Atmos. Meas. Tech.*, 14, 1655–1672, <https://doi.org/10.5194/amt-14-1655-2021>.
- Zhang, J., Campbell, J. R., Hyer, E. J., Reid, J. S., Westphal, D. L., and Johnson, R. S. (2014), Evaluating the impact of multisensor data assimilation on a global aerosol particle transport model, *Journal of Geophysical Research: Atmospheres*, 119, 2013JD020975, 10.1002/2013jd020975.
- Zheng, Y., Q. Zhang, Y. Liu, G. Geng, and K. He (2016), Estimating ground-level PM<sub>2.5</sub> concentrations over three megalopolises in China using satellite-derived aerosol optical depth measurements, *Atmospheric Environment*, 124, 232-242, doi:<https://doi.org/10.1016/j.atmosenv.2015.06.046>.



## Appendix A:

### Summary of Individual Satellite Sensors that Provide Aerosol Information

This Appendix describes in detail the sensors with observation capabilities covering the lower troposphere that are relevant for PM monitoring. Individual sensors on current and planned satellites are summarized in Table A1 (LEO satellites) and Table A2 (GEO satellites).

#### A1. Geostationary Sensors

##### A1.1. The INSAT Series

The Indian national geostationary satellite, INSAT-3D, has been providing continuous data since 2013 over the region of South Asia bounded by 44.5 °E to 105.5 °E and 10 °S to 45.5 °N (Mishra et al., 2018, Lima et al., 2019). The Imager on-board INSAT-3D makes observations at a temporal interval of 30-min with visible (0.55-0.75  $\mu\text{m}$ ), short-wave infrared (1.55-1.70  $\mu\text{m}$ ), mid-wave infrared (3.80-4.0  $\mu\text{m}$ ), water vapor (6.50-7.10  $\mu\text{m}$ ) and thermal infrared (10.3-11.3  $\mu\text{m}$  and 11.5-12.5  $\mu\text{m}$ ) channels. The spatial resolutions of the visible, short-wave infrared, and water vapor channels are 1 km, 1 km, and 8 km respectively, whereas the resolution of the mid- infrared and thermal infrared channels are 4 km. Mishra (2018) developed the INSAT-3D AOD algorithm by adopting the GOES AOD GASP algorithm. GASP uses a fixed value of background AOD for correcting the darkest observation to derive surface reflectance. A similar approach is used in the INSAT-3D AOD algorithm but instead using a dynamic value of background AOD due to high aerosol loading and high seasonal and geographical variability of AOD over Asian countries. Mishra et al. (2014) include a thorough discussion of the algorithm, including the retrieval and validation of the AOD product from INSAT-3D. AOD from INSAT-3D agrees with ground-based instruments within 45% and 30% over land and ocean, respectively. These differences are expected as the current INSAT-3D AOD algorithm uses a single broad visible channel (0.55-0.75  $\mu\text{m}$ ) with a static aerosol model (rural model over land and maritime model for oceans) leading to significant uncertainties.

Currently, the accuracy of INSAT-3D AOD over land is being enhanced by selecting an appropriate set of spatially and temporally dynamic aerosol models based on ground-based measurements and on multispectral sensors on-board polar-orbiting satellites. The aerosol product from INSAT-3D described here has been made operational on the MOSDAC and VEDAS data portals (<https://vedas.sac.gov.in>). Furthermore, implementation of the present algorithm on both INSAT-3D and INSAT-3DR will provide AOD at an interval of 15 minutes (as the former provides observations at HH:00, HH:30 and the latter at HH:15 and HH:45, where HH represents hour) over the South Asia region. In addition, there are plans to launch future geostationary satellites for enhanced real-time monitoring with higher spatial and spectral resolution, which is expected to help in retrieving not only AOD, but also other aerosol optical parameters with improved accuracy.

##### A1.2. The GOES-R Series

The launch of the GOES-R Series ABI has advanced the capabilities of operational aerosol and air quality monitoring many fold with 5-min observations routinely over the CONUS (Schmit et al., 2017; Kondragunta et al., 2020). More importantly, the new generation ABI has 16 channels, with multiple channels in the visible and short-wave IR, compared to one broad visible band on the legacy GOES imagers. NOAA launched GOES-R (16) on November 19, 2016 as GOES-East and GOES-S (17) on March

**Table A 1.** Characteristics of sensors on current and planned LEO satellites relevant for PM monitoring.

Sensor	Sensor Class*	Satellite(s)	Launch Date	Daytime Equatorial Crossing Time	Number of Spectral Bands	Spectral Wavelength Range†
3MI	PMI-M	MetOp-SG A series	Expected in 2024	9:30	12	VIS-NIR-SWIR (410-2130 nm)
MAP	MI-M	AOS-P1	Expected in 2030	13:30	TBD	VIS-NIR
PACE	HyperSpectral		Expected in 2024	13:30	>70	UV-VIS-NIR-SWIR (340-2130 nm)
ATLID	L	Earthcare	Expected in 2023	14:00	1	355 nm
CALIOP	L	CALIPSO	April 2006	13:30	2	532, 1064 nm
HSRL	L	AOS-P1	Expected in 2030	13:30	2	532, 1064 nm
DPC	PMI-M	GaoFen-5	May 2018, Sept 2021	98.12	8	VIS-NIR (443-910 nm)
EMI	IS	GaoFen-5	May 2018 and Sept 2021	13:30		240-790 nm
MAIA	PMI-M	OTB-2	Expected 2025	10:30	14	UV-VIS-NIR-SWIR
METImage (VII)	MI	MetOp-SG A series	Expected in 2024	9:30	20	VIS-NIR-SWIR-MWIR-LWIR (443 nm to 13 µm)
MISR	MI-M	Terra	December 1999	10:30	4	VIS-NIR (446, 558, 672, 866 nm)
MODIS	MI	Aqua	May 2002	13:30		
OCM	MI	OceanSat-2	September 2009	12:00	8	VIS-NIR
TROPOMI	IS	S5P	October 2017	13:30		UV-VIS-NIR-SWIR
VIIRS	MI	SNPP	October 2011	13:30 (50 min offset)	22	VIS-SWIR-MWIR-LWIR (0.41 µm to 12.01 µm)
		NOAA-20	November 2017			
S5/UVNS	IS	MetOp-SG A series	Expected in 2024	9:30		UV-VIS-NIR-SWIR

\*Sensor Class abbreviations:

L: lidar

MI: multispectral imager

MI-M: multispectral imager with multiple viewing directions

PMI-M: polarimetric multispectral imager with multiple viewing directions

IS: imaging spectrometer

MAP: Multi-Angle Polarimeter

†Wavelength range abbreviations:

Near-infra-red (NIR): 0.75-1.4 µm

Short-wave-infra-red (SWIR): 1.4-3 µm

Middle-wavelength-infra-red (MWIR): 3-8 µm

Long-wave-infra-red (LWIR): 8-15 µm

Table A 2. Characteristics of sensors on current and planned GEO satellites relevant for PM monitoring.

Sensor	Sensor Class*	Satellite(s)	Date Launched	Central Longitude (°)	Number of Spectral Bands	Spectral Wavelength Ranges†
ABI	MI	GOES-16	November 2016	-75.2	16	VIS-NIR-SWIR-MWIR-LWIR (0.47, 0.64, 0.86, 1.37, 1.6, 2.2, 3.9, 6.2, 6.9, 7.3, 8.4, 9.6, 10.3, 11.2, 12.3, and 13.3 μm)
		GOES-17	March 2018	-137.2		
AGRI	MI	FY-4	December 2016	105	14	VIS-SWIR-MWIR-LWIR
AHI	MI	Himawari-8	October 2014	140.7	16	VIS-SWIR- MWIR-LWIR (0.47, 0.51, 0.64, 0.86, 1.61, 2.26, 3.9, 6.19, 6.95, 7.34, 8.5, 9.61, 10.35, 11.2, 12.3, and 13.3 μm)
		Himawari-9	November 2016	140.7		
AMI	MI	GEO-KOMPSAT-2A	December 2018	128.2	16	VIS-NIR- MWIR-LWIR (0.48, 0.51, 0.64, 0.86, 1.38, 1.61, 3.8, 6.2, 6.9, 7.3, 8.6, 9.6, 10.4, 11.2, 12.3, 13.3 μm)
GEMS	IS	GEO-KOMPSAT-2B	February 2020	128.2	1000	UV-VIS (300-500 nm)
GOCI	MI	GEO-KOMPSAT-2A	December 2018	128.2	8	VIS-NIR (412, 443, 490, 555, 660, 680, 745, and 865 nm)
GOCI-2	MI	GEO-KOMPSAT-2B	February 2020	128.2	12	UV-VIS-NIR (380, 412, 443, 490, 510, 555, 620, 660, 680, 709, 745, and 865 nm)
Imager	MI	INSAT-3D	July 2013	82	6	VIS-SWIR-MWIR-LWIR (0.55-0.75 μm, 1.55-1.70 μm, 3.80-4.0 μm, 6.50-7.10 μm, 10.3-11.3 μm and 11.5-12.5 μm)
SEVIRI	MI	Meteosat-8 (MSG)	August 2002	41.5	12	VIS-NIR-SWIR-MWIR-LWIR (0.635, 0.81, 1.64, 3.92, 6.25, 7.35, 8.7, 9.66, 10.8, 12.0, 13.4 μm)
		Meteosat-9 (MSG)	December 2005	3.5		
		Meteosat-10 (MSG)	July 2012	9.5		
		Meteosat-11 (MSG)	July 2015	0		
TEMPO	IS		Expected in 2022	100		UV-VIS (290-490 nm, 540-740 nm)
S4/UVN	IS	MTG-S series	Expected in 2024	0	3	UV-VIS-NIR (305-400 nm, 400-500 nm, 750-775 nm)

\*Sensor Class abbreviations:

MI: multispectral imager

MI-M: multispectral imager w/ multiple viewing directions

PMI-M: polarimetric multispectral imager w/ multiple viewing directions

IS: imaging spectrometer

†Wavelength range abbreviations:

Near-infra-red (NIR): 0.75-1.4  $\mu\text{m}$

Short-wave-infra-red (SWIR): 1.4-3  $\mu\text{m}$

Middle-wavelength-infra-red (MWIR): 3-8  $\mu\text{m}$

Long-wave-infra-red (LWIR): 8-15  $\mu\text{m}$

12, 2018 as GOES-West. A notable difference between the ABI and the Himawari AHI is the missing green band (525 nm), due to which a true color image like those from MODIS and VIIRS cannot be made; NOAA, however, developed algorithms to create a pseudo green band and generates GeoColor images for users (Miller et al., 2020).

ABI aerosol products are expected to meet specific performance requirements for accuracy and precision, and also the availability at high temporal resolution (every 5 min) and spatial resolution (~2 km) increases the value to operational users. The GOES-R ABI also provides aerosol detection (smoke and dust mask), and various false color imagery to help operational end users interpret aerosol events of different types and scales in real time. This is a new feature of the ABI and was not available from the legacy GOES imagers. The aerosols/air quality relevant products currently generated and distributed to science and operational users are GeoColor imagery, dust RGB imagery, fire temperature imagery, fire detection and characterization (includes fire radiative power), smoke/dust detection, and aerosol optical depth.

NOAA has found that applying the heritage aerosol optical depth algorithms, developed for polar-orbiting sensors (e.g., MODIS) to geostationary imagers creates some challenges. In particular, NOAA found that significant effort needs to be devoted to understanding spectral surface reflectance relationships prescribed in most AOD algorithms. The relationships derived for MODIS or VIIRS (e.g., SWIR vs. red/blue bands) are not adequate for geostationary geometry; consequently, there can be a diurnal bias in retrieved ABI AOD. NOAA tested both its AOD product as well as the NASA DT algorithm applied to GOES-16 ABI and found that both products have a diurnal bias at some AERONET stations (Zhang et al., 2020). Overall, over land, based on an analysis of five months of data (August-December 2018), the GOES-16 ABI AOD has a mean bias of 0.01 compared to AERONET and a RMSE difference of 0.06. Despite these good performance metrics, in conditions of low AODs (background values), the diurnal bias is quite significant. NOAA developed an empirical bias correction algorithm that minimizes the bias and the technique can be applied to any geostationary satellite AOD algorithm (Zhang et al., 2020).

The GOES-16 ABI product is recommended for use from July 25, 2018 and the GOES-17 ABI product is recommended for use from January 1, 2019. The default “flex mode” scan mode of the GOES-16 satellite changed to Mode 6 (full disk every 10 minutes) on April 2, 2019. The GOES-17 ABI experienced an anomaly soon after launch which does not significantly impact the AOD product as the anomaly is associated with thermal wavelengths.

### **A1.3. The Himawari Series**

The Japan Meteorological Agency (JMA) launched the Himawari-8 geostationary meteorological satellite on 7 October 2014; the satellite became operational in July 2015. Himawari-9, which is identical to Himawari-8, was launched on 2 November 2016 and entered a backup status in March 2017 extending until 2022. The AHI onboard Himawari-8/9 is capable of frequent and flexible observations, providing full disk images of the earth every 10 minutes. AHI is also capable of target area observations, which provide regional imagery covering a 1000 km x 1000 km area every 2.5 minutes with flexibility for location changes. The nominal resolution for AHI bands is 1 km in the visible to near infrared and 2 km from the shortwave to thermal infrared, with the exception of the red band which is at 0.5 km resolution. AHI has 16 observation bands at 0.47, 0.51, 0.64, 0.86, 1.61, 2.26, 3.9, 6.19, 6.95, 7.34, 8.5, 9.61, 10.35, 11.2, 12.3, and 13.3  $\mu\text{m}$  (Bessho et al., 2016), which enables the retrieval of aerosol properties. The three wavelengths in the visible spectrum allow for true color imagery; however, AHI lacks a 1.38  $\mu\text{m}$  band sensitive to upper-level clouds. The AHI aerosol optical properties (AOP; AOD and AE) products have been developed and released from the Earth Observing Research Center (EORC) of the Japan Aerospace Exploration Agency (JAXA), which are available via the Himawari Monitor website

(<https://www.eorc.jaxa.jp/ptree>). The Level 2 aerosol products include full disk AOD and AE at a wavelength of 500 nm every 10 min in near real-time (Yoshida et al., 2018). The Level 3 product consists of hourly AODs derived from a combination of the Level 2 10-min AODs. Taking advantage of Himawari-8's high-frequency observations, the combination of Level 2 AODs enables minimization of the number of AOD pixels missing because of cloud and sun glint and removes degradation due to cloud contamination (Kikuchi et al., 2018). Himawari-8 AOD is utilized in the aerosol DA of the global aerosol model for the aeolian dust forecast.

#### **A1.4. The GEOKOMPSAT Series**

The AMI onboard the Geostationary Earth Orbit-Korea Multi-Purpose SATellite-2A (GEO-KOMPSAT-2A or GK-2A) is providing imagery every 10 minutes at 500 m (VIS Red), 1 km (VIS Green & Blue, NIR), and 2 km (SWIR to TIR) resolution. The AMI has 16 channels centered at visible (0.48, 0.51, 0.64  $\mu\text{m}$ ), NIR (0.86  $\mu\text{m}$ ), SWIR (1.38, 1.61  $\mu\text{m}$ ), MWIR (3.8, 6.2, 6.9, 7.3  $\mu\text{m}$ ), and TIR (8.6, 9.6, 10.4, 11.2, 12.3, 13.3  $\mu\text{m}$ ) wavelengths. AMI is basically the same instrument as ABI and AHI, but it is missing the 2.2  $\mu\text{m}$  band. This complicates the surface reflectance retrieval, but the YAER algorithm was applied using the 1.6  $\mu\text{m}$  band instead (Lim et al., 2018; Lim et al., 2021). Two types of algorithms were developed for AMI using AHI data as a proxy: one with the minimum reflectance method (MRM), and the other with estimation of surface reflectance (ESR) in the visible using the 1.6  $\mu\text{m}$  band. Comparison with AERONET for four months in each season of 2016 showed correlation coefficients of 0.78 to 0.89 (MRM) and 0.63 to 0.89 (ESR) over land and 0.87 to 0.95 (MRM) and 0.74 to 0.93 (ESR) over ocean. Merged products using MRM and ESR at both the surface reflectance level and AOD product level show improved statistics (Lim et al., 2018).

#### **A1.5. The MetoSat Series**

The EUMETSAT is the operational agency in Europe that partners with the European Space Agency (ESA) and launches weather satellites into geostationary orbits (Meteosat series). The current Meteosat Second Generation (MSG) series of satellites carry the Spinning Enhanced Visible and Infrared Imager (SEVIRI) with 12 channels (2 visible, 1 near infrared, one high resolution visible, and 8 thermal infrared) at  $\sim 3$  km nadir view resolution with 15 minutes revisit time. There are various SEVIRI AOD products developed by research groups available (e.g. Popp et al., 2007; Bernard et al., 2011; Zawadzka and Markowicz, 2014; Zawadzka-Manako et al., 2020). SEVIRI false color spectral composite data are exploited by the WMO dust and sand storm warning system (Martinez et al., 2009). The SEVIRI AOD product produced operationally in the Cloud-Aerosol-Water-Radiation Interactions (ICARE) data center (Bernard et al., 2011) is planned to be used in the CAMS global real-time forecast system. EUMETSAT's next generation of geostationary satellites, the Meteosat Third Generation (MTG) series, will carry the 16-channel Flexible Combined Imager (FCI). The FCI is similar to ABI, AHI, and AMI and offers imaging of aerosols at 10 to 15 minutes temporal refresh rate. The added value of assimilating FCI observations for monitoring aerosol has been shown in an Observing System Simulation Experiment (OSSE) by Descheemaeker et al. (2019).

#### **A1.6. The FengYun-4 (FY-4) Series**

The Chinese Meteorological Administration (CMA) operates its second generation of FY-4 series of satellites with an Advanced Geosynchronous Radiation Imager (AGRI), which is similar to ABI, AHI, and AMI. The AGRI instrument, launched on FY-4A in December 2016, became operational in June 2018. It has three visible, three shortwave infrared, and eight infrared channels. The red visible band has 0.5 km

resolution, similar to ABI, AHI, and AMI. The nominal nadir view resolution of the visible bands is 1 km, the shortwave infrared bands is 2 km, and the infrared bands is 4 km. The FY-4A instrument is a pathfinder mission for the series and is centered in CMA's East location at 105 °E with a 15-minute temporal refresh rate (Yang et al., 2017).

The FY-4B satellite, with an identical instrument suite to FY-4A but with improved spatial resolution, is expected to launch in the 2020s. CMA maintains two operational meteorological satellites, one in its East location (105 °E) and one in its West location (86.5 °E). When launched, FY-4B and FY-4C will provide continuous monitoring of AOD, aerosol detection, and various false color aerosol imagery into the 2040s. The FY4 series of satellites is expected to make a significant contribution to the GeoRing for aerosols and air quality. Zhang et al. (2019) presented a preliminary assessment of AGRI AOD retrievals via comparison to MODIS AOD and AHI AOD and found that the AGRI AOD correlates well with MODIS AOD at the 10% level and with AHI AOD at the 20% level for an optical depth of unity. The authors offered an opinion that dust and volcanic ash detections will improve with the FY-4B satellite because the AGRI instrument will be enhanced by improving the infrared channel resolution to 2 km and also by expanding the number of channels from 14 to 18. that the dust and ash detection algorithms utilize infrared channels and the expectation is that retrievals will improve with improved spatial resolution.

### **A1.7. The Geostationary Ocean Color Imager (GOCI) Series**

The GOCI onboard the GK-1 satellite, also known as the Communication, Oceanographic, and Meteorological Satellite (COMS), has provided hourly imagery since 2011. GOCI is the first multi-channel instrument in geostationary orbit with visible- and near-infrared channels centered at 412, 443, 490, 555, 660, 680, 745, and 865 nm, covering the East Asia region every hour with a spatial resolution of 500 m x 500 m. Aerosol optical properties including AOD, fine mode fraction (FMF), SSA, and aerosol type are retrieved in 6 km x 6 km resolution by the YAER algorithm (Lee et al., 2010; Choi et al., 2016; Choi et al., 2018). Higher spatial resolution data are also available at 500 m resolution, but with slightly higher uncertainty (Lee et al., 2017). GOCI aerosol product version 1 (Choi et al., 2016) was based on a look-up table (LUT) approach and minimum reflectance method which required observations over a 30-day search window. GOCI aerosol product version 2 (Choi et al., 2018) is now available with its near real-time processing and improved accuracy, which utilizes a climatological database from the multi-year GOCI dataset. GOCI aerosol products have been validated against AERONET and correlative satellite observations including those from MODIS and VIIRS (Xiao et al., 2016; Choi et al., 2016; Choi et al., 2018, Choi et al., 2019). GOCI aerosol products have been used widely in data assimilation (Park et al., 2014; Saide et al., 2014; Jeon et al., 2016; Lee et al., 2017; Pang et al., 2018; Jung et al., 2019; Lee et al., 2020; Saide et al., 2020), detection of long-range aerosol transport (Lee et al., 2019), analysis of diurnal variation (Lennartson et al., 2018), and the estimation of surface PM concentrations (Xu et al., 2015; Park et al., 2019; Goto et al., 2019; Tang et al., 2019; Park et al., 2020; She et al., 2020).

The GOCI-2 onboard the GK-2B satellite was launched in February 2020, with additional channels in the ultraviolet (380 nm) and visible (510 nm, 620 nm, 709 nm). GOCI-2 has full disk imaging once per day, in addition to hourly East Asian coverage, with a spatial resolution of 250 m, which will allow for retrieval of aerosol products at a spatial resolution of 3 km or better. The YAER algorithm has been modified for GOCI-2 and is under in orbit test (IOT) for official data release in 2022.

## **A2. Geostationary Spectrometers**

### **A2.1. GEO-KOMPSAT-2B GEMS**

The GEMS was launched onboard the GK-2B satellite in February 2020. The objective of GEMS is to monitor air quality at an unprecedented spatial and temporal resolution from a geostationary Earth orbit for the first time (Kim et al., 2020). GEMS is a step-and-stare scanning UV-visible imaging spectrometer with a spectral resolution of 0.6 nm (3 samples/band) covering 300-500 nm. A UV-enhanced two-dimensional charge coupled device (CCD) takes images with east-west scanning every hour, with one axis spectral and the other north-south spatial. The GEMS instrument covers the Asian region (~5 °S to 45 °N latitude, ~75 °E to 145 °E longitude), which has large emission sources and about half of the global population. On orbit calibrations include daily solar measurements and weekly LED light source linearity checks. With its sophisticated retrieval algorithms, the GEMS instrument provides column amounts of atmospheric pollutants (e.g., O<sub>3</sub>, NO<sub>2</sub>, SO<sub>2</sub>, HCHO, CHOCHO, and aerosol). Aerosol optical properties including AOD, SSA, aerosol effective height (AEH), and UVAI are retrieved by optimal estimation (OE) and an OMI-type algorithm (Go et al., 2020; Kim et al. Details can be found in Kim et al. (2020). After the ongoing IOT, GEMS products are planned to be released from early 2022.

### **A2.2. Tropospheric Emissions: Measurement of Pollution (TEMPO)**

NASA's TEMPO instrument, to be launched by a commercial communications satellite as a hosted payload into a geostationary orbit at 91 °W longitude near the equator in 2022, will be the US's first atmospheric composition mission. TEMPO is ultraviolet-visible spectrometer with two detectors (290-490 nm and 540-740 nm) capable of measuring air quality and climate relevant trace gases and aerosols in the atmosphere. While some trace gases will be total column only, some trace gases will have tropospheric column amounts separated from total column amount, and for some trace gases like ozone, the retrievals will include PBL amount as well. GEMS, UVN, and TEMPO are expected to form a GeoRing for air quality and atmospheric composition, observing trace gases and aerosols on urban to continental and diurnal to seasonal scales to study air quality, climate, and their linkages, as well as documenting exceptional events and hemispheric transport for monitoring applications.

There are no legacy instruments for TEMPO; it is a pathfinder mission and the first of its kind for the US. The heritage instruments are NASA's OMI, and OMPS. The first of the two TEMPO detectors has 290-490 nm hyperspectral coverage (0.6 nm resolution and product spatial resolution of 2.1 km x 4.5 km) and is similar to OMI. TEMPO will make measurements similar to OMI but on hourly timescales and with enhanced spatial resolution. The scientific algorithms for TEMPO are adapted from OMI's UV AI algorithm, but additional approaches using synergy between TEMPO and NOAA's GOES-16 ABI are being explored. The synergistic algorithm is expected to provide a suite of aerosol products including improved surface PM<sub>2.5</sub>. Data from GEMS and the Himawari-8 AHI are being used to test the new algorithms prior to the launch of TEMPO.

### **A2.3. Sentinel-4 UVN**

The geostationary Copernicus mission Sentinel-4 (S4) will provide hourly observations of the atmospheric composition over Europe mainly for air quality applications (Ingmann, 2012; ESA, 2017). The key products of the missions are NO<sub>2</sub>, O<sub>3</sub>, SO<sub>2</sub>, HCHO, CHOCHO, and aerosols. The S4 Ultraviolet-Visible-Near-Infrared (UVN) instrument is an imaging spectrometer with spectral bands in the UV, visible, near infrared. The spatial sampling distance is 8 km x 8 km at a reference location at 45 °N, where a resolution of about 9 km N/S x 12 km E/W will be achieved. A series of two S4 instruments will be carried on the geostationary Meteosat Third Generation-Sounder (MTG-S) satellites. The mission has been developed by ESA and will be operated by EUMETSAT. S4 is an element of the geostationary air

quality constellation together with GEMS and TEMPO. The FCI instrument on the MTG-I satellite provides co-located cloud and surface information that can be used in synergy with the S4/UVN measurements to optimize the aerosol retrievals.

S4 will provide several data products relevant to PM monitoring:

- The ALH algorithm will provide information on the vertical aerosol distribution extracted from the relative depth and spectral shape of the O<sub>2</sub>-A band. Within the algorithm, the aerosol layer is approximated by one single homogeneous layer with a vertical thickness of 50 hPa. The output parameters include the mid-pressure of this layer and the associated geometric height in (labelled as ALH) and the AOD at 760 nm. The retrieved ALH is reported to be accurate (within 1 km) for cases with AOD > 0.3, ALH > 1.5 km, and a surface reflectance < 0.4. The product will help characterize events with pronounced emission plumes but will be of limited use for characterizing near-surface particle pollution with low optical thickness.
- The UV AI product will provide an index for detecting elevated UV absorbing aerosol. It is derived from the spectral contrast in the UV. This index can be used for detecting and tracking plumes of aerosols (e.g. desert dust, volcanic ash, smoke).
- A joint surface and aerosol product will be generated on a daily basis from temporally aggregated reflectance data in a set of spectral window bands. The product is based on the GRASP (Dubovik et al., 2014) algorithm. The output includes hourly data for surface bidirectional reflectance, AE (450-755 nm), and AOD at 342, 368, 410, 443, 490, and 755 nm.
- The NO<sub>2</sub> and SO<sub>2</sub> products will provide vertically integrated column densities of these trace gases derived from their absorption signatures in the UV-visible spectral range. Local formation rates of nitrate and sulfate aerosol particles can be predicted based on local concentrations of the precursor gases including NO<sub>2</sub> and SO<sub>2</sub>. For estimating the contribution of these processes to near-surface PM, additional information on the vertical distribution of the precursor gases is needed that is not provided by the satellite.

### *A3. Polar-Orbiting Imagers*

#### **A3.1. MODIS**

There are two MODIS instruments observing the Earth “system” on Terra since early 2000 and on Aqua since 2002. Offering wide swath views (~2300 km), each MODIS observes portions of the Visible, NIR, SWIR and TIR spectrum with nearly global daily coverage. MODIS offers measurements of solar reflectance in 20 spectral bands (0.41-2.11 μm) and Earth’s emittance in 16 spectral bands (3.9-14.2 μm). Most bands are at 1 km spatial resolution (nominal, at nadir view), however, five solar reflectance bands (SRB) are at 0.5 km, and two are at 0.25 km. The higher-resolution SRB (Bands #1 to #7 or B1-B7), having low gain settings to observe a wide dynamic range, are centered near 0.47 μm (blue), 0.55 μm (green), 0.66 μm (red), 0.86 μm and 1.24 μm (NIR), as well as 1.64 μm and 2.13 μm (SWIR). The lower resolution SRB bands (B8-19) include 0.412 μm (known as Deep Blue), bands with high gain settings (e.g. 0.443, 0.488, 0.531, 0.551, 0.667, 0.678, 0.748 and 0.869 μm) that were intended to measure the narrow dynamic range of ocean color, and three bands around 0.93 μm that are used to measure water vapor. There is one more SRB (B26) centered near 1.38 μm, which is in a water vapor absorption band, sensitive to detecting high altitude cirrus clouds. In addition to having many new bands compared to earlier sensors (such as AVHRR), the MODIS ground, flight and science teams have developed new methods for maintaining the stability of orbit (keeping the nominal 10:30 AM and 13:30 PM equator crossing times), and stability of calibration through on-board and vicarious calibration methods. This attention to orbit/calibration details has allowed the MODIS observational data record to be a possible basis of the long-term climate data record. The MODIS teams have also embraced the idea

of “Collections”, datasets encompassing the entire time series, using different versions of calibration and retrieval algorithms that evolve over time.

There is no single “aerosol” retrieval algorithm for MODIS. Prior to launch, the MODIS science team was separated into three disciplines, “ocean,” “land,” and “atmosphere,” and the separation has generally remained. For retrieval of Earth system variables, starting with land or ocean surface reflectance, aerosols provide obstacles and uncertainties for “atmospheric correction”. Therefore, aerosol retrieval is performed, but aerosol is considered a “secondary” product except for in MAIAC algorithm. Under the atmosphere umbrella, however, an aerosol retrieval product was a specific requirement at launch. This discussion focuses on the “atmosphere” aerosol products known as MxD04\_L2 (where the x represents “O” for the MODIS on Terra, and “Y” for the MODIS on Aqua, and L2 is for “Level 2”), and the MAIACMCD19A2 product offered under the ‘land’ discipline.

The products of MxD04\_L2 are provided by combinations of three different algorithms, at a nominal spatial resolution of 10 km x 10 km. Physically motivated by the general auto-correlation of in situ observations of aerosol (e.g. Anderson, 2003), the degraded spatial resolution also compensates for the relatively low SNR of single pixels, and allows for filtering/masking of cloudy and other non-retrievable pixels. The two algorithms considered “Dark Target” are directly based on the at-launch algorithms. These are separated into over-land (DT-L) and over-ocean (DT-B), where the Dark Target refers to using wavelengths where the land surface appears dark compared to the reflection of the aerosol above. Both DT algorithms make use of B1-7 (the higher spatial/lower gain bands), but there are differences in the way these bands are used. As DT-L was developed to retrieve AOD over vegetation and dark-soils (dark in the blue, red and SWIR wavelengths), this left a gap over arid and non-vegetated surfaces. The Deep Blue (DB) algorithm was developed in the early 2000s and makes use of the Deep Blue band (0.41  $\mu\text{m}$ ), which has lower reflection from desert surfaces. Both DT and DB algorithms (including assumed aerosol and surface properties, pixel selection and masking, inversion mathematics, radiative transfer, etc.) have significant differences in the assumptions and techniques. In the end, however, both algorithms provide estimates of total AOD in the mid-visible (e.g. 0.55  $\mu\text{m}$ ), along with a number of other aerosol parameters (e.g. fine mode fraction, AE, and/or SSA). In the current Collection (known as Collection 6.1), products of all three algorithms (DT-O, DT-L, and DB-L) are provided within the same MxD04 granule (5-minute time aggregation) file. As DT-L and DB-L both retrieve on vegetated (“dark”) surfaces, there are often two products over the same 10 km box.

There are strengths and weaknesses of each algorithm, and the accuracy of the retrieved product varies as a function of the scene being observed. The golden standard for product accuracy is global and site-by-site comparison with data from ground-based sun photometers (e.g. AERONET), and both DT and DB algorithms claim successful retrievals on a global scale. For example, DT-L claims that 66% of all global retrievals (that are collocated with AERONET within approximately  $\pm 15$  minutes and averaged over a 25 km radius from the AERONET site) match AERONET values of total AOD to within  $\pm (0.05 + 15\%)$ . Similar envelopes for global Expected Error are given for DT-O and for DB-L, however there may be additional functional constraints based on observation geometry or other variables. The DT and DB teams, however, have noted that these validations are only for collocated observations, as there is no easy way to quantify the accuracy of the retrieved MODIS AOD products when there is no collocated ground-truth.

Beginning in Collection 6 (data processing in 2013), the MxD04\_L2 product included a merge of DT-L and DB-L over land based on climatological Normalized Difference Vegetation Index (NDVI based on NIR and Red bands), where the DB value would be used for surfaces with low NDVI (non-vegetated), the DT value for surfaces with high NDVI (vegetated), and an average of the two for moderate NDVI conditions. However, even with the possibility of multiple retrieval techniques on any surface, only approximately 10-20% (depending on season) of the global observed 10 km boxes have valid aerosol

retrievals. Neither DT nor DB retrievals are made for scenes that are cloudy, ice/snow covered, or likely to be contaminated by sun-glint reflection.

MODIS DT 3 km AOD is a separate product created for air quality applications, but it is lesser used and the uncertainties for an individual retrieval are larger (reduced signal/noise and ability to mask/filter pixels).

The swath-based processing described above is associated with uncertainties because at the same location the footprint changes with the orbit and scan angle. At the same time, aerosol retrievals at high spatial resolution required for atmospheric correction and air quality research, need a good knowledge of the surface reflectance, in particular over heterogeneous urban surfaces. For this reason, the Multi-Angle Implementation of Atmospheric Correction (MAIAC) algorithm processing starts with gridding the TOA L1B MODIS 0.5km measurements to 1km grid. This way, observations from different orbits closely represent a given 1km grid cell allowing us to use a time series analysis to characterize surface properties for each grid cell. MAIAC uses a dynamic minimum reflectance method (Lyapustin et al., 2018) to characterize spectral surface ratios for aerosol retrieval. For each 1km grid cell, MAIAC also stores spatial and thermal contrasts, sub-pixel variability from 500m channels, full spectral BRDF retrieved using multi-angle observations accumulated for up to 16-day period, etc. A good knowledge of the surface helps MAIAC achieve a high accuracy cloud and snow detection and retrieve AOD at high 1km resolution globally over land except snow/ice. Due to its reliable good retrieval accuracy (~10-15%) and high 1km resolution regardless of the MODIS view zenith angle, which provides coverage in partly cloudy conditions when AOD from the coarse resolution standard aerosol products is often missing, MAIAC AOD has been widely adopted for PM predictions and air quality research. Many papers reporting validation of MAIAC AOD against AERONET show its reliable performance at a single 1km grid cell level, though depending on local aerosol variability the best performance metrics are often achieved at 3-7km or coarser scales.

MAIAC reports AOD at 1 km resolution on the global Sinusoidal grid (product MCD19A2), along with the 1km column water vapor and smoke plume injection height near detected active fires. The surface reflectance (BRF, or bidirectional reflectance factor) is reported in MCD19A1, and spectral BRDF model for bands 1-8 is in file MCD19A3. The upcoming MAIAC Collection 6.1 features a number of improvements, including updated regional aerosol models which will remove the known underestimation of MAIAC AOD at high AOD for the biomass burning smoke. MAIAC C6.1 also provides a gap-filled spectral BRDF, NDVI and snow properties (snow fraction and grain size) for detected snow at 1km resolution, which is a useful resource for the satellite data processing by other algorithms, data assimilation systems, for PM predictions etc.

### **A3.2. MISR**

The MISR instrument aboard the NASA Terra satellite has acquired continuous, near-global imagery about once per week for over two decades, beginning in late February 2000. MISR is comprised of nine cameras, viewing in an along-track configuration at angles of  $\pm 70.5^\circ$ ,  $\pm 60.0^\circ$ ,  $\pm 45.6^\circ$ ,  $\pm 26.1^\circ$ , and nadir, in each of four spectral bands centered at 446, 558, 672, and 866 nm (Diner et al., 1998). MISR is in a sun-synchronous orbit, with a 10:30 AM equatorial crossing time. As MISR is a passive imager, these data provide constraints on total-column AOD, and column-effective values of aerosol size, shape, and light-absorption properties under favorable retrieval conditions (Kahn and Gaitley, 2015). Aerosol retrievals can be performed at spatial resolutions up to individual 1.1 km pixels with a research algorithm (Limbacher and Kahn, 2014), though the MISR version 23 Standard product provides values at 4.4 km horizontal resolution. For good quality aerosol intensive-property retrievals, mid-visible AOD generally must exceed 0.15 or 0.2, and best retrieval results are obtained over darker, more uniform surfaces. However, the strengths of MISR include particle-type discrimination and steep slant-path

viewing that enhances the atmospheric signal over that of the surface. As such, aerosol air mass types can be mapped over complex urban areas provided the AOD is sufficiently high (e.g., Patadia et al., 2013).

For air quality applications, MISR's column-effective information must be applied as partial constraints on the quantities of greatest interest, nose-level, size-resolved and speciated aerosol mass concentration (e.g.,  $PM_{2.5}$ ). Aerosol transport modeling has been used to parse MISR AOD vertically for this application, to produce global (e.g., van Donkelaar et al., 2010; Hammer et al., 2020) or regional (e.g., Li, 2020) estimates of near-surface aerosol concentration. MISR constraints on particle shape were first used by Liu et al. (2007) to distinguish non-spherical mineral dust from spherical particles, with a transport model providing the vertical distribution and more detailed speciation within a regression modeling framework. More recent work has made use of MISR-retrieved particle size, shape, and light-absorption results combined with surface measurements, either in a statistical approach (e.g., Franklin et al., 2018), or to constrain a regional air quality physical model (Friberg et al., 2018). With these approaches, the model is weighted toward surface stations where available, and more heavily toward the MISR AOD and particle-type constraints progressively downwind. Further, deSouza et al. (2020) present a method that uses MISR constraints on particle size distribution to extrapolate size-resolved surface particle concentrations obtained from low-cost optical particle counters (OPCs); this makes it possible to capture the typical peak in pollution particle sizes that the OPCs miss, due to limited sampling ability for particle sizes below about 0.5  $\mu\text{m}$  in diameter, enhancing the value of low-cost OPC sensors for monitoring air quality in underserved regions.

### **A3.3. Visible Infrared Imaging Radiometer Suite (VIIRS)**

NOAA currently has two VIIRS instruments in orbit – one on the SNPP satellite launched on 28 October 2011 and one on the NOAA-20 satellite launched on 18 November 2017. The two VIIRS instruments continuously observe the earth with a 50-minute time difference. The VIIRS instrument is a follow-on to MODIS, which has been the workhorse for aerosol remote sensing for nearly two decades. Several instrument design changes, such as pixel resolution and limiting the pixel growth at the edge of the scan, have allowed for several improvements to VIIRS versus MODIS observations. The VIIRS aerosol products are derived from measurements made during the sunlit portion of the day. The VIIRS instruments have 22 bands with 16 of the bands in the visible to long-wave infrared at moderate resolution (750 m), five bands at imager resolution (375 m) covering 0.64  $\mu\text{m}$ , 0.86  $\mu\text{m}$ , 1.6  $\mu\text{m}$ , 3.7  $\mu\text{m}$ , and 11.4  $\mu\text{m}$ , and one broad Day-Night Band (DNB) band centered at 0.7  $\mu\text{m}$ . The NOAA VIIRS AOD algorithm over the ocean is based on MODIS heritage and over land the algorithm derives AOD for both dark targets as well as bright surfaces (Laszlo and Liu, 2016; Zhang et al., 2016; Huang et al., 2016). The bright surface aerosol optical depth algorithm developed by NOAA is unique to VIIRS and has been shown to perform well (Laszlo and Liu, 2016). In addition to AOD, NOAA also generates aerosol detection that qualitatively identifies the presence of smoke or dust in the atmosphere. This product is unique to VIIRS and is based on the absorbing aerosol index and dust smoke discrimination index, originally developed for MODIS (Ciren and Kondragunta, 2014; Zhang et al., 2018).

NOAA applies a modified version of the van Donkelaar et al (2012) algorithm to scale AOD to surface  $PM_{2.5}$  for air quality applications in the US (see Section 4.2 for details). The SNPP VIIRS AOD product has been extensively validated by comparing it to AERONET AODs, and the VIIRS 550 nm AOD is shown to have a global bias of  $-0.046 \pm 0.097$  for AODs over land  $< 0.1$  and for AODs between 0.1 and 0.8, the bias is  $-0.194 \pm 0.322$ . In the US, for VIIRS AODs ranging between 0.1 and 0.8, the bias is  $-0.008 \pm 0.089$  and for AODs  $> 0.8$ , the bias is about  $0.068 \pm 0.552$  (Zhang and Kondragunta, 2021).

### A3.4. METImage

EUMETSAT and ESA have partnered to develop aerosol imagers such as METImage (also referred to as VII for Visible Infrared Imager) to fly on a series of MetOp-SG A satellites. The METImage is a VIIRS like instrument with multiple visible and infrared bands that will fly in a mid-morning orbit around the globe. The instrument is expected to launch in 2023 as the current era of MetOp series comes to an end. METImage has 20 spectral bands ranging from 443 nm to 13  $\mu\text{m}$  and takes measurements at 500 m spatial resolution. The spectral bands are similar to VIIRS except for the 412 nm band, which is missing on METImage. As a result, METImage will have gaps in global coverage of the AOD and aerosol detection (smoke/dust mask) products; for AOD retrievals over bright surfaces, both MODIS and VIIRS instruments use the 412 nm measurements as the surface is relatively dark in that channel. According to the METImage science plan ([https://www-cdn.eumetsat.int/files/2020-04/pdf\\_science\\_epssg\\_metimage\\_plan.pdf](https://www-cdn.eumetsat.int/files/2020-04/pdf_science_epssg_metimage_plan.pdf)), METImage will fly along with the Sentinel-4 UVN instrument on the same satellite and thus will take advantage of synergy between UVN and METImage to retrieve a suite of aerosol properties such as optical depth, aerosol layer height, single scattering albedo, and aerosol type.

### A3.5. MAIA

While most health effects studies have focused on the effects of exposure to the mass concentration of  $\text{PM}_{2.5}$  and  $\text{PM}_{10}$  (e.g., Pope and Dockery, 2006; US Environmental Protection Agency, 2019), the relative toxicity of different compositional mixtures of PM is less well understood (Bell et al., 2007; Adams et al., 2015). This is due in part to the sparseness of surface monitors that measure chemical speciation (US Environmental Protection Agency, 2013). The National Research Council (2004), WHO (2007), and scientific literature (e.g., Li et al., 2019) have stressed the importance of improving our understanding in this regard.

Satellite remote sensing, combined with surface data and chemical transport model information, offers a means of filling in the spatial gaps between surface monitors, thereby enabling improved estimates of human exposure to different types of particulate air pollution. Motivated by this objective, the Multi-Angle Imager for Aerosols (MAIA) investigation was selected as part of NASA's Earth Venture Instrument program in 2016 (Liu and Diner, 2017; Diner et al., 2018). MAIA defines particle type as aerosol mixtures having different proportions of sulfates, nitrates, organic carbon, elemental carbon, and dust.

A key element of the MAIA investigation is a satellite-based instrument that measures the radiance and polarization of sunlight scattered by the Earth's atmosphere and surface. The instrument contains a pushbroom spectropolarimetric camera capable of providing multi-angle imagery. Unlike MISR, which contains multiple cameras pointed at discrete along-track view angles, MAIA's single camera is mounted on a gimbal assembly that can point it in two axes. The along-track (scan) gimbal has a  $\pm 60^\circ$  range of motion, while the cross-track (pan) gimbal and camera field of view provide a  $\pm 48^\circ$  cross-track field of regard. The targeting nature of the MAIA instrument enables routine multi-angle observations of a globally distributed set of study sites. The pan capability permits access to targets that are not directly situated on the sub-spacecraft track, making it possible to observe targets 3-4 times per week. Over most targets, images of the same area will be observed at a set of discrete view angles in a "step-and-stare" sequence (see Figure A1). MAIA is to be hosted aboard the General Atomics Orbital Test Bed (OTB)-2 spacecraft in an ascending, sun-synchronous (near-polar) orbit at 740 km altitude and 10:30 AM equator crossing time. Launch is planned for mid-2025 for a baseline mission duration of 3 years.

The MAIA instrument (Figure A2) uses several remote sensing methodologies. In addition to the multi-angular capability provided by the gimbal, the camera has 14 spectral bands spanning the UV, VNIR, and SWIR. VNIR and SWIR spectral bands help discriminate particle size, while the UV provides sensitivity to absorption. Multi-angle polarimetry provides sensitivity to particle size and compositional proxies such as refractive index. Polarimetric imaging is acquired in 3 of MAIA's 14 spectral bands by using a specialized modulation technique designed for high accuracy (Diner et al., 2007, 2010).

The MAIA instrument operations system defines four different types of target areas: Primary Target Areas (PTAs), Secondary Target Areas (STAs), Calibration/Validation Target Areas (CVTAs), and Targets of Opportunity (TOOs). Primary Target Areas (PTAs) are major population centers designated for conducting epidemiological investigations by the MAIA Science Team, and measure 352 km (E/W) x 420 km (N/S). A dozen PTAs in North America, Europe, Africa, Middle East, and Asia are the main focus of the investigation. Privacy-protected health data geolocated by home addresses, postal codes, or census block groups will be used to examine linkages to acute, sub-chronic, and chronic exposure to total and speciated PM. STAs are regions of interest for air quality or other aerosol and cloud research. CVTAs will be observed routinely for instrument calibration, stability monitoring, and product validation. Acquisitions over TOOs may be acquired over episodic events such as major wildfires or dust storms.

Aerosol retrievals will be performed in ground data processing. Output parameters include total AOD; fractional AODs associated with two size modes (each corresponding to a lognormal distribution of particles), spherical, nonspherical, absorbing, and nonabsorbing aerosols; size parameters and complex refractive indices of the two aerosol modes; and phase function asymmetry parameter. An optimal estimation strategy with constraints on spatial and spectral smoothness will be used (Xu et al., 2017).

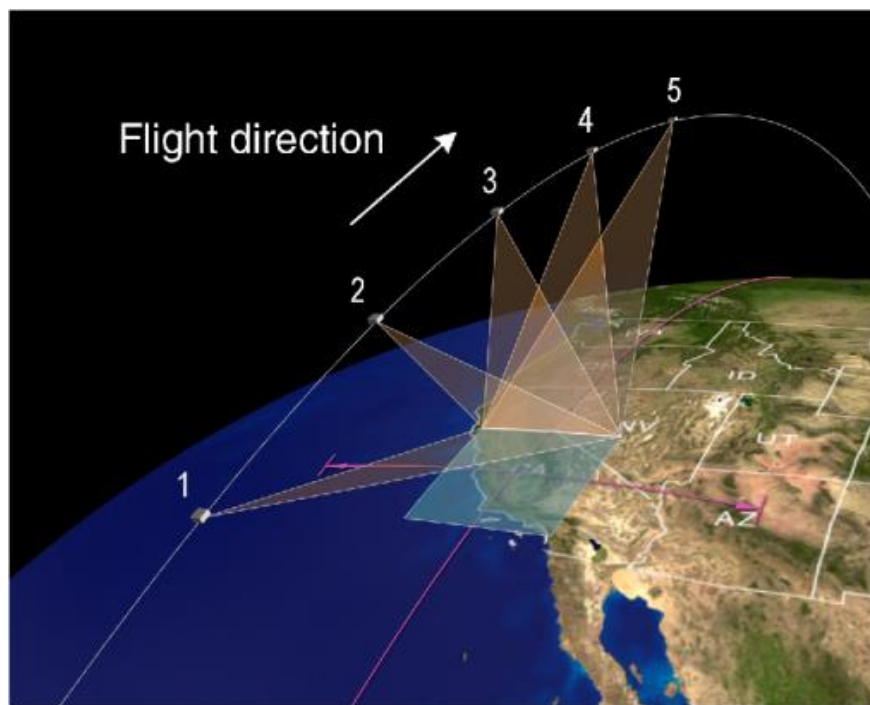


**Figure A 1.** Example MAIA step-and-stare sequence, showing the case of 5 discrete view angles.

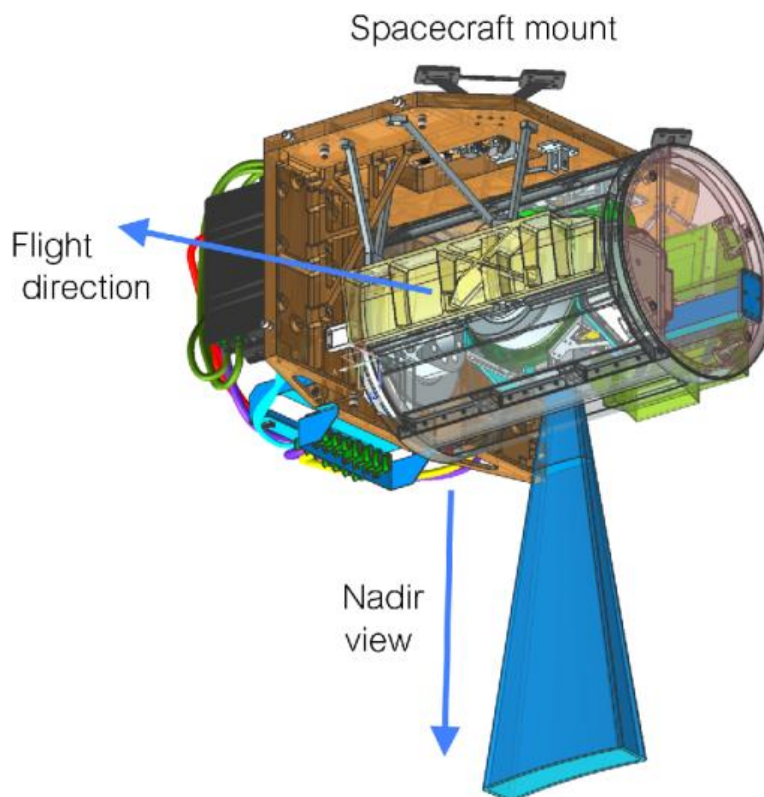


**Figure A 2.** Layout of the MAIA satellite instrument.

### A3.6. OceanSat

OceanSat-1, launched in 1999, is the first Indian satellite primarily built for ocean applications in a sun-synchronous orbit. The satellite consists of the Ocean Colour Monitor (OCM) sensor, which provides multi-spectral imagery at a ground resolution of 360 m via eight narrow spectral bands in the VNIR region ( $\mu\text{m}$ ): B1: 0.402-0.422, B2: 0.433-0.453, B3: 0.480-0.500, B4: 0.500-0.520, B5: 0.545-0.565, B6: 0.660-0.680, B7: 0.745-0.785, and B8: 0.845-0.885. The sensor is mainly designed to cater to ocean applications globally and accordingly, it has high radiometric sensitivity with a large dynamic range. AOD at 0.765  $\mu\text{m}$  (Das et al., 2002, 2003; Dey et al., 2002) and 0.865  $\mu\text{m}$  (Chauhan et al., 2009) over oceans are retrieved using OCM data, assuming the ocean surface perfectly dark in near infrared (NIR) wavelengths. The inter-comparison of OCM AOD retrievals with AOD from SeaWiFS and MODIS show good agreement, with linear correlation coefficients of 0.88 and 0.75, respectively (Mishra et al., 2008). The mean percentage difference indicates that OCM AOD is +12% higher compared to SeaWiFS and +8% higher compared to MODIS. The mean absolute percentage between OCM AOD and SeaWiFS is found to be less (16%) compared to OCM and MODIS (20%) (Mishra et al., 2008). However, the quality of the AOD product is enhanced with an improved algorithm using OceanSat-2 data, which was a continuity mission to the applications of OceanSat-1.

OceanSat-2 is the second satellite in the ocean series, which was successfully launched in September 2009 with the same OCM sensor but with improved channels. AOD at 865 nm over the oceans is regularly retrieved from OCM on-board the OceanSat-1 (1999-2010) and OceanSat-2 (2010-present) satellites. Due to the unavailability of short-wave infrared channels on OCM, the AOD retrieval over land is challenging using existing DT and enhanced DB aerosol retrieval algorithms (Levy et al., 2017; Hsu et al., 2013). Recently, an advanced algorithm to retrieve AOD and fine mode fraction at

spatial resolution of 750 meters utilizing OCM measurements in three visible and one NIR bands over land has been developed (Mishra et al., 2021). The OCM AOD product over land is operationally available on the VEDAS air quality portal (<https://vedas.sac.gov.in>) since December 2020. The validation of OCM AOD retrievals over land with in-situ AOD acquired at different AERONET station located in India show good agreement, with linear correlation coefficients of around 0.8 (Mishra et al., 2021).

In addition, the Indian Space Research Organization (ISRO) is envisaging launching another OceanSat class satellite in the near future to provide service continuity for the operational OCM data from OceanSat-2; this new satellite will improve the repeatability of OCM AOD measurements.

#### *A4. Polar-Orbiting Spectrometers*

##### **A4.1. Sentinel-5P TROPOMI**

TROPOMI has been flying on the Sentinel-5 Precursor (S5P) satellite since 13 October 2017. TROPOMI is a high spectral resolution spectrometer covering eight spectral windows from the UV to SWIR, and operating in a push-broom configuration, with a 2600 km swath width at a nadir resolution 5.5 km x 3.5 km. The objective of the mission is operational monitoring by the ESA of trace gas (O<sub>3</sub>, NO<sub>2</sub>, SO<sub>2</sub>, CO, CH<sub>4</sub>, and CH<sub>2</sub>O) concentrations for atmospheric chemistry and climate applications. ESA aerosol products include UV AI and O<sub>2</sub>-A band ALH. Currently, no ESA-produced AOD products are available from TROPOMI observations.

The NASA OMI aerosol retrieval algorithms for cloud free conditions (OMAERUV; Torres et al., 2007, 2013, 2018), and for above-cloud aerosols (OMACA; Torres et al., 2012; Jethva et al., 2018) have been combined into a single NASA research aerosol algorithm (TropOMAER) and applied to TROPOMI observations (Torres et al., 2020). TropOMAER standard aerosol products are the UV Aerosol Index (UVAI), total column AOD and SSA. As discussed in a recent evaluation of retrieval results (Torres et al., 2020), TropOMAER improvements in relation to the heritage OMAERUV algorithm are associated with TROPOMI's dramatic improvement in spatial resolution, and the availability of a VIIRS-based cloud mask that facilitates the identification of minimally cloud-contaminated TROPOMI pixels suitable for aerosol AOD/SSA retrieval.

The UV AI parameter is TROPOMI's aerosol product most relevant to PM estimation. The magnitude of the aerosol UV AI signal depends on AOD, ALH, and aerosol absorption exponent (AAE) of UV-absorbing aerosols such as carbonaceous and desert dust. The ALH dependence can be particularly useful in the identification of aerosol layers above the PBL. As shown in Figure 1 of Torres et al. (2020), absorbing aerosols at 3 km or lower typically yield UV AI values lower than about 4 and AOD lower than about 2. Thus, the UV AI magnitude can be used as a first initial step to separate aerosols above the PBL (generally long range transported smoke and desert dust aerosols) from aerosols in the PBL.

##### **A4.2. Sentinel-5 UVNS**

The Copernicus mission Sentinel-5 (S5) will provide observations of the atmospheric composition with daily global coverage for air quality and climate applications (Ingmann, 2012; ESA, 2019). The key products of the mission are NO<sub>2</sub>, O<sub>3</sub>, SO<sub>2</sub>, HCHO, CHOCHO, CO, CH<sub>4</sub> and aerosols. The S5 instrument is an imaging spectrometer with spectral bands in the UV, visible, near infrared, and shortwave infrared (UVNS). The spatial sampling distance will be close to 7 km x 7 km at nadir. A series of three S5 UVNS instruments will be launched on the LEO MetOp-SG A satellites. The mission is developed by ESA and will be operated by EUMETSAT. The first MetOp-SG A satellite with S5 UVNS on board is expected to be launched in 2023. S5 UVNS will provide several data products with information relevant to particle pollution, similar to S4 UVN and S5P TROPOMI, including Level 2 ALH, exploiting the

O<sub>2</sub>-A band, and UV AI; these products are common to S4, S5 and S5P and will be generated using very similar algorithms. The S5 AOD product will be generated using an algorithm based on the OMAEROUV scheme (Torres et al., 2018) that is extended to the visible.

#### A4.3. GaoFen-5 EMI

The objective of the Environmental Trace Gas Monitoring Instrument (EMI) flies on board the GaoFen-5 (GF-5) satellite as part of the Chinese civilian remote sensing satellite program GaoFen. Two GF-5 satellites with EMI on board have been launched in May 2018 and in September 2021. Each EMI instrument has a design lifespan of 8 years. Being primarily designed to measure trace gases such as NO<sub>2</sub>, SO<sub>2</sub>, and O<sub>3</sub>, EMI has similar aerosol observing capabilities as other imaging spectrometers. The strongest benefit is expected in the synergetic use of aerosol information from EMI and the Directional Polarization Camera (DPC, see Section 5.1).

### A5. Polarimeters

#### A5.1. GaoFen-5 DPC

The Directional Polarization Camera (DPC) has 8 channels between 443 nm and 910 nm with two visible bands and one near infrared band for polarization. The instrument sees the same scene from 9 different viewing angles. From these measurements, spectral AOD, AE, non-sphericity of particles, and fine mode AOD are derived. Xie et al. (2019) analyzed and applied the DPC retrievals to a smog event during 23-30 November 2018 and published the first global fine model aerosol optical depth map (Figure A3) and also reported that surface PM<sub>2.5</sub> values estimated from fine mode AOD are more accurate than those derived from total AOD.

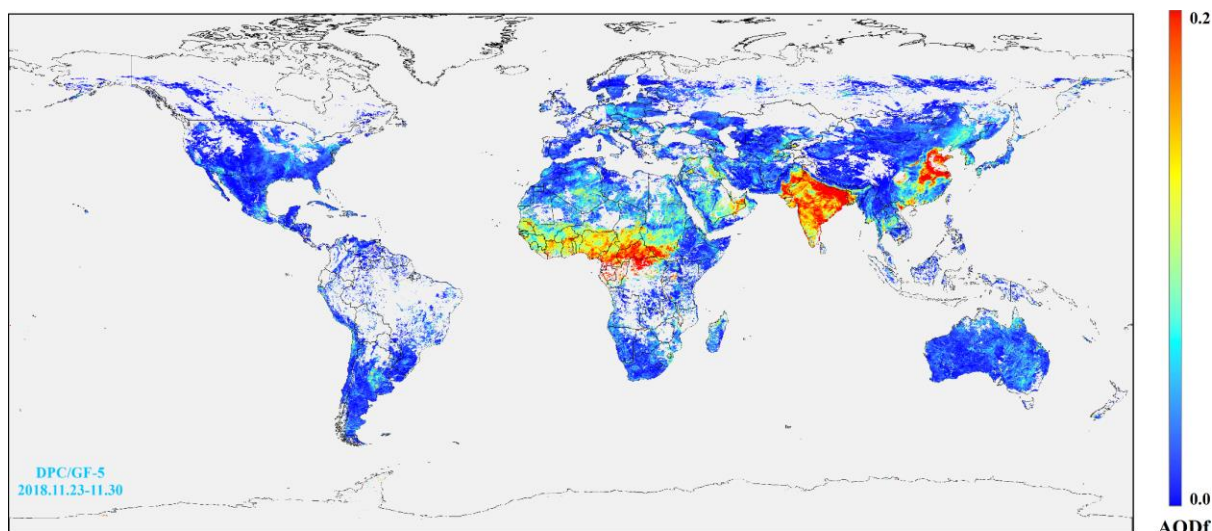


**Figure A 3.** DPC fine mode aerosol optical depth at 865 nm at 3.3 km x 3.3 km resolution for 23-30 November 2018.

The validation of polarimeter data needs to be carried out prior to recommending the use of the products in daily applications. This work is being done in earnest for the soon to be launched 3MI instrument by EUMETSAT (see Section A5.2). Most polarimeters fly in formation with imagers and

spectrometers, either on the same satellite or on a satellite flying ahead or behind in the same orbit. The GaoFen-5 DPC instrument flies on the same platforms (GF-5) as the Environmental Mapping Instrument (EMI), whose spectral coverage is in the ultraviolet to visible and provides additional aerosol information that can be used in conjunction with DPC aerosol properties.

### **A5.2. Metop-SG 3MI**

The second generation meteorological satellites to be launched by EUMETSAT in 2023 into a mid-morning orbit with an equator crossing time of 9:30 AM will include a multi angle, multi viewing (14 views), multi spectral imager with three polarizations (3MI) to observe and characterize aerosol properties. The instrument will have 12 wavelengths in the spectral window from 410-2130 nm with a spatial resolution of 4 km x 4 km. The instrument will be able to identify aerosol layer height, aerosol type, aerosol over clouds, fine mode fraction, aerosol optical depth, and aerosol absorption optical depth. In contrast, a visible-near infrared imager like MODIS or VIIRS is able to only provide optical depth and some qualitative information on aerosol type. 3MI's measured signal will come from measuring polarized light at different angles and wavelengths; spectral dependencies of various optical properties such as phase function and refractive index will be used to disentangle the signal and obtain information such as aerosol size distribution, composition, and layer height.

EUMETSAT is planning to apply the GRASP algorithm, which is a versatile code that can be applied to a variety of satellite and in situ sensors' spectral radiance measurements (Dubovik et al., 2011). The GRASP algorithm has been applied to polarization sensors such as POLDER and has been shown to provide accurate retrievals of single scattering albedo, size distribution, refractive index, in addition to total and absorption optical depths. Validation of various aerosol properties derived from POLDER-3 using AERONET data over China showed that the fine mode AOD retrievals were more accurate than total AOD (Tan et al., 2019). EUMETSAT is currently testing the GRASP algorithm on simulated 3MI data and NOAA is working with EUMETSAT in the evaluation process of proxy simulated retrievals.

### **A5.3. Copernicus Carbon Dioxide Monitoring (CO2M)**

Expected to be launched in 2025, the CO2M is a Copernicus mission consisting of three instrument suites: a combined CO<sub>2</sub>/NO<sub>2</sub> instrument, a multi-angle polarimeter, and a cloud imager. AOD, ALH, and other aerosol optical and physical properties will come from the polarimeter whose measurements will help in the atmospheric correction for CO<sub>2</sub> retrievals. Though the main purpose of the mission is to map urban area and power plant sources of CO<sub>2</sub> at 4 km<sup>2</sup> spatial resolution with a precision of 0.7 ppm or less, aerosols will be simultaneously retrieved using radiance and degree of linear polarization measurements at four different viewing angles and seven wavelengths (410, 443, 490, 555, 670, 753, 865 nm) from a polarimeter. The multiple cameras and multiple angles along track with 12 cross-track oriented detectors will allow for 1 km<sup>2</sup> aerosol retrievals. Full global coverage is expected every 10 days (<https://space.oscar.wmo.int/instruments/view/map>).

### **A5.4. CALIOP**

The need to fully map aerosols across the globe, including vertical profiles, propelled space agencies to consider flying an active lidar. NASA launched the first aerosol specific lidar, CALIOP on CALIPSO in 2006. CALIOP, with its two 532 nm channels (parallel and perpendicular polarization) and 1064 nm channel, is capable of retrieving aerosol extinction profiles and aerosol type using

depolarization ratio and color ratio information. The vertical resolution of the products is about 30 m and retrievals from the surface to 40 km are possible.

NASA also launched the Cloud and Aerosol Transport System (CATS) instrument on International Space Station with three wavelengths (355 nm, 532 nm, and 1064 nm) where polarized return signals from the atmosphere were measured. The CATS team adapted the CALIOP algorithms to process the data and kept the products consistent, but the instrument malfunctioned within the two years of launch; it operated successfully from January 2015 to October 2017.

The Atmospheric LIDAR (ATLID) on the Earthcare satellite is the ESA mission that has a single 355 nm laser whose return signals are filtered for molecular scattering and aerosol scattering to retrieve 100 m resolution vertical profiles of aerosol optical depth from near the surface to 40 km.

The planned NASA Aerosols Clouds Climate and Precipitation mission in response to the second decadal survey recommendations is also expected to carry a lidar in addition to a polarimeter and spectrometer.

### **A5.5. Atmosphere Observing System (AOS)**

The AOS is a multi-satellite mission with targeted observations of clouds, precipitation, and aerosols to learn about various feedback mechanisms tied to climate. Named AOS-P1, AOS-I1, AOD-I2, the platforms will carry a suite of different instruments. A combination of these measurements will provide relevant information on observables such as aerosols, clouds, and precipitation. Aerosol information can be obtained from a high spectral resolution Lidar (532 nm, 1064 nm), multi-angle polarimeter, and a UV-VIS spectrometer on AOS-P1. The expected spatial resolution for aerosol products is 0.5 km<sup>2</sup>. AOS-I2 will also have a backscatter Lidar and a multi-angle polarimeter. All satellites will be launched into inclined orbits and therefore be able to provide some diurnal information.

### *A6. Ground-Based Sensors*

Monitoring surface PM<sub>2.5</sub> using an integrated approach of satellites and models requires a host of in situ observations, ranging from AOD and PM<sub>2.5</sub> to aerosol vertical distribution, aerosol composition, and optical properties. While not all observations are made routinely, significant number of networks that observe diverse information exist.

#### **A6.1. Surface PM<sub>2.5</sub>**

PM<sub>2.5</sub> is one of the criteria pollutants identified by environmental agencies worldwide. The standard measurements are often made in temperature- and humidity-controlled (~40%) environments, and therefore are referred to as dry mass concentration.

The systematic regulatory measurement of PM<sub>2.5</sub> in the US started in late 1997 with few monitors, and grew over the past two decades to more than 1000 continuous monitoring stations currently. Most other countries started monitoring PM<sub>2.5</sub> in the 21<sup>st</sup> century. US EPA makes PM<sub>2.5</sub> data available (<https://www.epa.gov/outdoor-air-quality-data>) in various formats, including API access. Several other countries around the world also make data available in the public domain.

In 2015 a private company (now a non-profit organization) called openAQ ([openaq.org](http://openaq.org)) started archiving PM<sub>2.5</sub> and other pollutant data from US embassy locations around the world into an easy-to-access data format. Gradually, openAQ extended its database to include other standard air quality networks specifically operated by individual countries. The openAQ database started with few stations and has grown over the last five years to include PM<sub>2.5</sub> data from more than 4000 stations worldwide, including 86 countries. OpenAQ only archives data in forward processing, meaning that even though

many of the stations may have longer data records, openAQ only contains data from the date the station was added to their data record. OpenAQ data can be downloaded from their website, including API access. OpenAQ metadata includes station information and original source of data but does not have any details on data collection instruments. A recent study (Christopher and Gupta, 2020) used these global data sets and collocated with MODIS AOD records to understand the data availability in different parts of the world and its impact on AOD-PM<sub>2.5</sub> relationships. Over the years, more than 100 other studies have utilized data records from openAQ to perform various air quality analyses, including those with satellite observations.

There are also growing networks of low-cost sensors from private sectors and citizen scientists that are relevant for PM<sub>2.5</sub> monitoring. The most popular low-cost network is PurpleAir (PA) with 10,000 plus monitors operating around the world. The PurpleAir sensor uses two identical sensors in a single unit for cross-calibration and consistency checks. In addition to PM<sub>2.5</sub>, PM<sub>10</sub>, PM<sub>1</sub>, the unit also records temperature and relative humidity. The PA sensor records PM<sub>2.5</sub> every 2-minutes; sensors connected to the internet send their measurements to the PA cloud where it becomes publicly available in real-time in the form of a map and chart. The most significant advantage of PA data is its open access through API and download tools. Over the years, several research groups have deployed PA sensors in large numbers and attempted to calibrate with US EPA regulatory FRM/FEM monitors (Gupta et al., 2018; Feenstra et al., 2019) The sensors' accuracy varies as a function of aerosol type, aerosol concentration, temperature, relative humidity, and other environmental conditions. There can also be significant differences among identical PA units. More recently, US EPA has published correction factors for PA data so the data can be merged with data from regulatory monitors to fill in the gaps (Barkjohn, et al., 2021; Holder et al., 2020).

## A6.2. AERONET

AERONET utilizes Cimel Electronique Sun/Sky/Moon radiometers at more than 600 sites worldwide to measure total column AOD and retrieve aerosol characteristics such as volume size distribution, complex index of refraction, and SSA. Measurements of AOD are performed using eight (8) nominal spectral bands (340 nm, 380 nm, 440 nm, 500 nm, 675 nm, 870 nm, 1020 nm, 1640 nm) at 5-to-15-minute intervals (Holben et al., 1998; Giles et al., 2019). The AOD measurements are cloud screened and quality controlled according to the AERONET Version 3 algorithm (Smirnov et al., 2000; Giles et al., 2019). Uncertainty in the calibrated and temperature corrected AOD vary from  $\pm 0.01$  for the visible and near infrared wavelengths and  $\pm 0.02$  for the ultraviolet wavelengths (Eck et al., 1999; Giles et al., 2019). New nighttime AOD measurements are performed using the moon from waxing gibbous to waning gibbous lunar phase (Li et al., 2016; Barreto et al., 2016). The uncertainty in these nighttime AOD is estimated to be larger ( $\sim 0.03$ ) due to instrument and irradiance model uncertainties; and these data may be further affected by optically thin cirrus clouds.

Inverting AOD with the magnitude and angular distribution of sky radiances allows for the retrieval of aerosol characteristics utilizing the 440 nm, 675 nm, 870 nm, and 1020 nm nominal wavelengths (Dubovik and King, 2000; Dubovik et al., 2000, 2002, 2006; Sinyuk et al., 2020). In general, retrieved quality assured SSA has an uncertainty of  $\pm 0.03$  according to Dubovik et al. (2002). Sinyuk et al. (2020) determined that the uncertainty of SSA and imaginary part of the refractive index retrievals can vary depending on AOD magnitude with smaller uncertainties corresponding to larger AOD. Further, Schafer et al. (2014, 2019) showed excellent agreement between AERONET inversion products and column integrated in situ aircraft profiles of SSA and size distribution during the DISCOVER-AQ campaigns. The next iteration of the AERONET inversions will likely implement changes to algorithm constraints and include a up to three additional wavelengths (380 nm, 500 nm, and 1640 nm) to provide improved spectral range of aerosol absorption products and aerosol particle assessments (Sinyuk et al., in preparation).

AERONET's growth during nearly 30 years of operation is based on international participation and collaboration within the context of a federated network. Quality of the public domain database is maintained by imposing standardization of instruments, calibration, processing, quality assurance, and data distribution (Holben et al., 1998). Access to the historic and near real time aerosol products is available from <https://aeronet.gsfc.nasa.gov>. The network has largely stabilized in the number of active sites over the past four years owing to replacement and upgrades that has increased the capabilities of existing sites as described above. Expansion of the network is planned and ongoing in regions of low spatial coverage and as scientific opportunities and collaborations arise. The network deployments began with an emphasis on sites with elevated aerosol loading and regionally representative to support satellite validation research. For over 20 years, background sites, urban and agricultural, oceanic and coastal sites have been included at all latitudes and continents. The current highest deployment priorities are the continent of Africa and extending collaborations in central Asia, China and Russia. Co-location with the MPLNET and other ground based super sites is strongly encouraged.

NASA's AERONET contribution to PM is largely indirect where AOD is used to normalize lidar signals (e.g., MPLNET) or to develop a coefficient to relate ground based PM<sub>2.5</sub> to satellite retrievals (SPARTAN). Further, AERONET Distributed Regional Aerosol Gridded Observation Networks (DRAGON) campaigns have and continue to contribute to higher instrument spatial density to support large aircraft field campaigns such as TRACER-AQ, which is assessing air quality using the airborne GCAS sensor as a testbed for TEMPO (Holben et al., 2018; Judd et al., 2021). Data acquisition systems currently in development for AERONET may allow for expansion of instruments at select sites to include low-cost air quality sensors (e.g., PurpleAir). Future satellite missions such as MAIA will leverage AERONET instrumentation to provide multi-year monitoring at key primary and secondary target regions (Diner et al., 2018). AERONET measurements performed concurrently with ground-based in situ PM measurements and lidar is expected to provide a foundation for developing future PM retrievals from space.

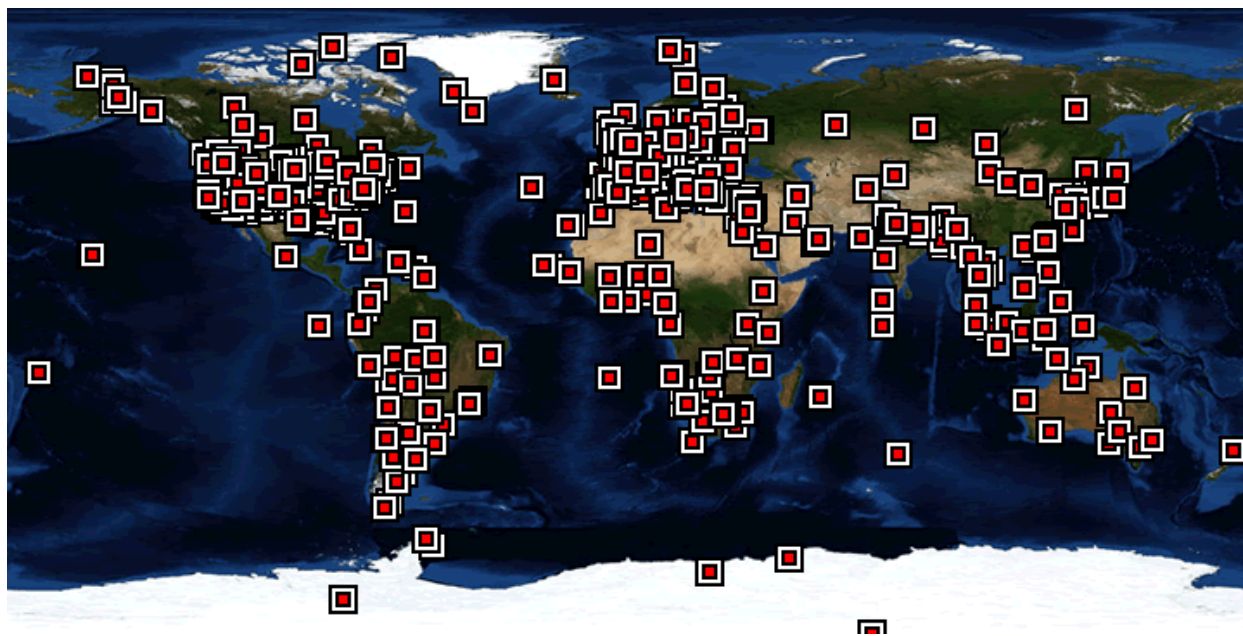


Figure A.4. Aerosol Robotic Network (AERONET) global site distribution in 2021

### A6.3. Ceilometer and Lidar Networks

Following critical maturation in lidar technology that has been on steady rise since the 1990s, ceilometers and lidars have become less distinct. The micro-pulse lidar was the first robust, commercially available lidar at visible wavelengths capable of running continuously and providing both ceilometer like data (multiple cloud and PBL heights) and retrievals of aerosol properties (when co-located with a sun photometer). Advanced lidar systems have been developed that provide direct retrieval of aerosol extinction, multi-wavelength profiling providing micro-physical retrievals, and doppler lidar for both wind and aerosol profiling. Ozone lidars have been upgraded to profile boundary layer ozone, and DIAL systems are on track towards a commercially available system for water vapor profiling (and aerosol extinction with HSRL channel). Ceilometers have also improved, as primarily newer instruments with increased SNR have enabled higher profiling and better ability to detect aerosols and even retrieve backscatter in some cases.

New networks have taken advantage of these developments to provide operational atmospheric profiling. Lidars have moved from the research realm to operational networks, starting around 2000 with EARLINET, ADNET, and MPLNET. The European Aerosol Research Lidar Network (EARLINET) was started as a research focused network of advanced lidars across Europe. The Asian Dust Lidar Network (ADNET) was also developed as a regional network providing lidar profiles of dust and pollution across Eastern Asia. In the US, the NASA MPLNET was created to provide global lidar profiling at key AERONET sites. In addition to these networks, the Network for the Detection of Atmospheric Composition Change (NDACC) pre-dates these networks and many sites have lidar data to contribute. More recently, new lidar and ceilometer networks have come online such as LALINET, a federated lidar network throughout Latin America. A successful example of exploiting new ceilometer capabilities is EUMETNET's E-PROFILE project, which provides data from European ceilometer networks. A new project called the Unified Ceilometer Network (UCN), funded by US EPA and NASA, will provide similar provision of ceilometer data in North America but with specific goal of supporting air quality programs. These lidar and ceilometer networks have continued to mature and develop more operational capabilities and data sets, coupled with viable data centers providing DAAC services and access to near-real-time data.

Coordination of ceilometer and lidar networks has been improving over time, but there are still challenges from a global perspective. In 2008 under WMO guidance, the Global Atmospheric Watch (GAW) Aerosol Lidar Observation Network (GALION) was created with existing lidar networks as members (EARLINET, ADNET, MPLNET, LALINET, and NDACC lidar) (Figure A4). The goal was to share information, best practices, develop frameworks and techniques for quality data, and improve ability to access network data.



**Figure A 5.** Global Atmospheric Watch (GAW) Aerosol Lidar Observation Network (GALION) stations.

#### **A6.4. Surface Particulate Matter Network (SPARTAN)**

A key source of uncertainty in the inference of  $PM_{2.5}$  from satellite retrievals of AOD is the spatiotemporal distribution of the relationship of  $PM_{2.5}$  with satellite retrievals of columnar AOD. The Surface PARTICulate mAtter Network (SPARTAN) of ground-based monitoring stations is designed to measure this relationship to evaluate and enhance satellite remote sensing of  $PM_{2.5}$ . SPARTAN is an ongoing, long-term project that measures aerosol mass, ions, trace elements, and aerosol optical properties at globally dispersed, densely-populated areas. Monitors are collocated with ground-based sunphotometers that measure AOD, to yield an empirical measure of the relation of AOD with  $PM_{2.5}$  mass, scatter, and composition.

Snider et al. (2015) provide an overview of the SPARTAN PM observation network, the cost-effective sampling methods employed, and initial post-sampling instrumental methods of analysis. Subsequent publications describe the initial analyses of major  $PM_{2.5}$  components (Snider et al. 2016), uncertainty characterization (Weagle et al. 2018), and elemental analyses (McNeill et al. 2020). The standard setup utilizes a combination of continuous monitoring by nephelometry and mass concentration via filter-based sampling. The instruments, a three-wavelength nephelometer and impaction filter sampler for both  $PM_{2.5}$  and  $PM_{10}$ , are highly autonomous. Nephelometer backscatter and total light scatter at three wavelengths provide high temporal resolution and some information on particle size. Nephelometer light scattering is constrained with filter-based measurements; the combination of these measurements yields estimates of hourly  $PM_{2.5}$  concentrations. SPARTAN filters are analyzed for mass, ions, carbonaceous material, and trace elements.

SPARTAN site-selection favors densely populated, globally dispersed regions that are underrepresented in terms of availability of representative and long-term air quality data. Local site-selection favors representative environments that avoid anomalous sources; low rooftops in urban environments are desirable to increase fetch, diminish local traffic influence, and offer

instrument security. Locations of SPARTAN sites are shown in Fig. A 5. As SPARTAN site selection prioritizes under-sampled locations, some regions that are well-represented in terms of air quality data have not established a SPARTAN site to date. Further expansion of the network is desired for the future, in order to cover regions not sampled by SPARTAN, as well as add more sites in underrepresented regions.

SPARTAN has undergone several upgrades since the original publications. Beginning in 2017, sampling stations were upgraded to the AirPhoton SS5 model, which uses a cyclone inlet to achieve a sharper size cut than the prior nucleopore filters. Beginning in 2018, filters have been routinely shipped to UC Davis for additional carbonaceous analysis (FTIR, HIPS). Beginning in 2019, manual gravimetric analyses were replaced with an automated weighing system (MTL AH500E) to improve precision and throughput, ICP-MS analysis transitioned to XRF (Malvern Panalytical Epsilon 5) to improve characterization of crustal elements, and the IC instruments were upgraded (ThermoFisher Integriion). Partnership with IMPROVE promotes consistency across both networks. Activities are ongoing to directly measure organics through Aerosol Mass Spectrometry. In early 2022, seven additional sampling stations were deployed at select MAIA primary target areas. These stations include communication modules to facilitate remote commanding of the instruments to sample at MAIA overpass times.

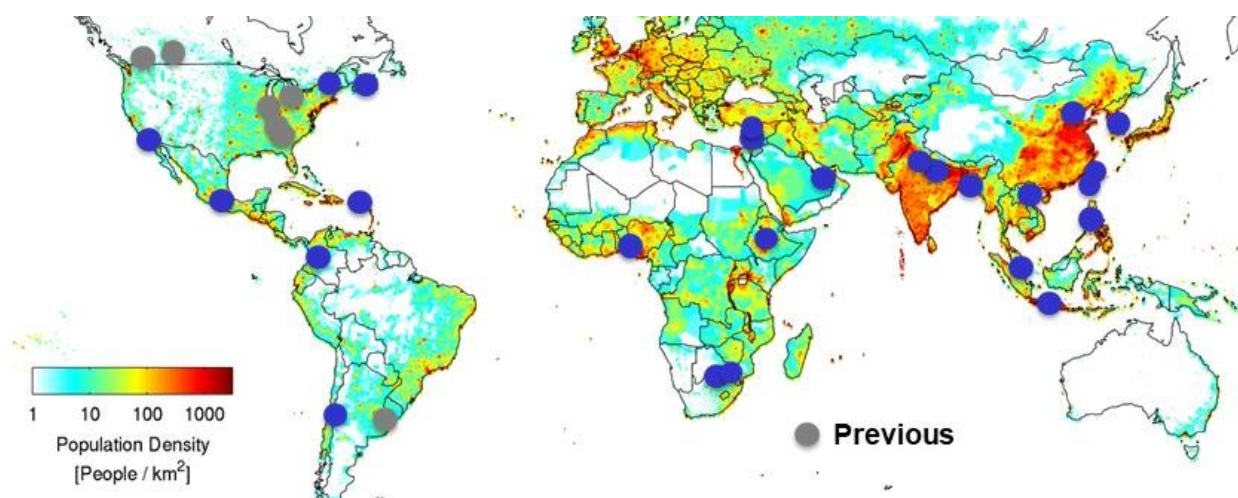


**Figure A 6.** Site locations of the Surface Particulate Matter Network (SPARTAN) that measures the relationship of columnar AOD with  $PM_{2.5}$  mass and chemical composition.